Discovery and Characterization of Novel Inhibitors for Bacterial rRNA Transcription

TSANG, Tsz Fung

A Thesis Submitted in Partial Fulfilment

of the Requirements for the Degree of

Master of Philosophy

in

Microbiology

The Chinese University of Hong Kong

September 2020

Table of contents

Declaration

I declared that this thesis has not been submitted for any degree or diploma to other University and it is the result of original research.

Tsang Tsz Fung

May 2020

Acknowledgements

I would like to thank my supervisor, Dr. Xiao Yang. I am grateful for your support and encouragement during the past three years. I have learnt a lot from your guidance and suggestion on the experimental techniques and the attitude toward my life plan. I am glad to have your precious advice on career planning and on my study.

Thank you to all members in Dr. Yang's group for their help in demonstration of experimental techniques and encouragement. I would like to thank Dr. Yang's collaborators: thanks to Dr. Cong Ma and his team for providing the nusbiarylins; thanks to Prof. Shannon Au for providing technical support for protein purification; thanks to Prof. Markus Wahl for hosting me for a three-month visit and training on protein structural works.

Last but not least, I want to thank my family and friends for their continuous support.

	Contributions
TSANG Tsz Fung	Performed the experiments. (NanoLuc PCA, reporter strain construction, dot blot, NusB crystallization)
Dr. Xiao Yang and teammates: Dr Adrian Chu, Miss Sophie Lam, Miss Lin Lin, Miss Rachel Harper, Miss Hoi Kiu Chan	Conceived the idea and provided guidance on data interpretation, and setup of experiments
Dr. Cong Ma and his group	Conceived the idea and synthesized the nusbiarylin compounds
Prof. Shannon Au and her group	Provided technical support on protein purification
Prof. Markus Wahl and his group	Collected and analyzed the X-ray diffraction data

Abstract

Antimicrobial resistance represents a growing worldwide crisis due to the overuse of antibiotics and the slowdown in new drug development. The most prevalent multi-drug resistant bacteria, methicillin-resistant *Staphylococcus aureus* (MRSA) can cause lethal infections. Hence, drugs with novel mechanisms of action are required. Bacterial transcription presents a proven but underutilized drug target for novel antimicrobial discovery.

Transcription is a process to make RNA from a DNA template, carried out by an enzyme RNA polymerase. In bacterial cells, ribosomal RNA (rRNA) is highly transcribed during the exponential growth phase. To enable a high level of rRNA to meet the demand for protein synthesis during the rapid cell growth, a class of conserved bacterial transcription factors N-utilization substance (Nus) family, RNA transcript, and other factors form antitermination complex with the RNA polymerase. The resulting complex passes through a premature terminator at the leader sequence, enabling a complete rRNA product. During the complex formation, transcription factors NusB and NusE dimerize, representing the first regulatory step of rRNA transcription.

Previously our team discovered the first-in-class bacterial transcription inhibitor hit compound **MC4**, which inhibited MRSA growth and specifically interacted with *Bacillus subtilis* NusB. A group of MC4-derivatives namely nusbiarylins were made with improved antimicrobial activities. Previous investigations of nubiarylins focused

on antimicrobial activities. However, nusbiarylins' mechanism of action remains unclear. The current study **aims** to characterize nusbiarylins through the lens of molecular biology. The NusB-NusE interaction is hypothesized as a novel target for antimicrobial discovery.

First, a novel *in vitro* protein-fragment complementation assay (PCA) was developed to characterize and screen for protein-protein interaction (PPI) inhibitors based on a split luciferase system. The newly developed *in vitro* NanoLuc PCA was validated by studying two essential PPIs in bacterial transcription and applied to study new nusbiarylin compounds. Second, *Escherichia coli* and *B. subtilis* reporter strains were made to examine the effects of nusbiarylins on promoter strength. Reporter gene expressions were inspected by a non-radioactive mRNA dot blot. Third, X-ray crystallography was applied to confirm the mode of interaction between NusB – nusbiarylins. The protein crystals from *Thermotoga maritima* NusB or NusB – nusbiarylins assemblies were subjected to X-ray diffraction for structural determination.

The present study facilitates future study on nusbiarylins and other transcription inhibitors. The *in vitro* NanoLuc PCA could be used to screen and characterize new nusbiarylin compounds and other PPI inhibitors. The reporter strains generated could be used to correlate nusbiarylins and rRNA transcription. Methods other than crystallography like mass spectrometry could be applied to confirm the formation of NusB-nusbiarylin complexes.

摘要

由於抗生素的過度使用和新藥開發的放緩，抗菌素耐藥性代表著全球日益嚴重的危機。最普遍的耐多藥細菌是耐甲氧西林的金黃色葡萄球菌（MRSA），如果 MRSA 進入血液，可引起致命感染。因此，需要具有新穎作用機制的藥物。細菌轉錄是一種經過驗證的但未充分利用的藥物靶標。

轉錄是通過 RNA 聚合酶從 DNA 模板製備 RNA 的過程。在細菌細胞中，核醣體 RNA（rRNA）在指數生長期被高度轉錄。為了使高水平的 rRNA 能夠滿足快速細胞生長過程中蛋白質合成的需求，一類保守的細菌轉錄因子 N 利用物質（Nus）家族，RNA 轉錄物和其他因子與 RNA 聚合酶形成了抗終止複合物。產生的複合物在前導序列處通過一個過早的終止子，從而形成完整的 rRNA 產物。在復合物形成過程中，轉錄因子 NusB 和 NusE 二聚化，代表 rRNA 轉錄的第一個調控步驟。

以前，我們的團隊發現了一流的細菌轉錄抑製劑 MC4，該抑製劑可抑制 MRSA 的生長，並與枯草芽孢桿菌 NusB 發生特異性相互作用。為了獲得更強的抗菌作用，製備了一組 MC4 衍生物，即 nusbiarylins。先前對 Nubiarylins 的研究集中在抗菌活性上。但是，努斯比芳林素對 NusB 和 rRNA 轉錄的作用仍不清楚。本研究旨在通過分子生物學的角度表徵努比聯芳烴。 NusB-NusE 相互作用被假定為新型藥物靶標。

本研究具有三個目標。首先，開發了一種新型的體外蛋白質片段互補測定法（PCA）來表徵和篩選蛋白質-蛋白質相互作用（PPI）抑製劑。基於稱為

NanoLuc™（美國 Promega，美國）的熒光素酶拆分系統，設計並構建了 PCA 質粒系統，用於將 PPI 對融合到兩個熒光素酶片段上。特定的 PPI 允許兩個互補片段結合為功能性螢光素酶。通過研究細菌轉錄中的兩種基本 PPI，驗證了新開發的體外 NanoLuc PCA，並將其用於篩選新的努斯比林化合物。其次，製備大腸桿菌和枯草芽孢桿菌報導菌株，以檢查努斯比芳林對 rRNA 轉錄的影響。通過非放射性 mRNA 點印跡檢查報告基因的表達。第三，應用 X 射線晶體學確定 NusB – nusbiarylins 之間的相互作用方式。將來自濱海嗜熱菌的 NusB 或 NusB –努比聯芳烴裝配體的蛋白質晶體進行 X 射線衍射以進行結構測定。最終，在分離的結構中未鑑定出努斯比芳林分子。

本研究促進了對努斯比芳林和其他轉錄抑製劑的未來研究。試管內 NanoLuc PCA 可用於篩选和表徵新的努斯比林化合物和其他 PPI 抑製劑。本研究所產生的報告株可用於研究努斯比芳林和 rRNA 轉錄的關係。未來研究可以採用晶體學以外的方法（如質譜法）來確定 NusB-nusbiarylin 配合物的形成。

List of abbreviations

AIM	Auto-induction media
ATP	Adenosine triphosphate
Bp	Base pair
CAT	Chloramphenicol acetyltransferase
CH	Clamp helix
CTD	C-terminal domain
DNA	Deoxyribonucleic acid
DTT	Dithiothreitol
EDTA	Edetate disodium
ELISA	Enzyme-linked immunosorbent assay
FRET	Fluorescence resonance energy transfer
HTS	High throughput screening
HRP	Horseradish peroxidase
IC_{50}	Half-maximal inhibitory concentration
IPTG	Isopropylthiogalactoside
ITC	Isothermal titration calorimetry
K_d	Dissociation constant
LB	Luria broth media
MIC	Minimum inhibitory concentration
MQW	MilliQ water

mRNA	Messenger RNA
NanoLuc	NanoLuciferase
NusA	N-utilization substance A
NusB	N-utilization substance B
NusE	N-utilization substance E
NusG	N-utilization substance G
Nut	N-utilization
NTD	N-terminal domain
NTP	Nucleoside triphosphate
Ops	Operon polarity suppressor
PCA	Protein-fragment complementation assay
PCR	Polymerase chain reaction
PPI	Protein-protein interaction
Qut	Q-utilization
RLU	Relative light unit
Rpm	Revolution per minute
RNA	Ribonucleic acid
RNAP	RNA polymerase
rRNA	Ribosomal RNA
Rut	Rho-utilization
SDS	Sodium dodecyl sulfate
SDS-PAGE	SDS-polyacrylamide gel electrophoresis
TBE	Tris-borate-EDTA

TEC	Transcription elongation complex
TRAP	Tryptophan RNA attenuation protein
Trp	Tryptophan
tRNA	Transfer RNA
UP element	Upstream element

Chapter 1: Introduction

1.1 RNA Polymerase

In all organisms, transcription is the first step in gene expression and is carried out by an enzyme DNA-dependent RNA polymerase (RNAP) (Kireeva and Kashlev, 2013). In eukaryotic cells, there are three distinct RNAPs; RNAPI transcribes ribosomal RNA (rRNA), RNAPII produces messenger RNA (mRNA), and RNAPIII synthesizes transfer RNA (tRNA) (Carter and Drouin, 2009). In bacteria and archaea, a single type of RNAP is responsible for transcribing all kinds of RNA (Carter and Drouin, 2009).

Bacterial RNAP is a multi-subunit enzyme that exists in two states: core and holoenzyme (Murakami, 2015). A core is composed of five subunits including two α, β, β', and ω (Murakami, 2015; Figure 1.1). The core enzyme can catalyze RNA synthesis but is incapable of binding to a specific promoter (Murakami, 2015). The second form of RNAP, namely holoenzyme is able to synthesize RNA and recognize a promoter (Murakami, 2015). The RNAP holoenzyme is formed by the core associated with an initiation factor σ (Kireeva and Kashlev, 2013). In addition to σ, RNAP interacts with various transcription factors throughout transcription (Balleza *et al.*, 2009). To fully elucidate the protein-protein interactions (PPIs) that occur during transcription, the subunits of RNAP has been explored by numerous prior studies (Borukhov and Nudler, 2008).

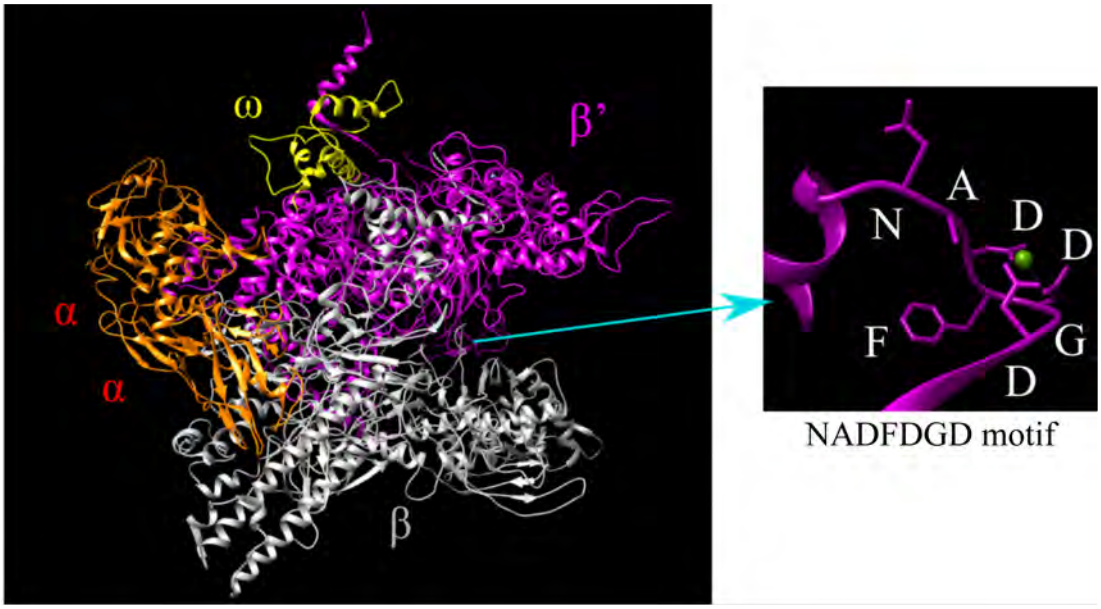

E. coli RNAP core $\alpha_2\beta\beta'\omega$

Figure 1.1 The *Escherichia coli* RNAP core EM structure (PDB ID: 3LU0) (Opalka *et al*., 2010). RNAP core has the characteristic crab-claw shape with the $\alpha_2\beta\beta'\omega$ composition. β and β' are larger parts constituting two clamps. The catalytic activity of RNAP is due to the conserved motif NADFDGD that chelates a Mg^{2+} ion. The cation Mg^{2+} is electrostatically attracted to two residues of aspartic acid. α: orange, β: grey, β': magenta, ω: yellow.

Previous researches explored functions of the RNAP subunits (Borukhov and Nudler, 2008). α has three functions; First, α stimulates transcription through interacting with the transcription factors (Ishihama, 1992). Second, α facilitates holoenzyme-promoter binding by interacting with the upstream (UP) element in a promoter (Murayama and Ishikawa, 2015). Third, α supports RNAP core assembly (Mathew and Chatterji., 2006; Figure 1.2).

β and β' are two large subunits that resemble two pincers in the 'crab claw'-like structure of RNAP (Murakami, 2015, Figure 1.1). The central cavity between β and β'

accommodates the primary, secondary channels (Borukhov and Nudler, 2008). The primary channel has a diameter of 27 Å that holds the hybrid of the DNA template and RNA strand (Borukhov and Nudler, 2008). In the primary channel, a new nucleoside triphosphate (NTP) is added to the 3' end of RNA transcript by the active center (Borukhov and Nudler, 2008). The active center is the catalytic part of RNAP attributed to the evolutionarily conserved motif NADFDGD (Murakami, 2015; Nudler, 2009; Figure 1.1). The secondary channel directs an NTP to the primary channel and is bound by different modulators for regulation (Nickels and Hochschild, 2004; Marr and Roberts, 2000). Apart from the primary and secondary channels, RNAP has the RNA exit channel that comprises three domains, namely the β' zipper, β' zinc finger, and β flap (Nudler, 2009). These three elements assist the release of newly synthesized RNA, transcriptional pausing, and termination (Borukhov and Nudler, 2008).

ω is the smallest subunit. The essentiality of ω used to be disregarded because the RNAP core enzyme was previously defined as $\alpha_2\beta\beta'$ (Mathew and Chatterji., 2006). In the late 1990s, ω was proved to specifically interact with the β' subunit and to stimulate transcription (Gentry and Burgess, 1993; Dove and Hochschild, 1998). The specific ω - β' interaction supports RNAP core assembly (Ghosh, 2001). For a RNAP core to be formed, two α dimerize using the N-terminal domain (NTD) (Mathew and Chatterji., 2006). The α dimer provides a hydrophobic core to recruit β and the ω - β' subcomplex to constitute an active core (Mathew and Chatterji., 2006; Figure 1.2).

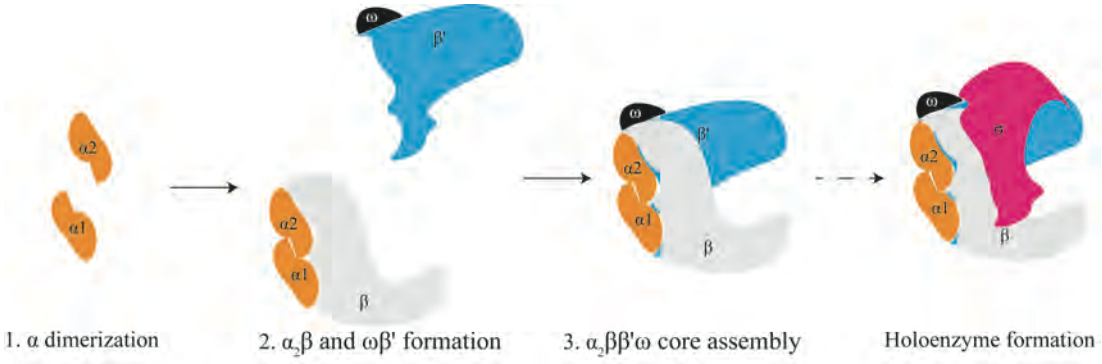

Figure 1.2 Assembly of the RNAP core. Two α form a dimer to recruit β and the ω - β' subcomplex. Ultimately, the RNAP core is formed by the assembly of $\alpha_2\beta\beta'\omega$. A core interacts with σ to form a holoenzyme.

RNAP has the conserved composition of $\alpha_2\beta\beta'\omega$ in bacteria like *Escherchia coli*. Notably, two additional subunits were found in Gram-positive model organism *Bacillus subtilis* in the previous studies (Opalka *et al*., 2010; Vassylyev *et al*., 2002). *B. subtilis* RNAP has two extra subunits δ and ε (Juang and Helmann., 1994; Keller *et al*., 2014). δ enhances RNA yield through the increase in RNAP recycling (Juang and Helmann., 1994). ε is presumed to confer phage resistance to *B. subtilis* (Keller *et al*., 2014). Hence, *B. subtilis* RNAP core is composed of $\alpha_2\beta\beta'\delta\varepsilon\omega$.

1.2 Overview of the transcription cycle

The transcription cycle is divided into three phases: initiation, elongation and termination (Stracy and Kapanidis, 2017; Figure 1.3). Following binding to the promoter DNA region, RNAP synthesizes the RNA strand by adding nucleotides to the 3' end of RNA . Eventually, RNA synthesis is ended by intrinsic or Rho-dependent termination. (Murakami, 2015; Figure 1.3).

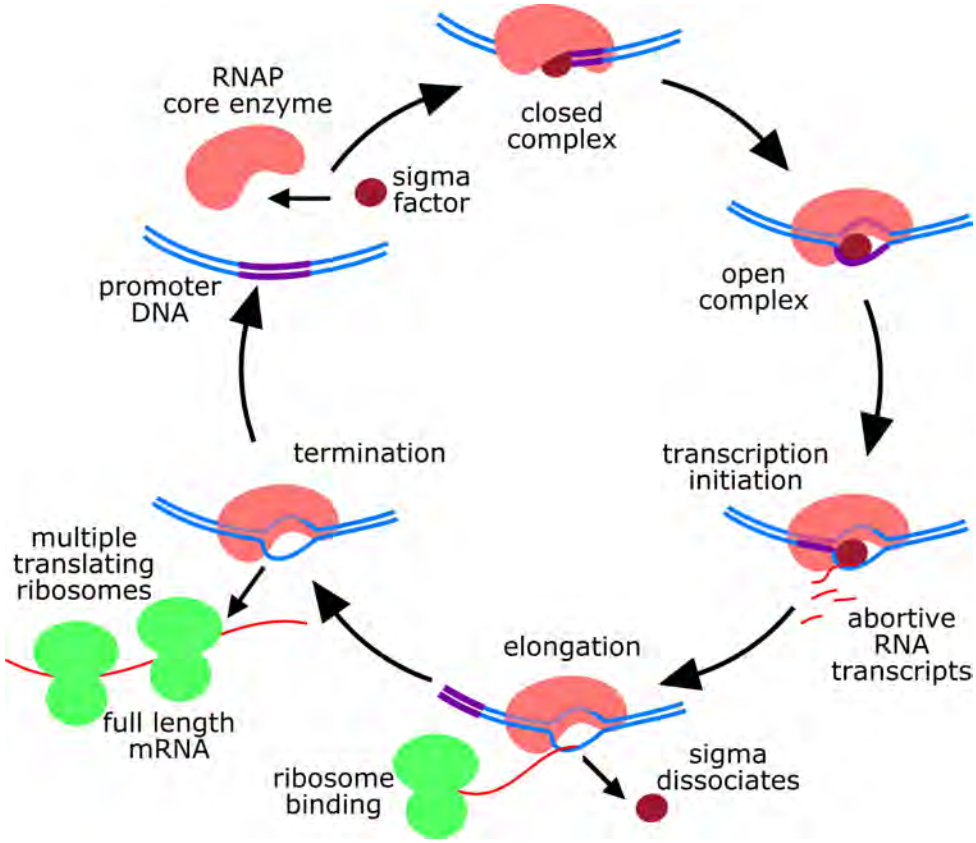

Figure 1.3 Overview of the transcription cycle. At initiation, a holoenzyme and the promoter DNA form the closed complex. σ melts the DNA duplex to form the open complex that makes abortive RNA transcripts for promoter escape. In early elongation, σ dissociates from RNAP. The synthesis proceeds until the production of full length RNA. Ribosome starts translation for protein synthesis. Adapted from Stracy and Kapanidis, 2017.

1.2.1 Initiation

To bind a specific promoter, RNAP must reach the promoter DNA region within whole chromosome (Dangkulwanich *et al*., 2014). Several prior studies purposed four promoter-searching mechanisms: sliding on chromosome, DNA hopping, translocation with a DNA loop, and random collision (Feklistov 2014; Friedman *et al*., 2013; Wang *et al*., 2013). Finally, RNAP reaches the promoter region and interacts with σ (Browning and Busby, 2004). Bacterial cells have multiple σ factors for transcribing different genes. For housekeeping gene transcription, bacterial cells make

use of the primary σ factor (Narayanan *et al*., 2018). σ^{70} and σ^{A} are the primary σ factors in *E. coli* and *B. subtilis* respectively (Narayanan *et al*., 2018; Juang and Helmann., 1994). In *E. coli*, σ^{70} contains domains 1, 2, 3, and 4 (Browning and Busby, 2004). Currently the biological importance of the domain 1 remains ambiguous, whereas the domain 2, 3, and 4 bind to the promoter elements (Browning and Busby, 2004).

A typical promoter encompasses four essential elements, namely the UP element, -10 box, -35 box, and extended -10 element (Narayanan *et al*., 2018). In a σ^{70}-specific promoter, the -10 box and -35 box contain the consensus sequence 'TTGACA' and 'TATAAT' respectively (Browning and Busby, 2004). The extended -10 element is located between the -35 box and -10 box. As illustrated in Figure 1.4, the region 2.4, 4.2, and the domain 3 of σ^{70} bind to these elements, whereas the UP element is bound by the α C-terminal domain (CTD) (Borukhov and Nudler, 2008; Browning and Busby, 2004). Holoenzyme and the promoter DNA form the closed initiation complex (Narayanan *et al*., 2018). In the closed complex, the DNA remains double stranded and outside the active center (Saecker *et al*., 2011). Subsequently, the β' clamp unwinds the duplex DNA of 13 base pairs (bp) upstream the -10 box to become the open complex (Glyde *et al*., 2018).

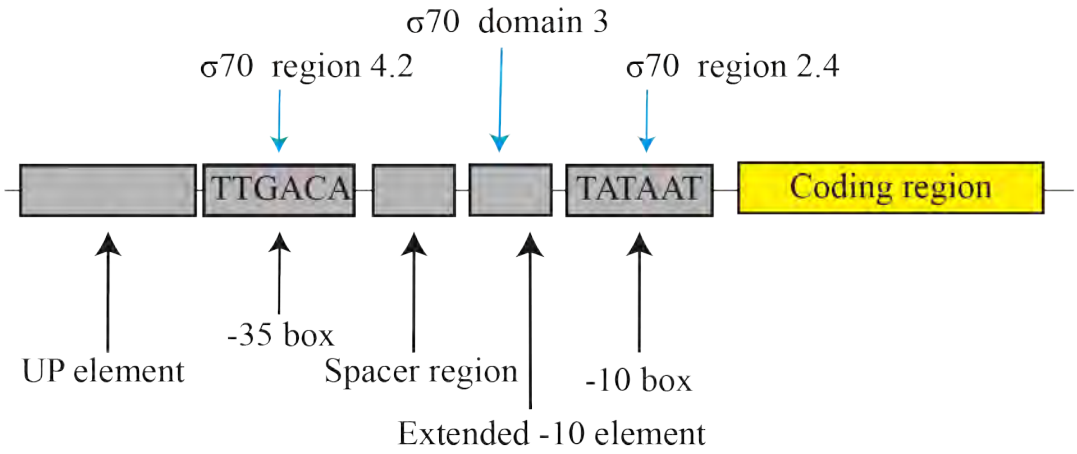

Figure 1.4 Location of the promoter components. The RNAP holoenzyme binds to the promotor region through the σ^{70} region 2.4, 4.2 and the domain 3.

The open complex repetitively synthesizes and releases short RNA transcripts without moving downstream, the process is called abortive initiation (Revyakin *et al.*, 2006). The nonproductive RNA synthesis is entitled DNA scrunching, a process to supply energy for promoter escape before elongation (Dangkulwanisch *et al.*, 2014).

1.2.2 Elongation

Following the synthesis of ~12 bp RNA strand, σ dissociates from the holoenzyme. Two transcription factors N-utilization substance (Nus) A and NusG are recruited to the elongating RNAP to form the transcription elongation complex (TEC) (Yang *et al.*, 2009; Burova *et al.*, 1995). The TEC can stably transcribe the coding sequence because both NusA and NusG can stimuate the transcription elongation rate (Burova *et al.*, 1995).

Throughout elongation, the DNA duplex remains melted as a 'transcription bubble' where the growing RNA hybridizes with the DNA template strand (Molnar and Gair,

2019; Figure 1.5). The TEC holds the transcription bubble and slides along the DNA template at up to 25 bp per second while NTPs are added to the 3’ terminus of RNA in the nucleotide addition cycle (Molnar and Gair, 2019; Brueckner *et al*., 2009). During the nucleotide addition cycle, an NTP goes to the insertion site within the active center (Brueckner *et al*., 2009). The active center adds this NTP to the RNA strand (Brueckner *et al*., 2009). Finally, the TEC is translocated by 1 bp toward the downstream (Nudler, 2009). The TEC keeps extending the RNA strand until being paused or terminated (Lee and Borukhov, 2016).

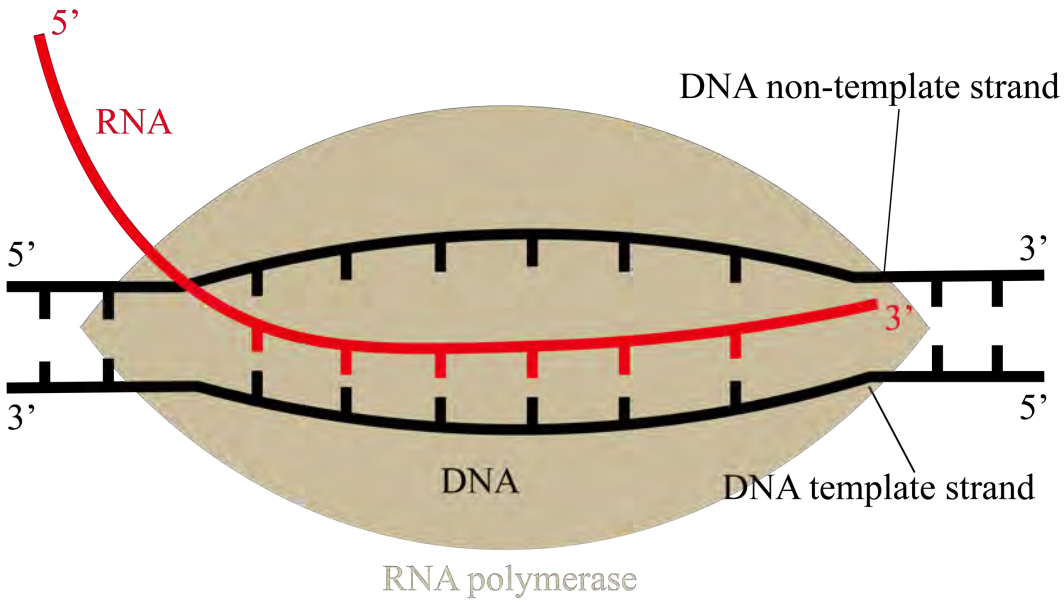

Figure 1.5 The transcription bubble in prokaryotic transcription. The DNA strand is separated like a bubble where NTPs are added to the 3’ end of RNA.

1.2.3 Termination

Transcription is ended through two major pathways: intrinsic or Rho-dependent termination (Borukhov *et al*., 2005). In the intrinsic pathway, a G/C-rich hairpin terminator destabilizes and releases RNAP (Gusarov and Nudler, 2001; Ray-Soni *et al*., 2016; Figure 1.6).

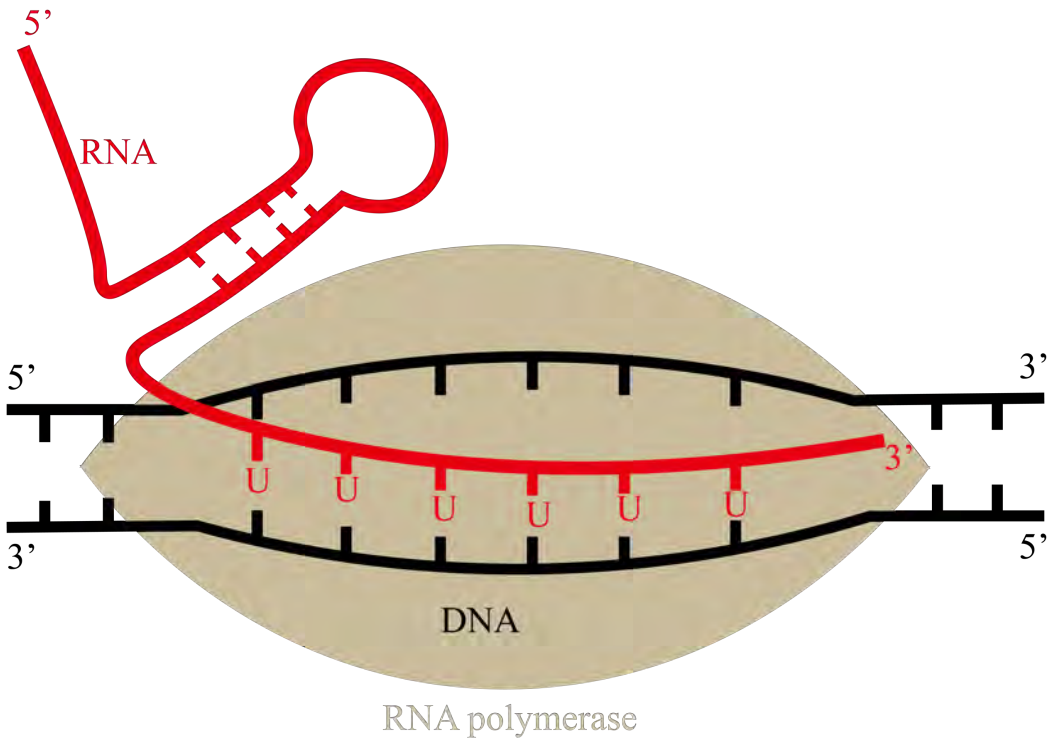

Figure 1.6 Intrinsic termination. A terminator RNA hairpin is trapped in the exit channel, leading to the transcriptional pause. The pause destabilizes the TEC, disengaging RNAP from DNA (Porrua *et al*., 2016).

Rho-dependent termination is mediated by the termination factor Rho. The complete mechanism of Rho-dependent termination has not been established yet (Porrua *et al*., 2016). Prior studies agreed that Rho is recurited at the Rho-utilization (*rut*) site to separate RNAP from the DNA template by ATP hydrolysis (Ray-Soni *et al*., 2016;

Figure 1.7). In previous studies, the *rut* sites were found to be C-rich G-poor or G-rich, but no universal *rut* sequence was reported (Ray-Soni *et al*., 2016). The C-rich G-poor *rut* site exists as the linear RNA, whereas the G-rich *rut* site adopts the hairpin-like structure that prevents Rho binding (Ray-Soni *et al*., 2016). To recruit Rho, NusG in the TEC prohibits the hairpin formation and interacts with Rho (Valabhoju *et al*., 2016). In addition to facilitate Rho-dependent termination, NusG also assists the coupling of translation and transcription by reacting with NusE (Burmann *et al*., 2010). NusE is known as a transcription factor and the ribosomal protein S10 (Burmann *et al*., 2010). The transcription-translation coupling can accelerate protein synthesis to support the rapid cell growth (Burmann *et al*., 2010).

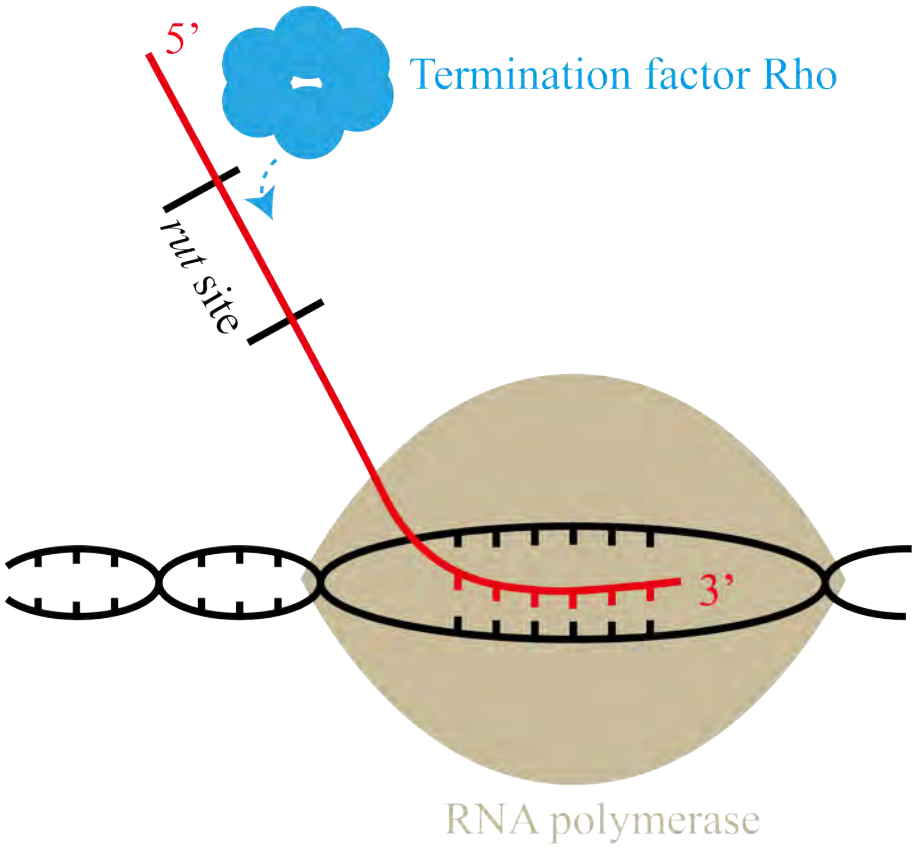

Figure 1.7 Rho-dependent termination. Rho accesses the newly made transcript *via* the *rut* site. Subsequently, Rho chases and precludes RNAP using the energy from ATP hydrolysis.

1.3 Antitermination as the regulation of gene expression

Transcription is a highly regulated step in gene expression. When a cellular protein is not urgently needed, the corresponding gene expression is stopped at the transcription level to avoid unnecessary energy expenditure (Santangelo and Artsimovitch, 2011). In some operons, the leader region contains a terminator to prevent transcription in response to any environmental change (Weisberg and Gottesman, 1999). Despite the surveillance role, this premature termination is problematic when gene expression is needed (Santangelo and Artsimovitch, 2011). To avoid the redundant premature termination, regulatory molecules attenuate the terminator or make RNAP resistant to

premature termination by a process called antitermination (Santangelo and Artsimovitch, 2011). For instance, the tryptophan biosynthesis in *B. subtilis* is normally adjusted according to the cellular tryptophan availability (Potter *et al*., 2011). In the tryptophan (*trp*) operon, the leader region contains the sequence acting as the terminator or antiterminator (Potter *et al*., 2011). When the tryptophan is required, the antiterminator preferably forms to enable transcription (Yakhnin *et al*., 2004; Figure 1.8A). Conversely, when the tryptophan is in excess, tryptophan RNA attenuation protein (TRAP) occupies the antiterminator sequence (Yakhnin *et al*., 2004). Thereby the terminator hairpin forms to prevent transcription (Yakhnin *et al*., 2004; Figure 1.8B).

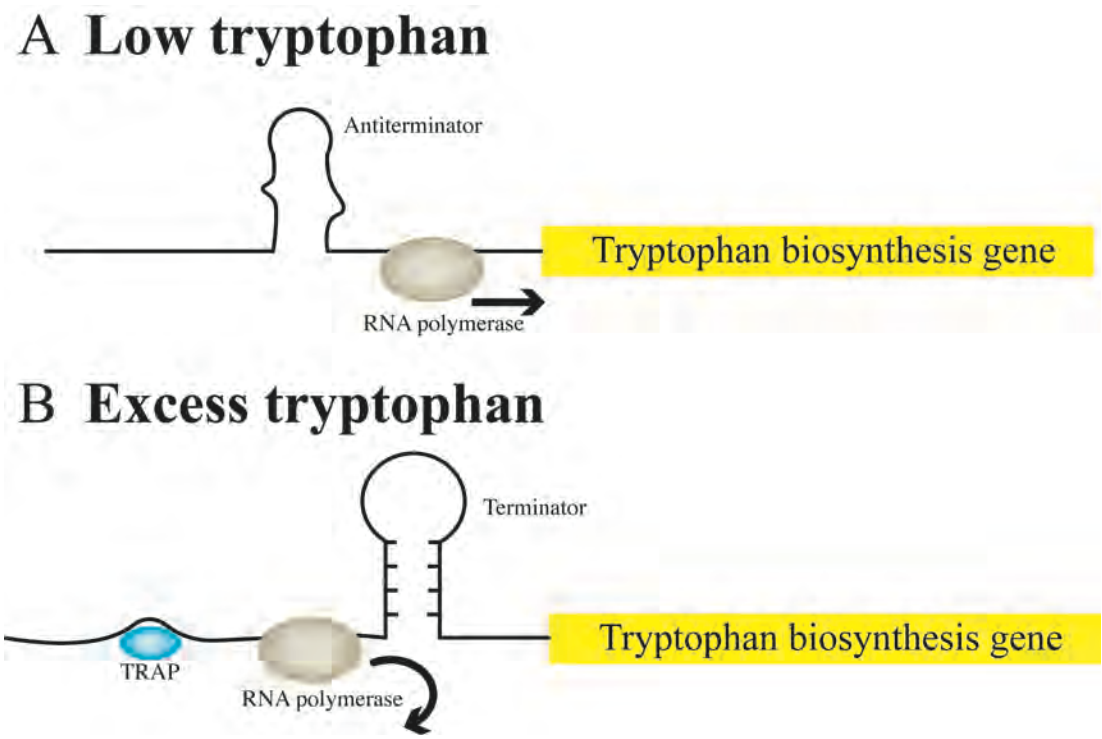

Figure 1.8 Transcription attenuation in the *B. subtilis trp* operon. **A.** At low tryptophan concentration, the antiterminator hairpin forms. **B.** At high tryptophan concentration, TRAP inhibits the antiterminator hairpin folding. Ultimately, the terminator hairpin forms to promote premature termination.

Instead of proteins, other molecules can be the regulators that suppress the terminator (Oda *et al*., 2004; Grundy *et al*., 2002; Serganov *et al*., 2004). For example, in the *E. coli trp* operon, two tandem tryptophan codons present in the leader region (Gong and Yanofsky, 2002). When the cellular tryptophan is inadequate, ribosome stalls at the tryptophan codons in the leader peptide so that the antiterminator hairpin can form (Gong and Yanofsky, 2002).

In addition to the attenuation of terminator, antitermination is also executed by rendering RNAP termination-resistant, namely the antitermination complex. (Santangelo and Artsimovitch, 2011). This type of antitermination was studied thoroughly using the model of phage λ genome transcription (Devito and Das, 1994; Rees *et al*., 1996; Yang *et al*., 1987). Phage λ infects bacteria and utilizes the bacterial transcription machinery to transcribe the phage genome. At the N-utilization (*nut*) site composed of *boxA*, *boxB,* and *boxC,* a number of bacterial transcription factors are recruited to form the antitermination complex (Das, 1992). These transcription factors are named Nus A, B, E, and G (Rees *et al*., 1996; Figure 1.9A). During the phage λ N-mediated antitermination, the host Nus factors are responsible to prevent intrinsic and Rho-dependent termination in the early and middle λ operon (Devito and Das, 1994). In the late λ operon, antitermination is usually mediated by protein Q. Protein Q is hired at the Q-utilization (*qut*) site where RNAP is stalled (Yang *et al*., 1987). The Q-RNAP-NusA complex disrupts the terminator hairpin folding and impedes Rho-dependent termination (Shi *et al*., 2019; Figure 1.9B).

Antitermination can also be mediated by the protein RfaH. RfaH enhances the gene expression of some bacterial operons (Santangelo and Artsimovitch, 2011). When operons consist of the operon polarity suppressor (*ops*) site, RfaH combines with RNAP to bypass termination (Belogurov *et al*., 2010; Figure 1.9C). In fact, RfaH occupies the RNAP β' clamp helices *via* the NTD, whereas the CTD interacts with ribosome and shields the NTD upon being recruited by the *ops* site (Belogurov *et al*., 2010).

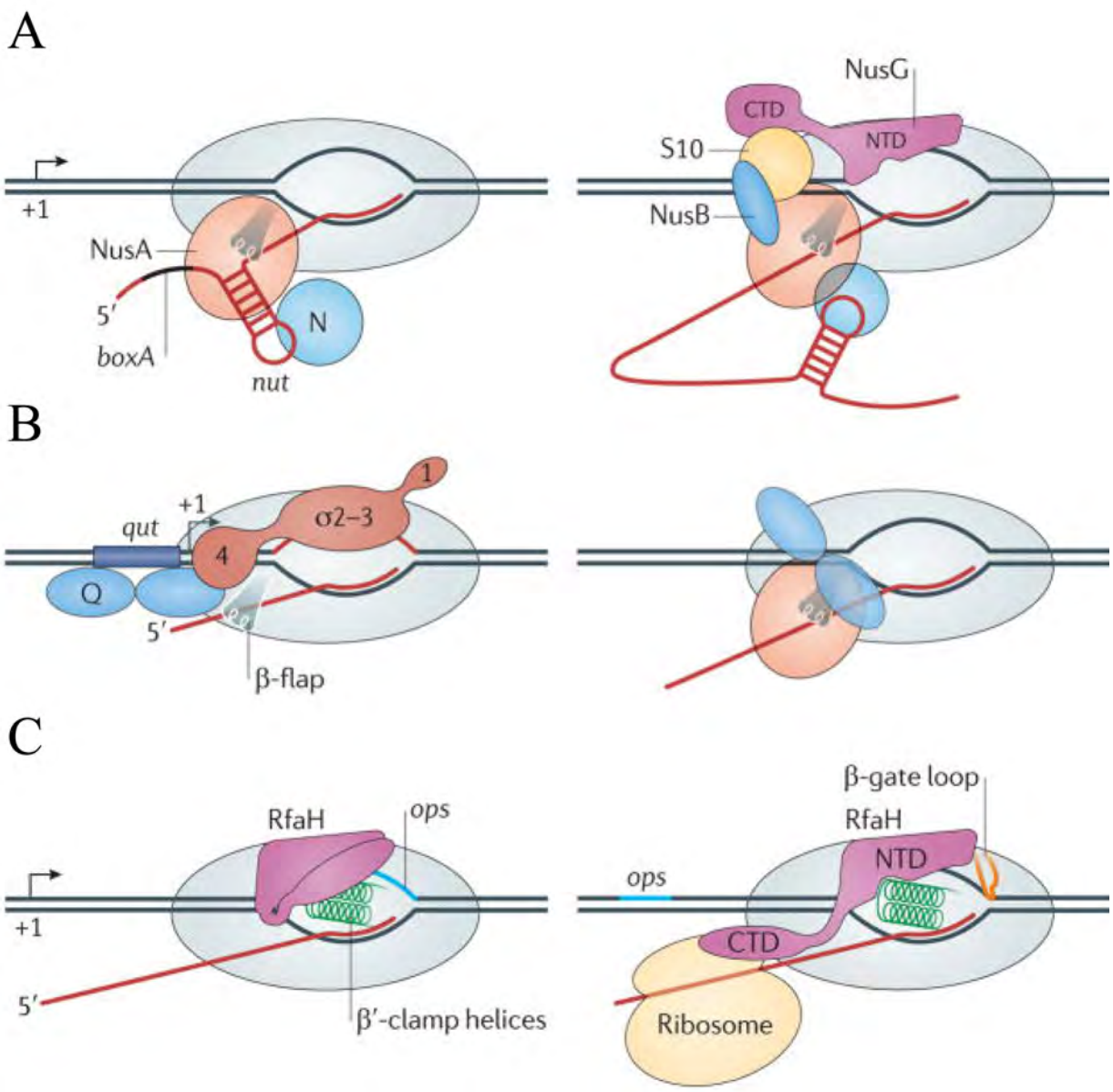

Figure 1.9 Antitermination complexes in the λ and *ops* operons. **A.** Phage λN utilizes four Nus factors to counteract the regulatory terminator in the early and middle λ operon. **B.** λ protein Q binds to the paused holoenzyme at the *qut* site. Protein Q, NusA, and RNAP form the antitermination complex in the late λ operon. **C.** RfaH coordinates antitermination in the *ops* operon. The RfaH NTD binds to the β' clamp helices, whereas the CTD interacts with ribosome to start translation. Adapted from Santangelio and Artsimovitch, 2011 with permission (Appendix IV).

1.4 Ribosomal RNA transcription for ribosome biogenesis

Ribosome biogenesis is an essential process regulated by the antitermination of rRNA (*rrn*) operons (Mayer and Grummt, 2006). Ribosome is responsible for translation in bacteria (Shajani *et al*., 2011). In the earlier studies, the components of ribosome were isolated as the small and large subunits by ultracentrifugation (Aboulhouda *et al*., 2017). The intact ribosome and the subunits were defined as the 70S, 30S, and 50S molecules described in the Svedberg unit S (Mehta *et al*., 2012; Figure 1.10).

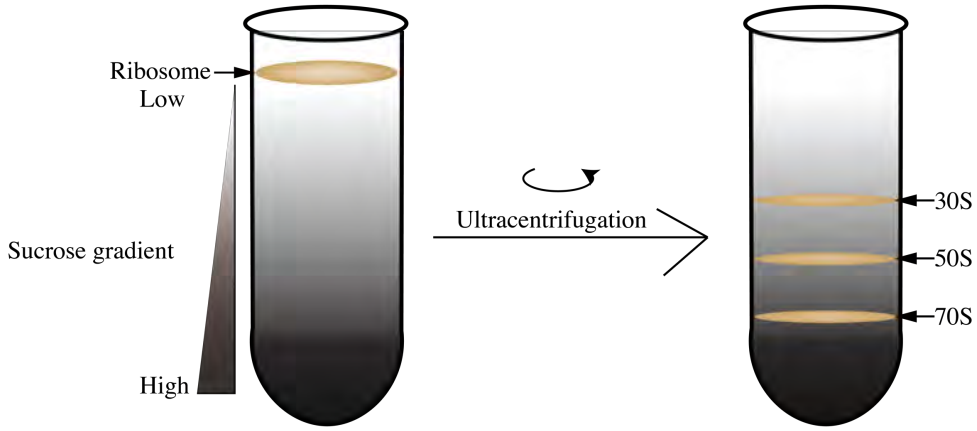

Figure 1.10 The separation of the ribosome subunits by sucrose gradient. Ultracentrifugation separates the intact ribosome and the components in different layers of the sucrose gradient. The sedimentation rates are described in the Svedberg unit S.

Bacterial ribosome is composed of small 30S and large 50S subunits (Shajani *et al*., 2011; Figure 1.11). In the 30S subunit, the 16S rRNA, and S-proteins S1-21 are identified (Shajani *et al*., 2011). The 16S rRNA serves as the biological barcode to identify unknown organisms, recognizes the ribosome binding site, and excludes the umatched tRNA (Janda *et al*., 2007; Zimmermann *et al*., 1972). The 50S subunit is formed by the 23S, 5S rRNA, and L-proteins 1-36 (Shajani *et al*., 2011). The 23S

rRNA directs the tRNA carrying an amino acid to the growing peptide chain (Bocchetta *et al.*, 1998). The 5S rRNA was previously assumed to enhance the translation elongation rate (Szymanski *et al.*, 2002).

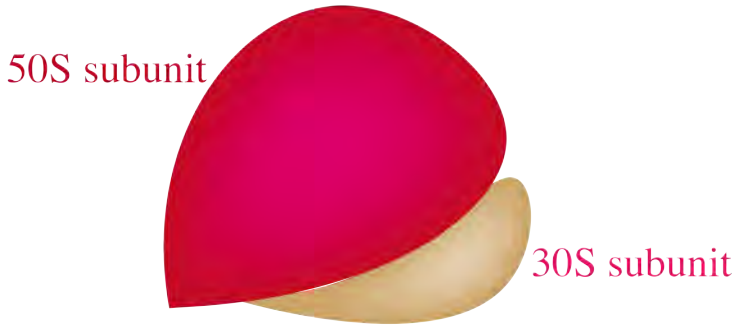

Figure 1.11 Bacterial 70S ribosome. A bacterial ribosome is composed of the small and large subunits. The 30S subunit includes the 16S RNA and S-protein. The 50S subunit is formed by the 23S rRNA, 5S rRNA and L-proteins.

1.4.1 16S, 23S and 5S rRNA transcription

In *E. coli*, rRNA transcription are carried out in seven *rrn* operons: *rrnA*, *rrnB*, *rrnC*, *rrnD*, *rrnE*, *rrnG*, and *rrnH* (Maeda *et al.*, 2015). The typical structure of the *rrn* operon is illustrated in Figure 1.12. The promoter P_1 supports rRNA transcription during the exponential growth, whereas the promoter P_2 maintains the basal level of rRNA synthesis (Maeda *et al.*, 2015). The terminators T_1 and T_2 end the synthesis (Orosz *et al.*, 1991). Antitermination occurs downstream P_2 and upstream the 23S region (Maeda *et al.*, 2015). This can enable high level of rRNA to support protein synthesis during the exponential growth phase (Maeda *et al.*, 2015; Mayer and Grummt, 2006).

In *E. coli rrn* operons, the *nut*-like region is conserved for antitermination (Berg *et al.*, 1989). The linear *boxA*, *boxB* stem-loop, and GT-rich *boxC* regions exist (Gource *et al.*, 1996). *boxA* (UGCUCUUUA) is the conserved part required for the antitermination complex assembly, whereas *boxB* and *boxC* are dispensable in *E. coli* (Berg *et al.*, 1989). At the *boxA* sequence, RNAP, Nus factors, RNA transcript and other molecules form the antitermination complex (Maeda *et al.*, 2015; Stagno *et al.*, 2011). Nevertheless, T_1 and T_2 are able to end the synthesis (Orosz *et al.*, 1991). The mechanism of how the terminators overcome antitermination is poorly understood. Notably, the T_1-T_2 cluster was previously found incapable of stopping the antitermination complex (Orosz *et al.*, 1991). Hence, the antitermination system is supposed to be disrupted by uncharacterized elements upstream T_1 and T_2. (Ghosh *et al.*, 1991; Orosz *et al.*, 1991).

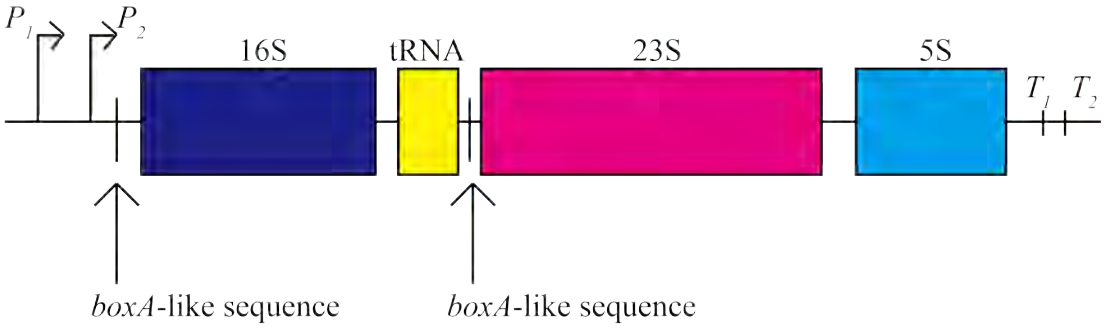

Figure 1.12 Schematic diagram of a typical *E. coli rrn* operon. Each *E. coli rrn* operon consists of the promotors P_1 and P_2, the coding sequences of the 16S, tRNA, 23S and 5S as well as the terminators T_1 and T_2. *boxA* can be found upstream the 16S and 23S regions.

A complete rRNA transcript matures following post-transcriptional modifications executed by RNase III, RNase E, RNase T and unknown nuclease (Nachtergaele and

He, 2017; Figure 1.13). First, the linkers between the components are removed, releasing the tRNA molecule, 16S and 23S rRNA with the immature ends (Nachtergaele and He, 2017; Figure 1.13). RNase E, RNase T and unknown nuclease further restrict these ends, resulting in the mature rRNA as the primary part of ribosome (Shajani *et al*., 2011; Figure 1.13).

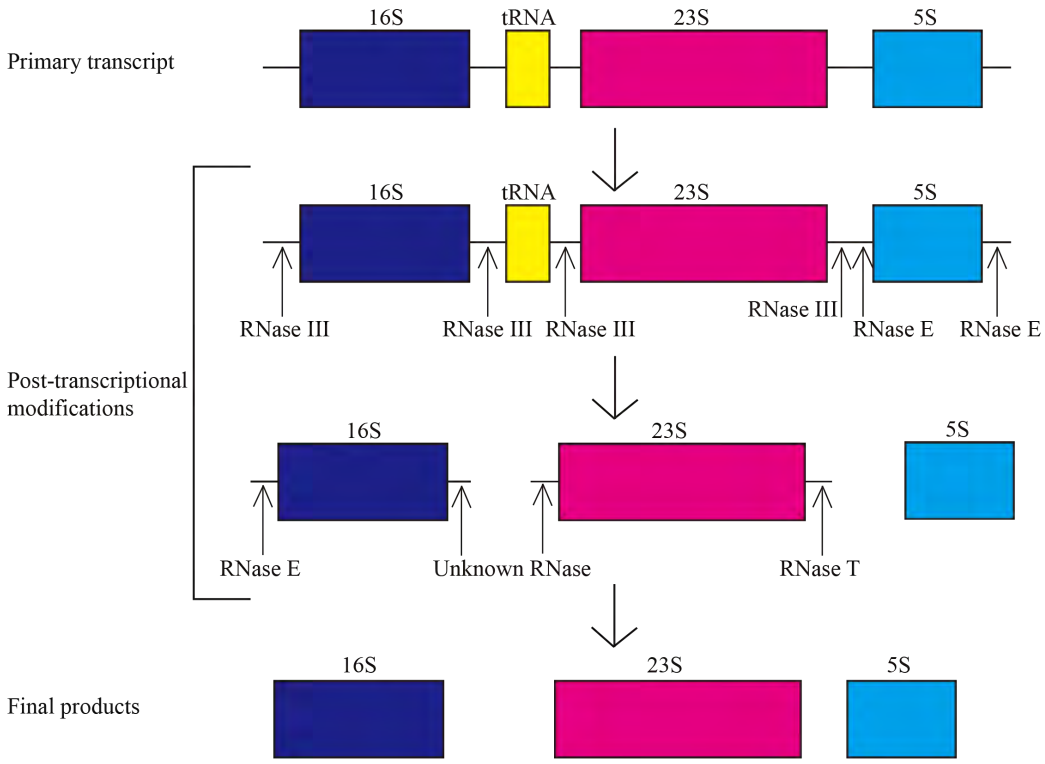

Figure 1.13 rRNA maturation by splicing. The primary transcript is subjected to the cleavages by RNase III, RNase E, RNase T and unknown nuclease. The recognition sites of the nucleases are indicated by the black arrows.

1.4.2 Transcription factor NusB in transcribing the 16S, 23S and 5S rRNA

The interaction between the Nus factors and RNAP has been thoroughly investigated by a number of studies (Santangelo and Artsimovitch, 2011). To form the antitermination complex, NusB dimerizes with NusE for recognizing the conserved *boxA* sequence (Santangelo and Artsimovitch, 2011). Following the interaction between the NusB-NusE-RNA complex and the TEC, the antitermination complex forms (Luo *et al*., 2008; Stagno *et al*., 2011; Krupp *et al*., 2019). Among the four Nus factors, NusB is the central mediator for *rrn* antitermination (Altieri *et al*., 2000). A number of previous studies showed the NusB protein structures include merely α-helices in *E. coli*, *Mycobacterum tuberculosis,* and *Thermotoga maritima*, suggesting a universal antitermination system (Altieri *et al*., 2000; Gopal, 2000; Bonin *et al*., 2004; Stagno *et al*, 2011; Figure 1.14; Figure 1.15).

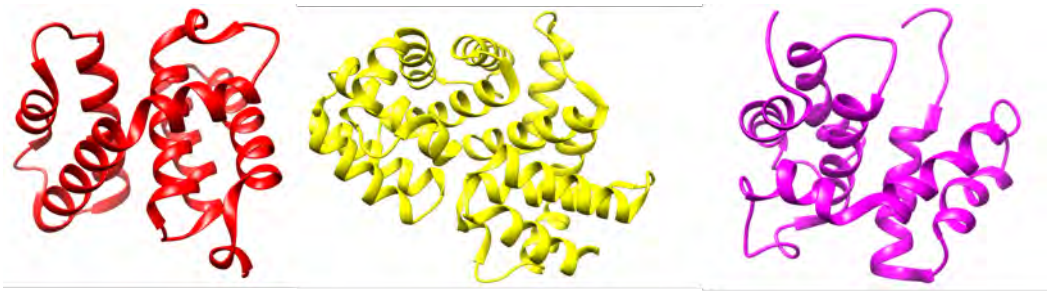

T. maritima NusB | *M. tuberculosis* NusB | *E. coli* NusB

Figure 1.14 The crystal structures of NusB from *T. maritima* (PDB ID: 1TZU), *M. tuberculosis* (PDB ID: 1EYV) and *E. coli* (PDB ID: 1EY1). *M. tuberculosis* NusB exists as the homodimer in crystal and solution at 18-120μM, whereas *T. maritima* and *E. coli* NusB exists as the monomer in solution and crystals.

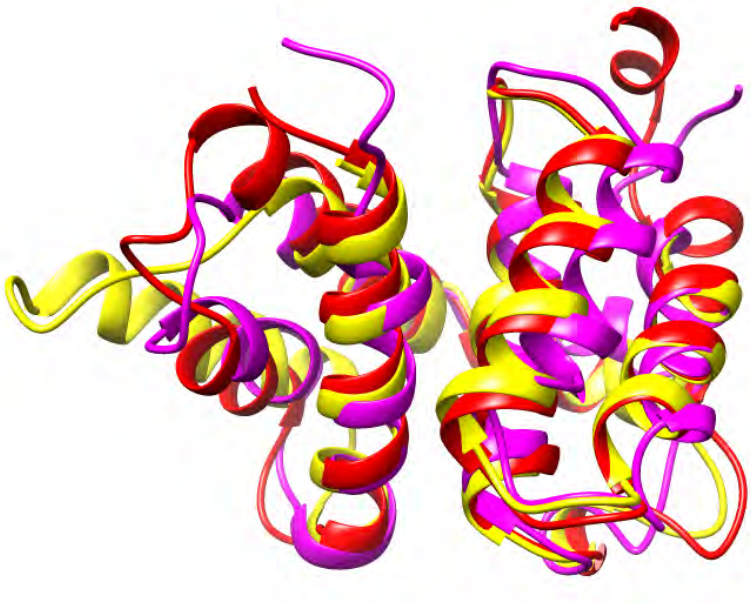

Figure 1.15 The structural alignment of the homologous NusB from *T. maritima* (PDB ID: 1TZU), *M. tuberculosis* (PDB ID: 1EYV) and *E. coli* (PDB ID: 1EY1).

The essentiality of NusB in the bacterial rRNA transcription was advocated by earlier mutational studies (Friedman and Baumann, 1976; Sharrock *et al*., 1985). The point mutation Y18D in NusB is correlated to premature termination in the *rrn* operons (Friedman and Baumann, 1976; Sharrock *et al*., 1985). In fact, the Y18 residue contributes to the structural integrity through hydrophobic interactions with V80 and Q79 (Altieri *et al*., 2000; Figure 1.16). The point mutation Y18D destroys the hydrophobic interactions (Altieri *et al*., 2000). Eventually the protein structure is collapsed, abolishing the biological function.

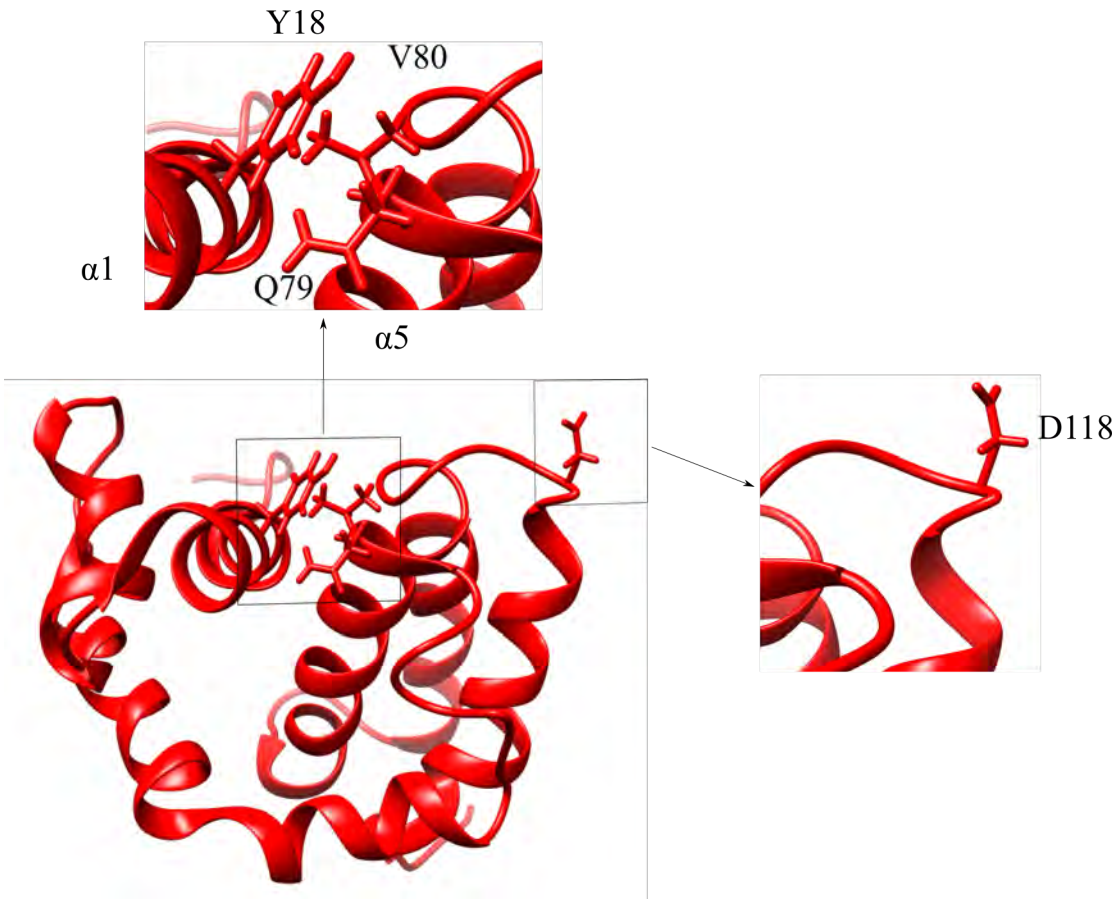

Figure 1.16 The NMR solution structure of *E. coli* NusB (PDB ID: 1EY1). The Y18 residue is in hydrophobic interactions with Q79 and V80 at the α5, contributing to the structural integrity, whereas D118 locates at the loop region contacted for RNA binding.

In the first regulatory step of the antitermination complex assembly, NusB and NusE form the heterodimer. NusE is a protein with dual functions in transcription and translation (Stagno *et al.*, 2011). In transcription, NusE participates in the antitermination complex assembly in the *rrn* operons (Burmann and Rösch, 2011). Additionally, NusE is known as ribosomal protein S10 as a part of the ribosome for translation (Friedman *et al.*, 1981). Prior crystallographic investigations disclosed the importance of the NusB-NusE interaction (Luo *et al.*, 2008; Stagno *et al.*, 2011). During the NusB-NusE heterodimer formation, the NusE NTD contacts NusB and triggers the confirmational change in NusB (Luo *et al.*, 2008; Figure 1.17A). This

conformational change eventually causes the NusB E75 residue to be interacting with the NusE R16 residue (Luo *et al*., 2008; Figure 1.17B). Since the NusE NTD is the part inserted into ribosome, suggesting NusE cannot function in translation while interacting with NusB for *rrn* antitermination (Luo *et al*., 2008). Although the NusB-NusE-*boxA* RNA complex is supposed to form, the monomers of NusB and NusE exhibit mild affinities to the *boxA* RNA (Das *et al*., 2008). In contrast, the NusB-NusE heterodimer demonstrated 10-folded increased affinity to *boxA* compared to the monomers in the previous biophysical study (Das *et al*., 2008). To characterize the NusB-NusE-RNA complex in atomic detail, a recent crystallographic investigation was conducted on *Aquifex aeolicus* NusB and NusE (Stagno *et al*., 2011). In both *E. coli* and *A. aeolicus*, NusB and NusE are shown to interact through hydrophobic and electrostatic interactions (Stagno *et al*., 2011). This similarity suggests the conserved interaction mode and thus the conserved antitermination mechanism (Stagno *et al*., 2011; Luo *et al*., 2008). Additionally, The NusB-NusE dimer is found to interact with *boxA* (GGCUCCUUG) and the duplex RNA (Stagno *et al*., 2011). Since *boxB* exists as a stem-loop that resembles the duplex RNA, the NusB-NusE-*boxB* interaction is suggested (Stagno *et al*., 2011).

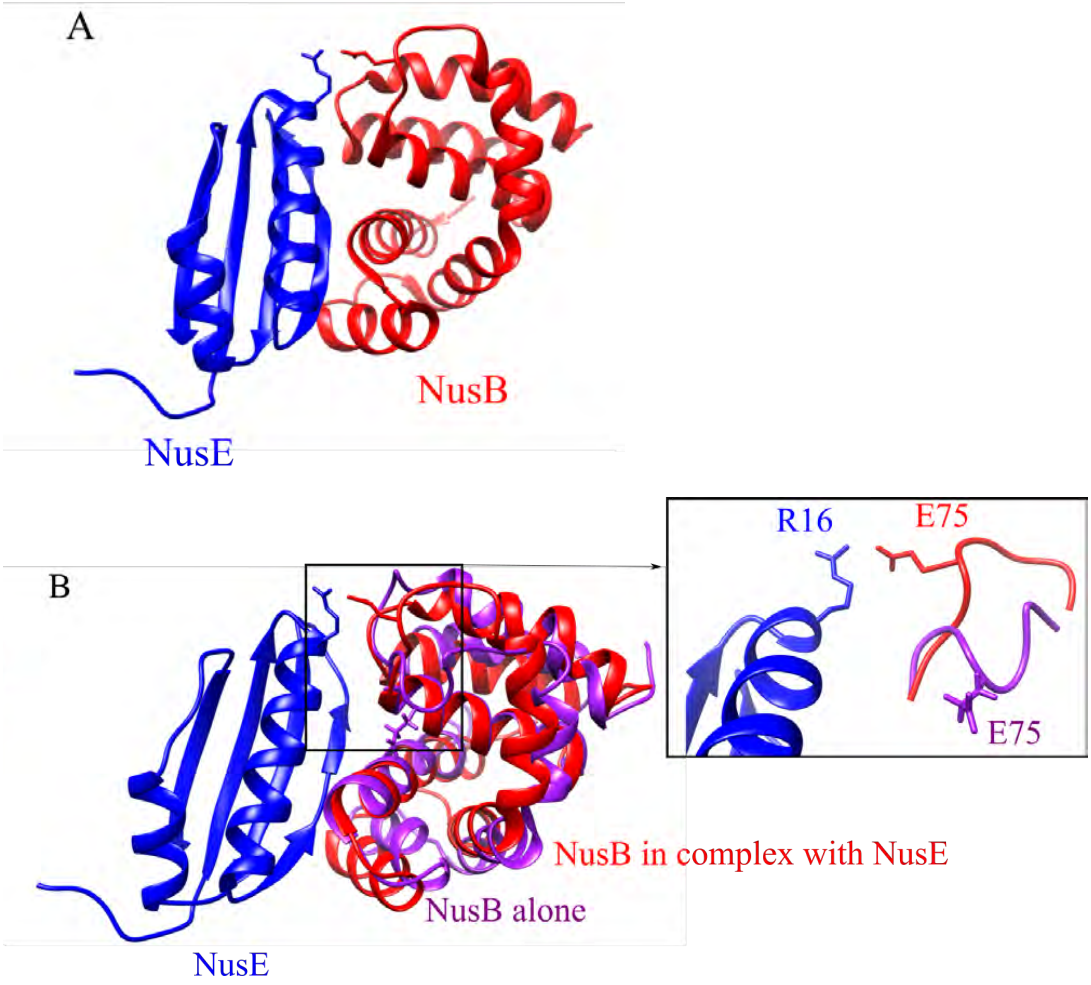

Figure 1.17 A. The *E. coli* NusB-NusE complex crystal structure (PDB ID: 3D3B). **B.** The structural alignment of the free NusB (PDB ID:1EY1) and NusB in complex with NusE (PDB ID: 3D3B), The NusB local induced fit is triggered upon NusE binding, placing the E75 residue near to R16 in NusE.

The essentiality of the NusB-NusE interaction in rRNA transcription was previously established by a number of mutational studies (Sharrock *et al*., 1985; Ward *et al*., 1983). The point mutation A86D in NusE was associated to premature termination in the *rrn* operons, whereas this defective antitermination can be rescued by the gain-of-function mutation D118N in NusB (Sharrock *et al*., 1985; Ward *et al*., 1983). In fact, the D118 residue of NusB presents in the loop region where the mutation does not influence the

protein folding (Altieri *et al*., 2000; Figure 1.16). The substitution by the positively charged amino acid can strengthen electrostatic interaction with the negatively charged RNA (Altieri *et al*., 2000). Hence, the proper NusB-NusE-RNA interaction is needed for the normal rRNA transcription.

The NusB-NusE-RNA complex contacts the TEC to form the antitermination complex (Burmann *et al*., 2010). The interaction between the NusB-NusE-RNA complex and the TEC was examined by recent structural studies (Said *et al*., 2017; Krupp *et al*., 2019). In the NusB-NusE-RNA complex, NusE interacts with NusA in the TEC while NusG in the TEC stabilizes the antitermination complex. (Krupp *et al*., 2019; Figure 1.18). With other molecules, four Nus factors render RNAP termination-resistant (Krupp *et al*., 2019). The antitermination complex enables a complete rRNA transcript, rRNA maturation, and ribosome assembly (Said *et al*., 2017).

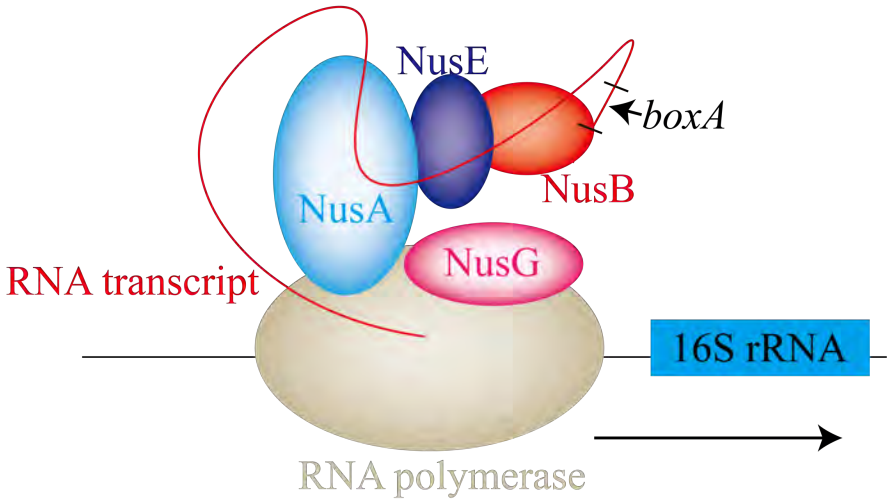

Figure 1.18. The *rrn* antitermination complex. The NusB-NusE heterodimer are recruited to *boxA*. The resulting NusB-NusE-RNA complex contacts NusA in the TEC to form the antitermination complex.

1.4.3 Other regulators in rrn antitermination

An increasing number of recent studies purposed other cellular molecules involved in the *rrn* antitermination (Squires *et al*., 1993; Singh *et al*., 2016; Torres *et al*., 2001; Grinwald and Ron 2013). In the earlier study, RNAP and the four Nus factors were purified to transcribe a DNA template *in vitro* (Squires *et al*., 1993). Although RNAP, Nus factors and the *nut* site presented, premature termination was detected at the Rho-terminator site (Squires *et al*., 1993). The production of full transcript was only observed when cell lysate was added to the reaction mixture (Squires *et al*., 1993). This suggests some other cellular molecules are indispensable for bypassing the Rho-terminator (Squires *et al*., 1993). Recent studies have found that the conserved innositol phosphatase SuhB, the ribosomal protein S4 and the heat shock protein YbeY function in *rrn* antitermination (Singh *et al*., 2016; Dudenhoeffer *et al*., 2019; Torres *et al*., 2001; Grinwald and Ron 2013). For example, SuhB is recruited to the *nut* region and in complex with RNAP and NusA throughout rRNA transcription (Singh *et al*., 2016; Dudenhoeffer *et al*., 2019).

1.5 NusB-NusE PPI as a novel drug target leading to new antimicrobial candidates

rRNA transcription is highly regulated at different stages of bacterial growth (Mayer and Grummt, 2006). During the exponential phase, ribosome synthesis is upregulated to support the demand for protein synthesis, whereas the ribosome synthesis is prohibited at the stationary phase (Mayer and Grummt, 2006). This adjustment in the ribosome production is referred as the grow-dependent regulation, suggesting the

association between the ribosome and cell viability (Dennis *et al*., 2004). Thus, ribosome biogenesis is estimated to be a druggable target. During ribosome biogenesis, rRNA transcription is the rate-limiting step, during which the formation of the NusB-NusE heterodimer represents the first regulatory step (Neben *et al*., 2017; Ma *et al*., 2016). Additionally, suboptimal cell growth occurs when the *nusB* gene is mutated (Dennis *et al*., 2004; Sharrock *et al*., 1985). This suggests the NusB-NusE interaction could be a novel drug target.

By rational design targeting the NusB-NusE interaction, a lead compound MC4 was selected (Yang *et al*., 2017; Figure 1.19). In antibiotic susceptibility test, MC4 exhibited antibacterial activity against *Staphylococcus aureus* strains including methicillin-resistant *S. aureus* (MRSA) (Yang *et al*., 2017). In addition to the antimicrobial activity, MC4 was demonstrated to specifically interact with *B. subtilis* NusB and to reduce the RNA content in the MC4-treated *S. aureus* 25923 (Yang *et al*., 2017). Although there was a decline, this does not fully explain how MC4 suppressed the bacterial rRNA transcription.

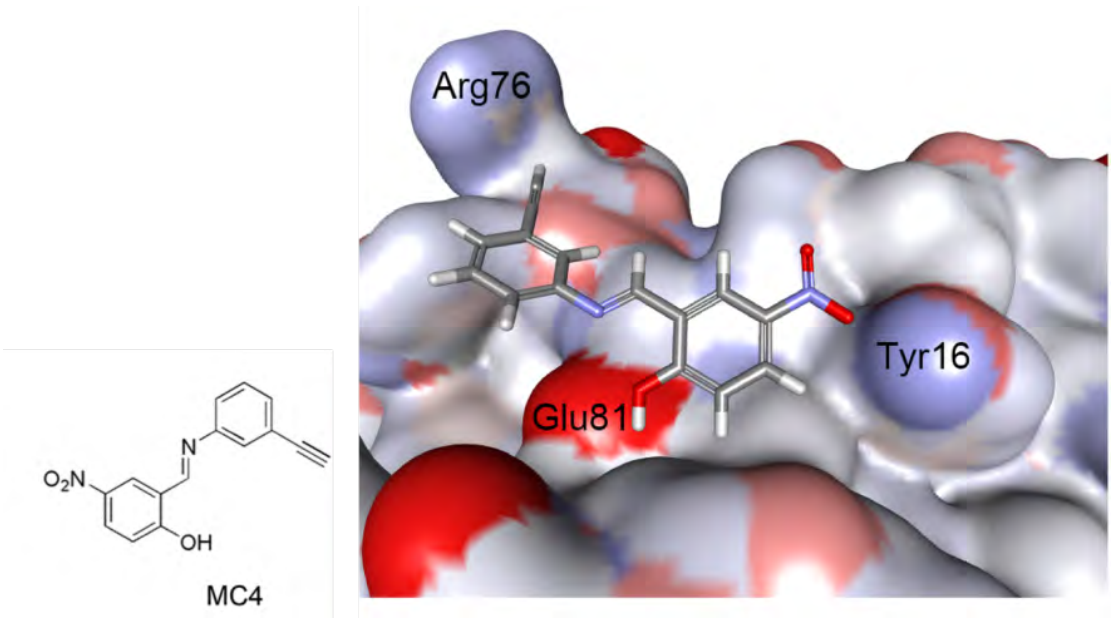

Figure 1.19 The chemical structure of MC4 (left) and the molecules docked into the buried surface of the NusB crystal structure (right). MC4 is deigned to interact with E81, Y16 and R76 in NusB. Adapted from Yang *et al*., 2017.

For improved antimicrobial activity, a group of MC4 derivatives were synthesized, namely nusbiarylins (Qiu *et al*., 2019; Figure 1.24). When *S. aureus* was treated with nusbiarylins at a lethal dose, the bactericidal effect was observed within 24 hours and the ATP production was drastically impaired (Qiu *et al*., 2019). However, the molecular mechanism of how nusbiarylins act on NusB and transcription is not fully established.

1.6 Aim and hypothesis

The interaction between bacterial transcription factors NusB and NusE is hypothesized to represents a novel target for antibiotics. The present study aims to characterize the action of nusbiarylins on NusB using biochemical, cell-based and structural approaches. The research consists of three objectives.

First, the novel *in vitro* protein-fragment complementation assay (PCA) for PPI inhibitor screening was developed. Based on a split luciferase system called NanoLuc™ (Promega, USA), a PCA plasmid system was constructed for tagging PPI pairs with the NanoLuc fragments and 6 x His tag. The *in vitro* assay was used to quantifiy PPI when two NanoLuc fragments combined as a functional luciferase during the PPI. Also, The effect of PPI inhibitors was quantified because the inhibitors blocked the PPI and thus the luciferase reconstitution. To validate the assay, two essential PPIs in bacterial transcription: NusB-NusE and RNAP-σ^A were studied. Using the PCA plasmid system, the protein overproduction plasmids of NusB, NusE, the RNAP clamp helix (CH) fragment and σ^A were made. The recombinant proteins were purified and tested for luminescence emission. The assay was further applied to characterized the previously discovered PPI inhibitors of NusB-NusE and RNAP-σ^A (Yang *et al*., 2017; Yang *et al*., 2015). Compared to the previous studies, the PPI inhibitory effects were similarly quantified by the *in vitro* NanoLuc PCA. This suggests the potential application of the *in vitro* NanoLuc PCA in screening for PPI inhibitors in early drug discovery.

Second, the reporter strains were generated to confirm the suppression of nusbiarylins on the bacterial rRNA transcription. The reporter strain constructions were performed by introducing a reporter plasmid to *E. coli* and *B. subtilis*. The *E. coli* reporter strains were generated to express the reporter gene *chloramphenicol acetyltransferase* (*cat*) under the control of *E. coli rrnG* promoter P_2. The reporter gene expression was regulated by the *nut* site and the Rho-terminator downstream P_2. To extend the

investigation to Gram-positive bacteria, the *B. subtilis* reporter strain was generated to express the reporter gene *nanoLuc* upon xylose induction. The present study suggested the use of reporter strains to characterize the transcription-suppressing effect of nusbiarylins. Also, the non-radioactive detection was found feasible to inspect the reporter gene expression using the *E. coli* reporter strain generated in the study.

Third, a crystallographic approach was carried out to confirm the NusB-nusbiarylins interaction mode. *Thermotoga maritima* NusB was purified and crystallized with nusbiarylins. The resulting crystals were used in X-ray diffraction but the nusbiarylin molecules were not identified in the collected dataset. Prior to repeating the crystallization, the formation of NusB-nusbiarylin complex will be examined by other means like mass spectrometry.

Chapter 2: Materials and Methods

2.1 Plasmids and bacterial strains

The plasmids and strains used in this study are shown in Table 2.1. All cloning experiments were performed in *E. coli* DH5α. The following bacteria strains were used in this study for the microdilution assay: *Enterococcus casseliflavus* 25788, *Staphylococcus epidermidis* 12228, *Staphylococcus saprophyticus* 15305, *Streptococcus pneumonia* 49619, *Streptococcus pyogenes* 19615, *Streptococcus agalactiae* 12386, and *S. aureus* ATCC 25923, ATCC 29213, ST239, ATCC BAA-43, ATCC BAA-44, HA W-231 ST45, CA W-47 ST30, CA W-45 ST59, CA W-46 ST59, USA 300, ST22, CA W-4 ST338, CA W-48 ST217, HA W-235 ST5.

Table 2.1 Plasmids and strains used in the study

Plasmids	**Genotype**	**Source/construction**
Cloning vectors / genome DNA		
pETMCSIII	*bla* $P_{\varphi 10}$-*6×His*-T_{φ}	Neylon *et al*., 2000. N-terminal his-tagging vector.
pET51b(+)_S-Luc_CLIP	*bla* $P_{\phi 10}$-*nanoLuc-CLIP*-T_{ϕ}	Hiblot *et al*., 2017
pNG209	*bla* $P_{\varphi 10}$-*6×His*-T_{φ}	Yang *et al*., 2009. C-terminal his-tagging vector.
pNG130	*bla* $P_{\varphi 10}$-*6×His-bsubnusB*-T_{φ}	Yang *et al*., 2017.
pNG134	*bla* $P_{\varphi 10}$-*6×His-bsubnusE*-T_{φ}	Yang *et al*., 2017
pNG590	*bla* $P_{\varphi 10}$-*6×His-sigA-Tφ*	Johnston *et al*., 2009
pNG908	*bla* $P_{\varphi 10}$-*rpoC (aa220-*	Ma *et al*., 2013

	315) -PKA-3C-GST-T_{φ}	
T. maritima MSB8 genome DNA	-	ATCC
NanoLuc PCA plasmids		
Commercial plasmids		
pBiT1.1-N[TK/LgBit]	*bla $P_{HSV\text{-}TK}$ - LgBiT - linker- polyA*	Promega
pBiT2.1-N[TK/SmBiT]	*bla $P_{HSV\text{-}TK}$- SmBiT - linker –polyA*	Promega
pBiT1.1-C [TK/LgBiT]	*bla $P_{HSV\text{-}TK}$- linker -LgBiT-polyA*	Promega
pBiT2.1-C [TK/SmBiT]	*bla $P_{HSV\text{-}TK}$-linker - SmBiT-polyA*	Promega
Cloning vectors		
pCU179	*bla $P_{\varphi 10}$-6×His-LgBiT-linker-T_{φ}*	Tsang *et al*., 2019. For N-terminal LgBiT and his-tagging.
pCU180	*bla $P_{\varphi 10}$-6×His-SmBiT-linker-T_{φ}*	Tsang *et al*., 2019. For N-terminal SmBiT and his-tagging.
pCU197	*bla $P_{\varphi 10}$-6×His-MCS –Lg/SmBiTLinker-T_{φ}*	Tsang *et al*., 2019
pCU198	*bla $P_{\varphi 10}$-MCS-C-hislinker -T_{φ}*	Tsang *et al*., 2019
pCU199	*bla $P_{\varphi 10}$-6×His-linker-SmBiT-T_{φ}*	Tsang *et al*., 2019. For C-terminal SmBiT and N-terminal his-tagging
pCU200	*bla $P_{\varphi 10}$-6×His-linker-LgBiT-T_{φ}*	Tsang *et al*., 2019. For C-terminal LgBiT and N-terminal his-tagging.
pCU201	*bla $P_{\varphi 10}$-SmBiT-linker-*	Tsang *et al*., 2019. For N-

	6×His-T_{φ}	terminal SmBiT and C-terminal his-tagging
pCU202	*bla $P_{\varphi 10}$-LgBiT-linker-6×His-T_{φ}*	Tsang *et al*., 2019. For N-terminal LgBiT and C-terminal his-tagging.
pCU203	*bla $P_{\varphi 10}$-linker-SmBiT-6×His-T_{φ}*	Tsang *et al*., 2019. For C-terminal SmBiT and his-tagging.
pCU204	*bla $P_{\varphi 10}$-linker-LgBiT-6×His-T_{φ}*	Tsang *et al*., 2019. For C-terminal LgBiT and his-tagging.
NanoLuc PCA protein overproduction plasmids		
NusB and NusE		
pCU231	*bla $P_{\varphi 10}$-6×His-SmBiT-bsubnusB-T_{φ}*	Tsang *et al*., 2019
pCU235	*bla $P_{\varphi 10}$-LgBiT-bsubnusE-6×His-T_{φ}*	Tsang *et al*., 2019
pCU236	*bla $P_{\varphi 10}$-bsubnusE-LgBiT-6×His-T_{φ}*	Tsang *et al*., 2019
pCU246	*bla $P_{\varphi 10}$-SmBiT-bsubnusE -6×His-T_{φ}*	Tsang *et al*., 2019
pCU247	*bla $P_{\varphi 10}$-bsubnusE-SmBiT-6×His-T_{φ}*	Tsang *et al*., 2019
pCU250	*bla $P_{\varphi 10}$-LgBiT-bsubnusB-6×His-T_{φ}*	Tsang *et al*., 2019
σ^A and RNAP		
pCU242	*bla $P_{\varphi 10}$-sigA-SmBiT-6×His -T_{φ}*	Tsang *et al*., 2019
pCU244	*bla $P_{\varphi 10}$-LgBiT-rpoC(aa220- 315)-6×His-*	Tsang *et al*., 2019

	T_{φ}	
pCU245	*bla* $P_{\varphi 10}$*-rpoC(aa220-315)-LgBiT-6×His-*T_{φ}	Tsang *et al*., 2019
pCU251	*bla* $P_{\varphi 10}$*-sigA-LgBiT-6×His -*T_{φ}	Tsang *et al*., 2019
pCU252	*bla* $P_{\varphi 10}$*-SmBiT-rpoC(aa220- 315)-6×His-*T_{φ}	Tsang *et al*., 2019
pCU253	*bla* $P_{\varphi 10}$*-rpoC(aa220-315)-SmBiT-6×His-*T_{φ}	Tsang *et al*., 2019
Reporter plasmids		
pSG1729	*bla amyE3' spc Pxyl – gfpmut1' amyE5'*	Lewis & Marston, 1999
pSL102	*bla* P_2*-cat-*T_1T_2	Li *et al*., 1984
pSL103	*bla* P_2*-*T_{16S}*-cat-*T_1T_2	Li *et al*., 1984
pSL115	*bla* P_2*-AT-*T_{16S}*-cat-*T_1T_2	Li *et al*., 1984
pCU314	*bla amyE3' spc Pxyl – nanoLuc amyE5'*	This work. The *nanoLuc* gene cloned into the *Acc65*I and *EcoR*I sites of pSG1729.
Protein overproduction plasmid		
pCU173	*bla* $P_{\varphi 10}$*-tmanusB-*T_{φ}	This work. The *tmanusB* gene cloned into the *Nde*I-*Acc65*I sites of pNG209.
Strains		
E. coli		
DH5α	*F- endA1 hsdR17 supE44 thi-1 λ- recA1 gyrA96 relA1 Δ(lacZYA-*	Gibco BRL

	argF)U169 φ 80 dlacZ ΔM15	
BL21	*F- ompT gal dcm lon hsdSB(rB- mB-) λDE3 pLysS (cmR)*	Studier *et al*., 1986
C41	*fhuA2 [lon] ompT gal (λ DE3) [dcm] ΔhsdS/ pLemo(CamR) λ DE3*	NEB
B. subtilis		
168	*trpC2*	Laboratory stock
BS2019	*trpC2 chr*::pCU314 (*spc Pxyl – nanoLuc*)	This work. *B. subtilis* 168 transformed with pCU314

spc: spectinomycin resistance gene. *bla*: ampicillin resistance gene, *cat*: chloramphenicol resistance gene. P_2: *E. coli rrnG* promoter P_2. P_{xyl}: xylose-inducible promoter. $P_{\phi 10}$: phage T7 promoter. $P_{HSV\text{-}TK}$: Herpes simplex virus (HSV) thymidine kinase (tk) promoter. T_ϕ: T7 transcription terminator. T_{16S}: *E. coli* 16S terminator. T_1T_2: *E. coli rrnG* terminator. *AT*: *E. coli rrnG* antiterminator.

2.2 Growth media

Growth media compositions and antibiotics are listed in Appendix I.

E. coli and *B. subtilis* strains were grown on Luria-Bertani (LB) agar supplemented with the appropriate antibiotics at 37^{o}C overnight.

2.2.1 Liquid media

For plasmids purification, *E. coli* DH5α single colonies were inoculated into 5 mL LB media supplemented with appropriate antibiotics and incubated at 37^{o}C for 16 hours with vigorous shaking at 180 rpm.

For RNA extraction, *E. coli* single colonies were inoculated into LB media at optical density at 600 nm (OD_{600}) equal to 0.04, supplemented with 100 μg/mL ampicillin and grown at 37^{o}C with vigorous shaking at 180 rpm until OD_{600} equal to 0.6.

2.3 Bacterial stocks

Transformed *E. coli* DH5α cells were plated on the LB agar supplemented with antibiotics, incubated at 37^{o}C overnight. The colonies were mixed with 1 mL 50% (v/v) glycerol broth, stored at -80^{o}C as a permanent stock.

2.4 Genetic manipulations

2.4.1 Polymerase chain reactions (PCR)

50 μL PCR reactions were prepared on ice and conducted in a T100™ thermocycler (Bio-Rad). Primers (Table 2.2) were synthesized by Invitrogen.

PCR reactions included the following:

2X Accuzyme mix (Bioline)	25 μL
5 μM forward primer	2 μL
5 μM reverse primer	2 μL
Plasmid DNA	1 μL
Distilled H_2O	20 μL

The PCR cycles contained the following:

Hot Start	95 ^oC	3 minutes
Denaturation	95 ^oC	30 seconds
Annealing	50 ^oC	30 seconds
Extension	72 ^oC	1 minute / 1 kb
Final Extension	72 ^oC	12 minutes
Storage	12 ^oC	

To screen for the positive clone, colony PCR was performed. Individual colonies were mixed with 20 μL PCR reactions, and empty vector was used as negative control.

The PCR screening reactions were as follows:

2X SapphireAmp fast PCR master mix (Takara)	10 μL
5 μM forward Primer	0.8 μL
5 μM reverse Primer	0.8 μL
Distilled H_2O	8.4 μL

The fast PCR cycles were as follows:

Hot Start	94 ^{o}C	1 minute
Denaturation	98 ^{o}C	5 seconds
Annealing	55 ^{o}C	5 seconds
Extension	72 ^{o}C	10 seconds / 1 kb
Storage	12 ^{o}C	

Table 2.2 Oliogonulceotides used in the study

Names	**Sequences (5' – 3')**	**Restriction sites**
NanoLuc cloning vectors		
N_smbit_F	TGGTAAAGCCCATATGGTCTTCACACTC	*Nde*I
N_lg/smbit_R	AGCGGCCCCATGGGGTACCTCTAGAAGATCTGCTAG	*Nco*I
N_lgbit_F	GGTAAAGCCCATATGGTGACCGGCTACC	*Nde*I
C_lg/smbit_1	TATGTCTAGAGGTACCCCATGGGGGCCCTAA	*Nde*I, *Xba*I, *Acc65*I, *Nco*I, *Apa*I, Stop codon
C_lg/smbit_2	CATGTTAGGGCCCCCATGGGGTACCTCTAGACA	*Nde*I, *Xba*I, *Acc65*I, *Nco*I,

		*Apa*I, Stop codon
C_lg/smbit_F	GCTAGCGCCATGGTAAGTGGGAGCTCAGG	*Nco*I
C_smbit_R	TAATCGGGGCCCCAGAATCTCCTCGAACAGC	*Apa*I
C_lgbit_R	CGATTAGGGCCCACTGTTGATGGTCGTTAC	*Apa*I
C_hislinker_1	TATGCCATGGGGGCCCCACCATCACCATCACCATTAA	*Nde*I, *Nco*I, *Apa*I, *6x his*, Stop codon
C_hislinker_2	CATGTTAATGGTGATGGTGATGGTGGGGCCCCCATGGCA	*Nde*I, *Nco*I, *Apa*I, *6x his*, Stop codon
NusB and NusE primers		
Bsub_nusB_F	CGGCGAGAATTCAGTCATGAAAAGAAG	*EcoR*I
Bsub_nusB_R	TCAGTTAGGGTACCTGATTGTCCAATATC	*Acc65*I
N_nusE_F	GGCTAATCGAATTCAGTCATGGCAAAAC	*EcoR*I
C_nusE_F	GGCTAATCGGTACCATGGCAAAAC	*Acc65*I
N_nusE_R	TGTACGAGGGTACCAAGTTTAATTTCG	*Acc65*I
C_nusE_R	TGTACGAGGAATTCAAGTTTAATTTCG	*EcoR*I

σ^A and RNA polymerase primer		
sigA_F	GTTCACTGGGTACCATGGCTGATAAACAAAC	*Acc65*I
sigA_R	CAGAGTCGAATTCCCTTCAAGGAAATCTTTC	*EcoR*I
N_CH_F	GTCTTGAGAATTCAGTCGGAAACAAGCC	*EcoR*I
C_CH_F	GCACTTCAGGTACCGGAAACAAGCC	*Acc65*I
N_CH_R	GGTACTCCGGTACCAGATTTTAACGG	*Acc65*I
C_CH_R	CAGAGTCGAATTCCCAGATTTTAACGG	*EcoR*I
NanoLuc reporter primers		
nlucF	ACAGGTCGGTACCATGGTCTTCACACTC	*Acc65*I
nlucR	ACAAAGTGAATTCTTACGCCAGAATGCGTTC	*EcoR*I
TmaNusB primers		
Tma_nusB_F	GAGGAGAAATTACATATGAAAACACCGAGGCGAAGAATG	*Nde*I
Tma_nusB_R	ATTCGTATAGGTACCTCAAAGTTCGAATTTTTCTTTTGGAGC	*Acc65*I
Sequencing primers		
PET_F	CGACTCACTATAGGGAGACCACAAC	
PET_R	GGGTTATGCTAGTTATTGCTCAG	

2.4.2 Agarose gel electrophoresis

1% (w/v) DNA agarose gels were made using the agarose powder (Lonza) melted in 1X TBE buffer with SYBR™ Safe DNA Gel Stain (NEB) added. 0.5 µL 100 bp ladder (NEB) and 2 µL PCR products in 6X loading dye (NEB) were loaded onto the gel. The run was started in 1X TBE buffer under 135 V for 25 minutes. The DNA bands were visualized using a Gel Documentation System (Bio-Rad).

2.4.3 PCR product purification

PCR clean-up and gel purification were performed using the Wizard® SV Gel and PCR Clean-Up system (Promega) according to the manufacturer's manuals.

2.4.4 DNA restriction digestion

Enzymes and 10X restriction buffers were purchased from NEB. 20 µL digestion reactions were set up as follows.

	PCR products	Vectors
DNA	8 µL	2 µL
10X restriction buffer	2 µL	2 µL
Enzyme 1	1 µL	1 µL
Enzyme 2	1 µL	1 µL
Distilled H_2O	8 µL	14 µL

The reaction was incubated at 37^{o}C for 1 hour followed by heat inactivation at 65^{o}C for 20 minutes.

2.4.5 DNA linker preparation

The forward and reverse linkers were annealed by incubation at 94^{o}C for 4 minutes followed by cooling down to room temperature.

The reaction mixtures were as follows:

Forward linker	2 µg
Reverse linker	2 µg
Annealing buffer	up to 50 µL

The annealed linker was used in ligation.

2.4.6 Ligation

T4 DNA Ligase and 10X T4 ligase buffer were commercially available from Thermofisher.

Insert DNA	14 µL
Vector DNA	3 µL
10X T4 ligase buffer	2 µL
T4 DNA Ligase	1 µL

The ligation product was set on ice and incubated at 4^{o}C overnight before heat inactivation at 65^{o}C for 20 minutes.

2.4.7 DNA transformation to competent E. coli

Competent *E. coli* DH5α were made by $CaCl_2$ / RbCl treatment (Kushner, 1987). The competent cells were freshly stored at -80^{o}C as 50 μL aliquots.

50 μL competent cells were thawed on ice and mixed with 1 μL plasmid DNA or 10 μL ligation product. The mixture was incubated on ice for 1 hour and heated at 42^{o}C for 90 seconds. 1 mL LB was added, the cells were recovered at 37^{o}C for 1 hour with vigorous shaking at 180 rpm. 50 μL reaction mixture was plated on the LB agar plate with appropriate antibiotics and grown at 37^{o}C for 16 hours.

2.4.8 DNA transformation to B. subtilis

Overnight culture of *B. subtilis* 168 in MM competence media (Appendix I) was inoculated into 10 mL MM competence media (Appendix I) for the incubation at 37^{o}C for 3 hours. The culture was then mixed with 10 mL pre-warmed starvation media (Appendix I) and incubated at 37^{o}C for 2 hours. 10 μL plasmid DNA was mixed with 0.4 mL culture prior to incubation at 37^{o}C for 1 hour. 100 μL reaction mixture was plated onto the LB agar plate supplemented with 15 μg/mL spectinomycin, incubated overnight at 37^{o}C.

To screen for the proper chromosome incorporation into the *amyE* gene, colonies were plated onto the LB agar plate containing 1 % starch, incubated overnight at 37^{o}C. The resulting plate was stained by iodine solution.

2.4.9 Plasmid DNA Extraction

Plasmid DNA was extracted from 5 mL *E. coli* liquid culture using the PureYield™ Plasmid Miniprep System (Promega) according to the manufacturer's manuals. DNA was quantified by a NanoDrop 2000 (Thermofisher), and stored at -20^{o}C.

2.4.10 Total RNA extraction

Bacterial total cellular RNA was extracted using the RNeasy Mini Kit (Qiagen) according to the manufacturer's instructions. The purified RNA was quantified using the Qubit^{TM} RNA BR Assay Kit (Thermofisher) according to the manufacturer's manuals. The purity was assessed using a NanoDrop 2000 (Thermofisher).

2.4.11 RNA dot blot

Purified RNA was denatured in 1 M NaCl / 10 mM NaOH buffer by heating at 65^{o}C. 100 µL denatured RNA were transferred to the BrightStar™-Plus Positively Charged Nylon Membrane (Thermofisher) using the Bio-Dot® Microfiltration Apparatus (Bio-Rad) by vacuum transfer. The RNA was fixed on the membrane by baking at 80^{o}C. The dry membrane was hybridized with 100 ng/mL biotinylated DNA probe (Invitrogen) in pre-warmed North2South^{TM} Hybridization Buffer (Thermofisher) at 50^{o}C overnight. The non-specific interaction was excluded by washing the blot three times in 1X North2South™ Hybridization Stringency Wash Buffer (Thermofisher) for 15 minutes at 50^{o}C and one time at room temperature. The detection was carried out using the Chemiluminescent Nucleic Acid Detection Module Kit (Thermofisher) according to the manufacturer's instructions and the HRP activity was detected by

using the Gel Documentation System (Bio-Rad).

2.4.12 DNA Sequencing

Plasmid DNA, above 50 ng/μL, was sequenced by BGI using the sequencing primers PET_F and PET_R.

2.5 Protein Work

2.5.1 SDS-polyacrylamide gel electrophoresis (SDS-PAGE)

Protein gels were prepared using the Mini-Protean® Tetra cell (Bio-Rad). A Stacking gel was made at 4% and a resolving gel was set at 10%. 20 μL protein samples were mixed with 4 μL 6X SDS-PAGE loading dye (Appendix I). 3 μL Precision Plus Protein™ Dual Color Standard and 20 μL samples were loaded onto the stacking gel. The gel was run under 200 V for 25 minutes in 1X tris-tricine running buffer (Thermofisher), and immersed into Instant Blue™ Coomassie Protein Stain (Expeden) until protein bands became visible.

2.5.2 Protein overproduction

Protein overproduction plasmid was transformed to *E. coli* competent BL21 or C41 treated by $CaCl_2$ / RbCl (Kushner, 1987). Recombinant colonies were inoculated into 2 mL Auto Induction Media (AIM) (Formedium) for solubility check or 800 mL AIM for protein purification. The culture was incubated at 37^{o}C overnight or at room temperature for two days with rocking at 180 rpm. The cells were harvested by centrifugation at 5000 g for 10 minutes. The resulting cell pellet was stored at -80^{o}C

before use.

2.5.3 Solubility check

Pellet from 1 mL cell culture was resuspended in lysis buffer (Appendix I) to an A_{600} equivalent of 10. The resuspension was subjected to sonication on ice prior to centrifugation at 20000 g for 3 minutes. The supernatant, representing soluble proteins, was kept for SDS-PAGE. The pellet was washed three times in 1X PBS. The resulting pellet, representing insoluble proteins, was resuspended in 1X PBS and used in SDS-PAGE.

2.5.4 His-tagged proteins purification by affinity chromatography

The cell pellet was resuspended in 5 mL/gram of lysis buffer (Appendix I) and sonicated on ice with 5 seconds burst and 5 seconds cool down until complete lysis. Soluble proteins were separated by centrifugation at 8000 g for 1 hour at 4^{o}C and filtered using 0.45 μm syringe filter.

The clarified supernatant was loaded into a 1 mL HisTrap FF column (GE Healthcare) connected to the NGC FPLC system (Bio-Rad). The column was pre-equilibrated with 10 CV lysis buffer (Appendix I) without B-PER^{TM} Complete Bacterial Protein Extraction Reagent (Thermofisher) before sample loading. The column was washed with 10 CV wash buffer (Appendix I). The His-tagged protein was eluted by an imidazole gradient to 500 mM imidazole. Supernatant, flow-through, wash and elution fractions were subjected to SDS-PAGE. Fractions with the His-tagged proteins were

pooled for dialysis into the 1X PBS and then into 1X PBS with 30% glycerol. Protein concentration was estimated by using the Pierce™ Coomassie Protein Assay kit (Thermofisher) according to the manufacturer's manuals. Purified proteins were stored at -80^{o}C before use.

2.5.5 T. maritima NusB purification

The cell pellet was resuspended in 5 mL/gram of lysis buffer (Appendix I) and sonicated on ice with 5 seconds burst and 5 seconds cool down until complete lysis. The lysate were separated by centrifugation at 8000 g for 1 hour at 4^{o}C and filtered using 0.45 μm syringe filter.

The clarified supernatant was heated at 80^{o}C for 20 minutes to remove the host *E. coli* proteins. Afterwards the lysate was cooled down on ice for 10 minutes. The denatured proteins were pelleted by centrifugation at 12000 g for 10 minutes at 4^{o}C. The supernatnat was loaded into a 5 mL haperin column (GE Healthcare) connected to the NGC FPLC system (Bio-Rad). The column was pre-equilibrated with 10 CV heparin binding buffer (Appendix I). The column was washed with 10 CV heaprin binding buffer (Appendix I). The bound protein was eluted by a gredient from 150 mM to 1 M NaCl. Input, flow through, wash and elution fractions were subjected to SDS-PAGE. Fractions with TmaNusB were pooled and concentrated to 2 mL using an Amicon® Ultra Centrifugal filters. The TmaNusB fractions were loaded into an HiLoad 16/600 Superdex 75pg column (GE healthcare) at a flow rate of 1 mL/min. The elution profile was monitored by absorbance at 280 nm.

2.5.6 in vitro NanoLuc PCA

The *in vitro* NanoLuc PCA was performed in a 96-well White Polystrene Microplate (PerkinElmer). 40 μL LgBiT tagged protein was mixed with 40 μL SmBiT tagged protein or 1X PBS, incubated for 10 minutes at 37^{o}C. Promega Nano-Glo® Luciferase Substrate was diluted 100-fold in Promega Nano-Glo® Luciferase Assay Buffer. 20 μL diluted substrates were added into the reaction mixture. The luminescence emitted was quantified using the PerkinElmer Victor X3 Multilabel plate reader. The experiments were done in triplicate and technical repeats were done to enable consistent results.

2.5.7 Compound titration assay

Chemical compounds in powder form were dissolved in DMSO to 10 mg/mL as the stock. For inhibitor titrations, compounds were diluted by two-fold serial dilution from 3 mM. For screening of nusbiarylin compounds, the compound final concentrations were 125 μM.

20 μL compounds were mixed with 40 μL the target protein- nusbiarylins with N-LgBiT-NusB and C5 with C-SmBiT-CH. The reaction mixture was incubated for 10 minutes at 37^{o}C. 40 μL complementary tagged protein was added before incubation for 15 minutes at 37^{o}C. 20 μL 100-fold diluted Promega Nano-Glo® Luciferase Substrate was added prior to the signal measurement by the PerkinElmer Victor X3 Multilabel plate reader. The experiments were done in triplicate and technical repeats were done to enable consistent results.

2.5.8 Crystallization

Crystallization experiments were conducted in the sitting-drop vapor diffusion format of 2 μL droplet and 100 μL reservoir. Crystallization conditions were probed by commercial kits at room temperature. After refinement of salt concentrations, the resulting crystals were stained by JBS True Blue (Jena Bioscience) in order to confirm protein crystals. For co-crystallization of TmaNusB with MC4-134, MC4-150 and MC4-152. The protein and compounds at 1 : 5 molar ratio were assembled for 1 hour at 30^{o}C or assembled during dialysis at 4^{o}C overnight before crystallizations.

2.5.9 Crystals soaking

Soaking was conducted in 48-well crystallization plates (Hampton research) with 200 μL of soaking buffer (Appendix I) as the reservoir. TmaNusB crystals were transferred to 3 μL droplet of inhibitors MC4-134, MC4-150 and MC4-152 in 0.5% and 5% DMSO at room temperature.

Chapter 3: Development of an *in vitro* system for screening PPI inhibitors

3.1 Protein-fragment complementation assay for PPI studies

This chapter describes the process to develop the *in vitro* NanoLuc PCA for PPI inhibitor screening by studying the PPIs of NusB-NusE and RNAP-σ^A.

High throughput screening (HTS) refers to an approach to identify candidates with the desired biochemical properties in a compound library. HTS is commonly employed to screen for enzyme inhibitors in early drug discovery process. Yet, an HTS for PPI inhibitors is not well established. Currently ELISA-based assay, fluorescence resonance energy transfer (FRET) are applied to studying PPI inhibitors (Yang *et al*., 2015; Zhou *et al*., 2016). The current methods are reliable but time-consuming, whereas the ideal HTS assay should be cost-effective, rapid and simple. These advantages can be achieved by a recently developed PCA in interactome studies (Zhou *et al*., 2016).

In a typical PCA, a reporter protein is divided into two fragments. The reporter protein fragments are fused to two interacting proteins respectively as two recombinant tags (Li *et al*., 2019). During a PPI, two complementary tags combine as the native-like conformation. The refolded enzyme catalyzes the signal emission such as luminescence and fluorescence (Michnick *et al*., 2011).

NanoLuc is a split-luciferase originated from a luciferase secreted by *Oplophorus*

gracilirostris (Dixon *et al*., 2016). The luciferase was previously engineered to become NanoLuc capable of releasing stable and strong luminescence (Hall *et al*., 2012). For NaonLuc to be used in PCA, the enzyme was divided into the small subunit SmBiT and the large subunit LgBiT (Dixon *et al*., 2016; Figure 3.1). In the NanoLuc PCA, two interacting proteins are tagged by SmBiT or LgBiT. A specific PPI brings the tags SmBiT and LgBiT together to form the native-like NanoLuc. The enzyme reconstitution results in the light emission in the presence of substrate (Dioxin *et al*., 2016). The NanoLuc PCA was intensively applied in some prior *in vivo* PPI studies (Yano *et al*., 2018). Conversely, the NanoLuc PCA is not generally employed as the *in vitro* assay despite the potentiality for *in vitro* use.

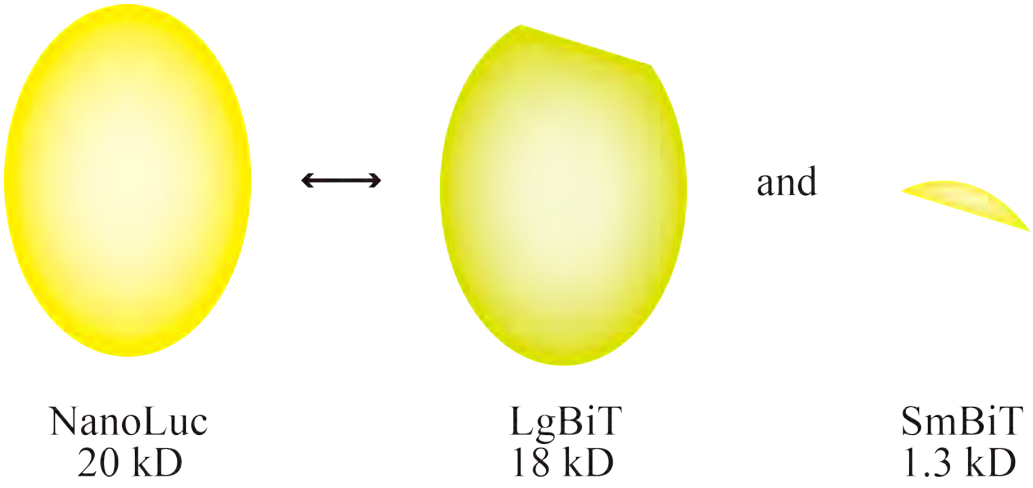

Figure 3.1 The NanoLuc protein divided into SmBiT and LgBiT. A peptide chain of 11 amino acid residues, namely SmBiT, is disserted from NanoLuc. The remaining part is LgBiT.

The present study developed the NanoLuc PCA to be an *in vitro* PPI inhibitor screening assay. A set of vectors were generated for single step cloning to tag proteins with one of the NanoLuc fragments and the His tag. To validate our system, the NusB-NusE

and RNAP-σ^A PPIs were examined by the *in vitro* NanoLuc PCA. Compared to previous studies (Yang *et al*., 2017; Yang *et al*., 2015), the PPIs and effects of inhibitors (MC4 and C5) were similarly quantified by the *in vitro* NanoLuc PCA. Subsequently the assay was simplified for large-scale screening. Our work demonstrated the potential application of the *in vitro* NanoLuc PCA for PPI inhibitor screening in a fast and simple manner.

Results

3.2 Design and construction of a NanoLuc PCA vector system

The investigation was initiated by generating a PCA plasmid system for tagging proteins with the NanoLuc fragments and the 6 x His tag. Eight plasmids were made for tagging proteins at NTD or CTD.

The N-terminal His tagging vectors were first designed and made. pETMCSIII was chosen as the parent vector for NTD His tagging (Neylon *et al*., 2000; Table 2.1). Four plasmids were cloned as described in Figure 3.2. The resulting vectors were used to clone protein overproduction plasmids (Table 2.1). However, potentially due to *E. coli* cellular protease activities, the N-terminal tag could be unstable for some recombinant proteins. For example, when the N-LgBiT fusion protein was overproduced, the N-LgBiT tag alone could exist at a significant amount that bound to the Ni-NTA column. To avoid the contamination, the C-terminal His tagging vectors were made to enable the complete recombinant proteins.

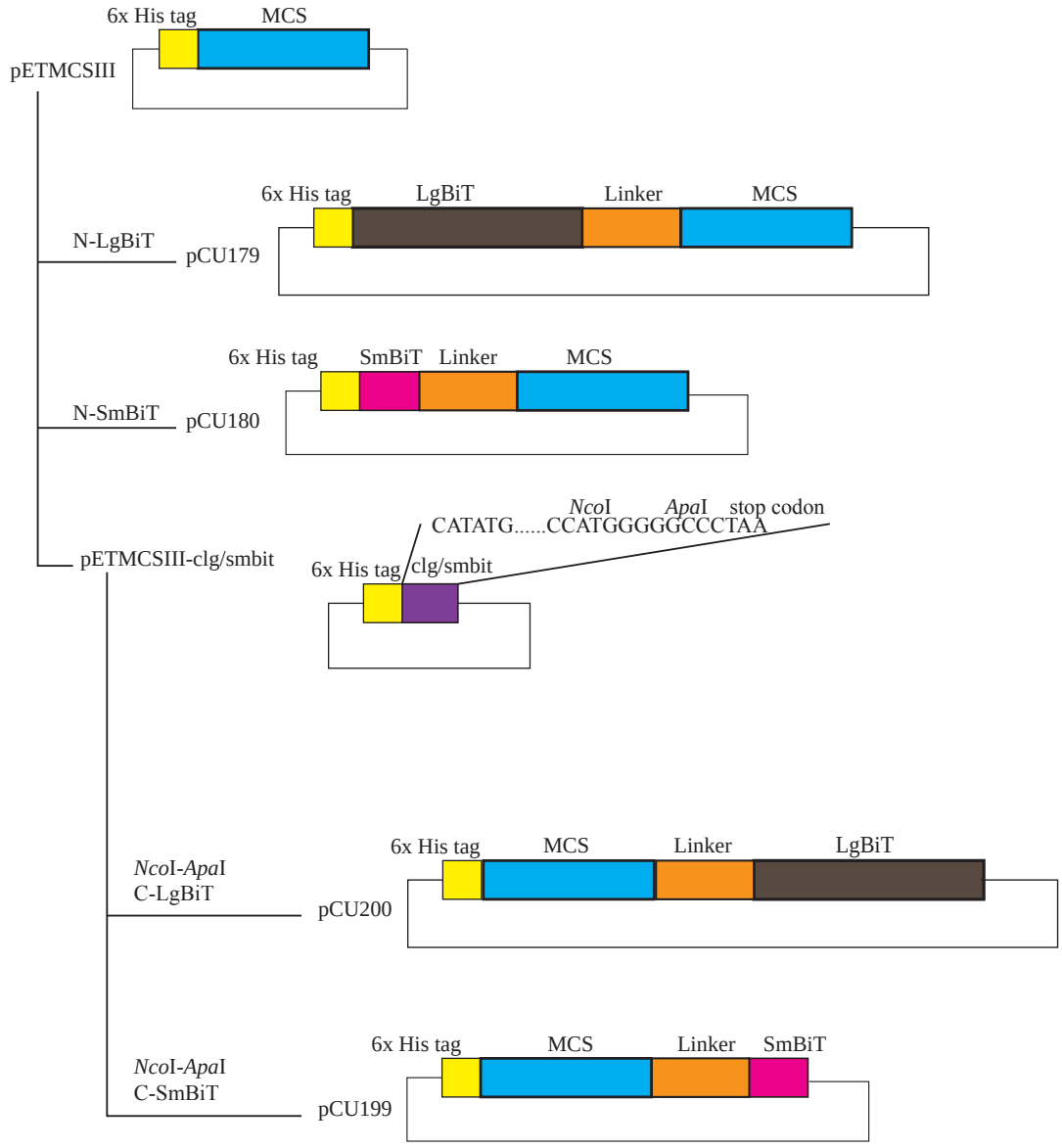

Figure 3.2 Schematic diagram summarizing the N-terminal His tagging vector constructions. The N-LgBiT and N-SmBiT vectors were first generated by simply cloning the genes *lgbit* and *smbit* into pETMCSIII, whereas the clg/smbit linker was cloned into pETMCSIII to introduce the *Apa*I restriction site prior to constructions of the C-LgBiT and C-SmBiT vectors.

To generate the C-terminal 6 x His tagging vectors, pNG209 was selected as the parent vector (Yang *et al*., 2009; Table 2.1). Since the *Nco*I and *Apa*I restriction sites were required for cloning the *smbit* and *lgbit* gene. The linker clg/smbit was cloned into pNG209 to introduce the necessary restriction sites (Yang *et al.*, 2009; Table 2.1). The

resulting vector was used to derive the C-terminal His tagging vectors (Figure 3.3)

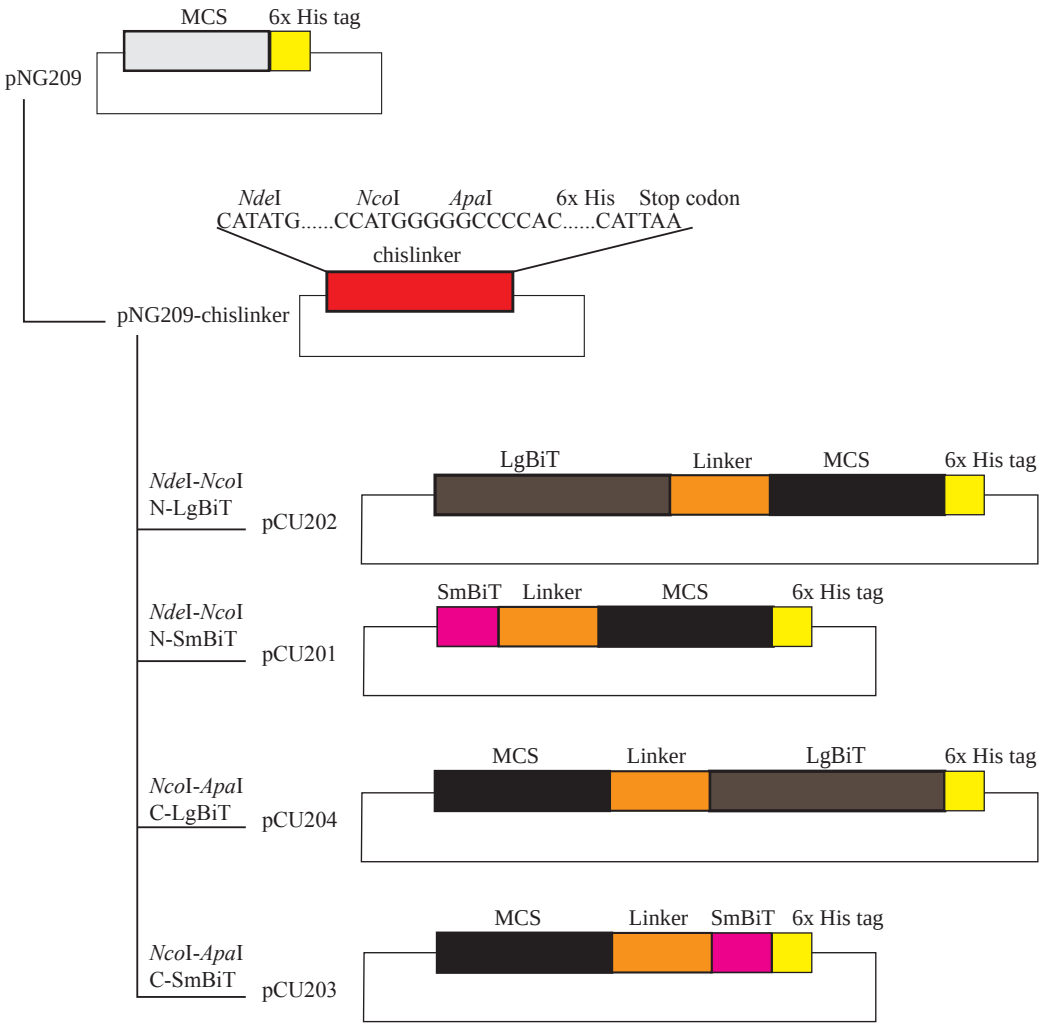

Figure 3.3 Schematic diagram showing the CTD 6 x His tagging vector constructions. The linker C_hislinker was cloned into pNG209 (Yang *et al*., 2009) to introduce the *Apa*I site prior to deriving the N-LgBiT, N-SmBiT, C-LgBiT and C-SmBiT vectors.

To justify the successful gene insertion, PCR colony screening was performed using the primers PET_F and PET_R (Table 2.2). In PCR, the region of *smbit* or *lgbit* inserts was amplified. The *smbit* and *lgbit* gene fragments were 400 bp and 700 bp respectively. To detect the length of the amplicons, DNA gel electrophoresis was performed. As the expected sizes of amplicons for successful recombinant vectors were observed in the DNA gel (Figure 3.4), the insertions of *smbit* and *lgbit* fragments were suggested. The nucleotide sequences were confirmed by Sanger sequencing.

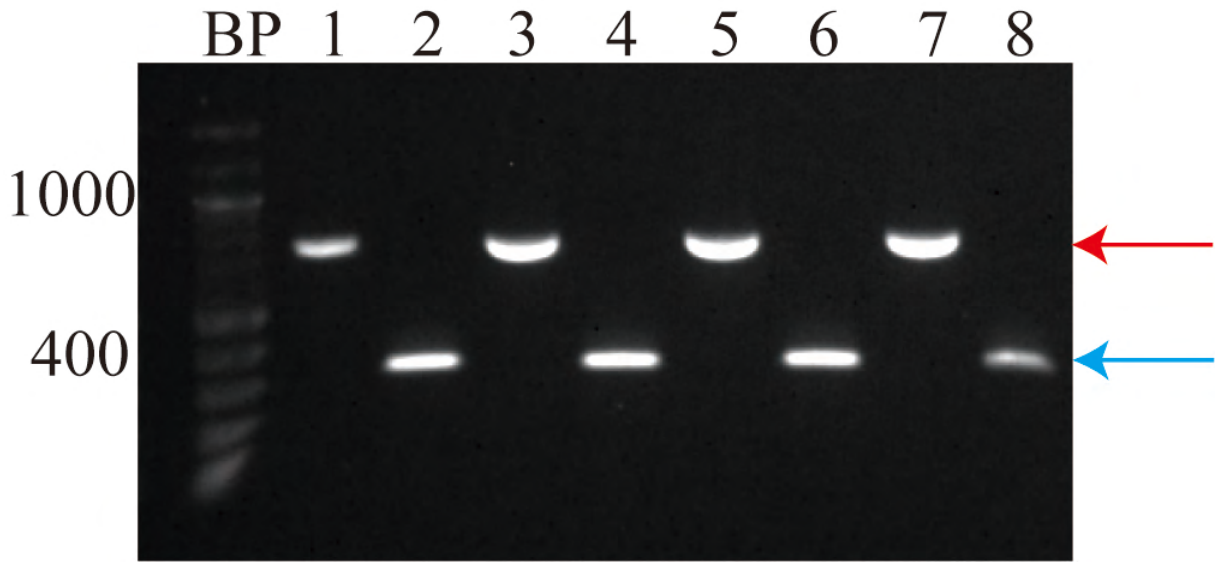

Figure 3.4 Amplified PCR products from the PCA plasmids generated in this study. The blue arrow indicates the *smbit* gene and the red arrow indicates the *lgbit* gene. 1- pCU179 (700bp); 2- pCU180 (400bp); 3- pCU200 (700bp) ;4- pCU199 (400bp) ;5- pCU202 (700bp); 6- pCU201 (400bp) ;7- pCU204 (700bp) ;8- pCU203 (400bp).

Eight vectors for the PCA tagging (Table 2.1) were finally made as shown in Figure 3.5. The plasmids provided an ampicillin resistance gene *bla* as the selective marker for identifying the transformants. A T7 promoter drove the recombinant gene expression. A multiple cloning site (MCS) served as the gene insertion site. Following gene insertion, protein overproduction could be induced by culturing the transformants with isopropylthiogalactoside (IPTG) or in AIM.

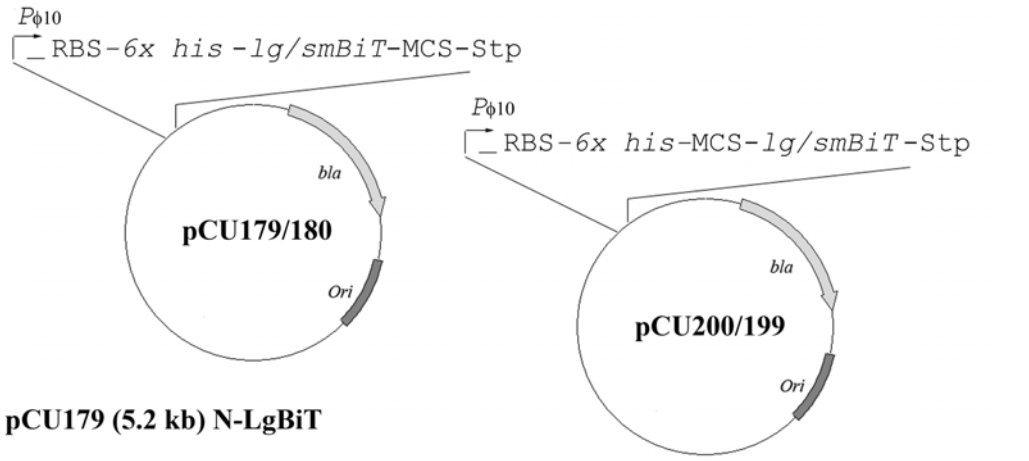

pCU179 (5.2 kb) N-LgBiT

6x his *NdeI* **LgBiT** linker

CAC...CAT*CATATG***GTCTTCACACTCGAAG**.....**CCATCAACAGT**GGGAGTTCCGGTGGTGGCGGGAGCGGAG

XhoI *SacI* *EcoRI* **Stp** *XbaI* *Acc65I* *NcoI* **Stp**

GTGGAGG*CTCGAGCGGTGGAGCTCAGGGGAATTC*AGTC**TAA**GCTAGCAGATCT*TCTAGAGGTACCCCATGG*...**TAA**

pCU180 (4.8 kb) N-SmBiT

6x his *NdeI* **SmBiT** linker

CAC...CAT*CATATG***GTGACCGGCTACCGGCTGTTCGAGGAGATTCTC**GGGAGTTCCGGTGGTGGCGGGAGCGGAG

XhoI *SacI* *EcoRI* **Stp** *XbaI* *Acc65I* *NcoI* **Stp**

GTGGAGG*CTCGAGCGGTGGAGCTCAGGGGAATTC*AGTC**TAA**GCTAGCAGATCT*TCTAGAGGTACCCCATGG*...**TAA**

pCU200 (5.2 kb) C-LgBiT

6x his *NdeI* *XbaI* *Acc65I* *NcoI* **Stp** *SacI* *EcoRI* *XhoI*

CAC...CAT*CATATGTCTAGAGGTACCCCATGG***TAA**GTGG*GAGCTCAGGGGAATTCTGGCTCGAG*CGGTGGT

linker **LgBiT** *ApaI* **Stp**

GGCGGGAGCGGAGGTGGAGGGTCGTCAGGT**GTCTTCACACTCGAAG**.....**CCATCAACAGT***GGGCCC***TAA**

pCU199 (4.8 kb) C-SmBiT

6x his *NdeI* *XbaI* *Acc65I* *NcoI* **Stp** *SacI* *EcoRI* *XhoI*

CAC...CAT*CATATGTCTAGAGGTACCCCATGG***TAA**GTGG*GAGCTCAGGGGAATTCTGGCTCGAG*CGGTGGT

linker **SmBiT** *ApaI* **Stp**

GGCGGGAGCGGAGGTGGAGGGTCGTCAGGT**GTGACCGGCTACCGGCTGTTCGAGGAGATTCTG***GGGCCC***TAA**

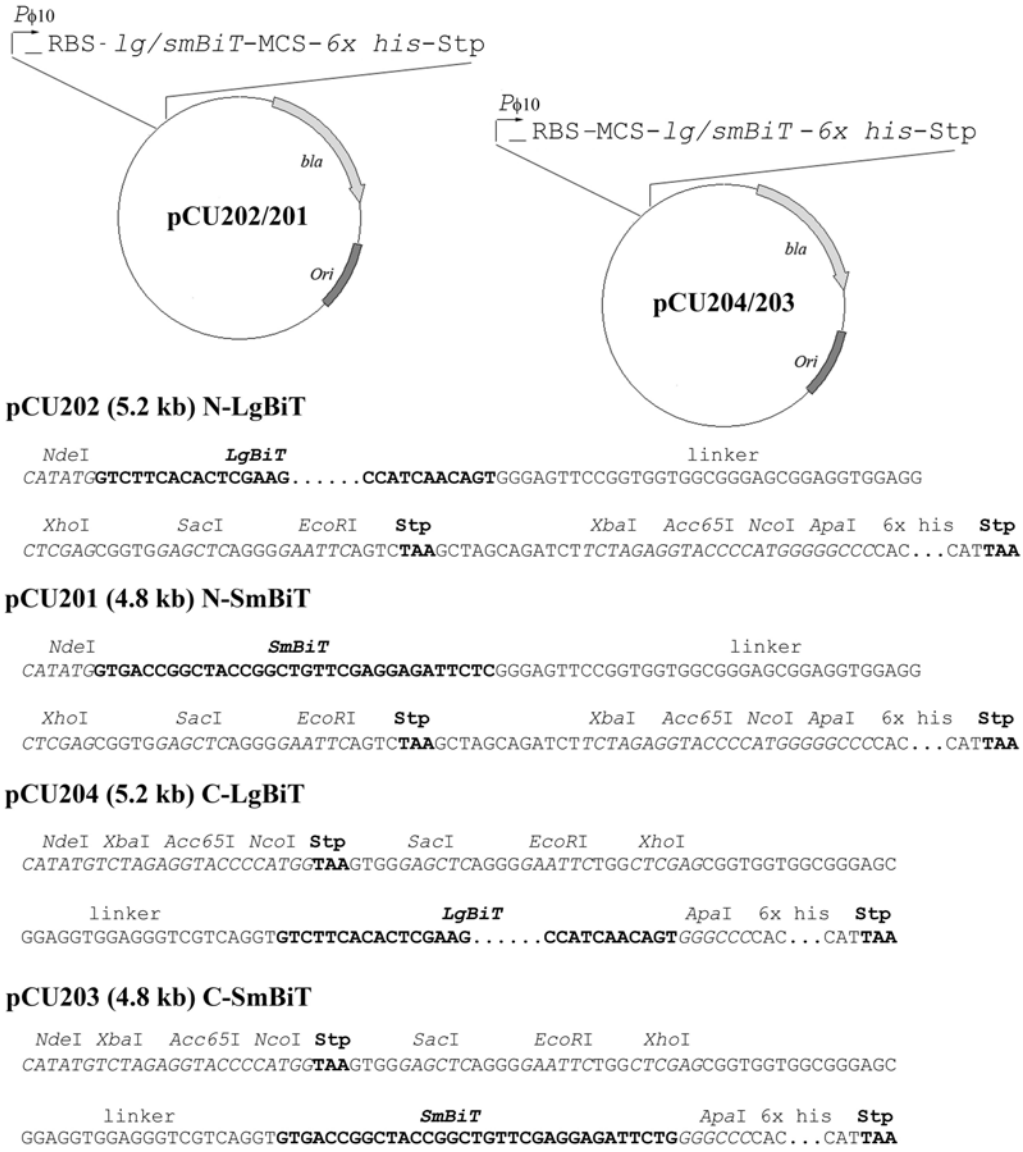

Figure 3.5 Summary of the PCA plasmid system generated for PPI studies. pCU179, pCU180, pCU200 and pCU199 were generated for the NTD His tagging, whereas pCU202, pCU201, pCU204 and pCU203 were generated for the CTD His tagging. The PCA plasmids contained the T7 promoter for the gene expression induction. The *bla* gene conferred ampicillin resistance to the transformants.

3.3 Application of the PCA system for studying *in vitro* NusB-NusE interaction

3.3.1 Design and construction of the PCA tagged NusB and NusE protein overproduction plasmids

The NanoLuc complementation fragments SmBiT and LgBiT could be fused to NTD or CTD of proteins. To ensure the NanoLuc complementation fragments could combine as the functional NanoLuc, the position of SmBiT and LgBiT should be carefully selected. The NanoLuc enzyme could not be formed when the complementation fragments did not contact each other during a PPI, whereas the maximized contact between SmBiT and LgBiT facilitated the NanoLuc reconstitution. Hence, different combinations of the tagging positions (NTD or CTD) should be tested for optimum luminescence emission. The *in vitro* NanoLuc PCA was first applied to characterize the NusB-NusE PPI, the essential PPI as aforementioned in chapter 1. The tagging strategy was decided by analyzing the *E. coli* NusB-NusE dimer crystal structure (Luo *et al*., 2008; Figure 3.6). The structural information revealed the spatial proximity between PPI partners. Compared to the NusB CTD, the NTD was anticipated to be in closer contact with NusE (Figure 3.6). Accordingly NusB was tagged at the NTD, whereas NusE was tagged at both NTD and CTD.

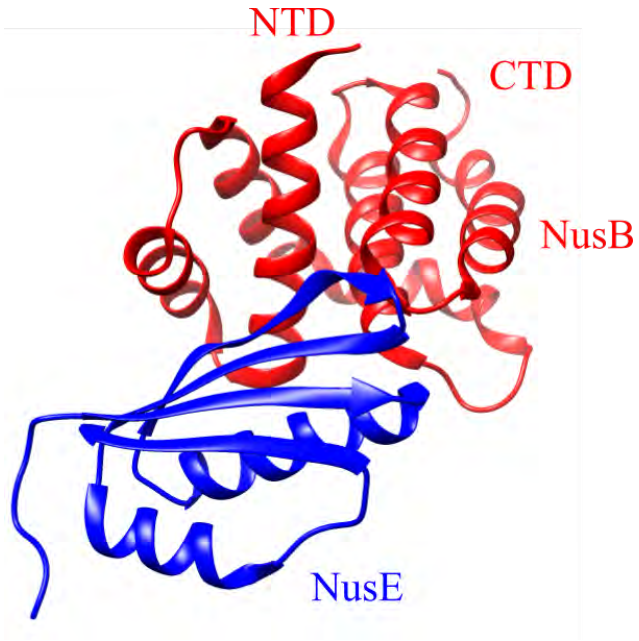

Figure 3.6 The crystal structure of NusB-NusE dimer (PDB ID: 3D3B). The NTD is in closer proximity to NusE when compared to the CTD. NusB is shown in red, and NusE is shown in blue.

The established plasmid system was applied for cloning the protein overproduction plasmid. NusB and NusE used in the study were original from the Gram-positive model organism *B. subtilis*. The *bsubnusB* gene was cloned into pCU180 and pCU202 (Table 2.1), whereas the *bsubnusE* gene was incorporated into pCU201, pCU202, pCU203 and pCU204 (Table 2.1).

Insertions of the *bsubnusB* and *bsubnusE* genes were checked by PCR colony screening using the PET_F and PET_R primers (Table 2.2). For example, the *bsubnusE* gene was ligated into pCU202, the correct gene insertion should result in an amplicon of 1000 bp. Compared to the negative control of pCU202, the expected amplicon of 1000 bp was identified (Figure 3.7A). This suggested the *bsubnusE* gene insertion.

The successful constructions of the NusB/NusE protein overproduction plasmids were checked by PCR using the primers PET_F and PET_R (Table 2.2). The distinct bands representing the expected sizes of the genes *bsubnusB* and *bsubnusE* were visualized (Figure 3.7B), suggesting the gene insertions. The DNA sequences were identified by Sanger sequencing.

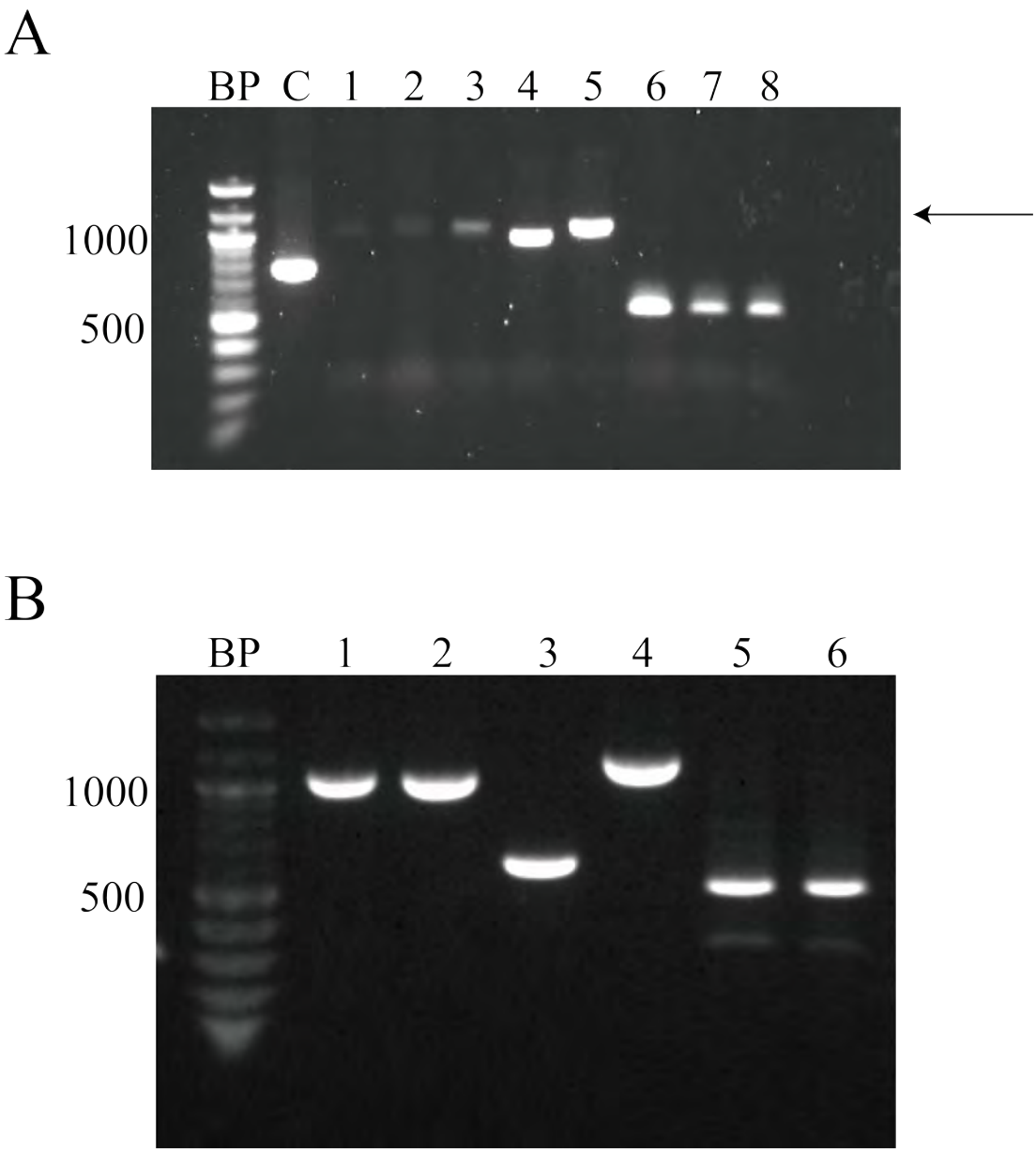

Figure 3.7 A. The colony screening result of the N-LgBiT-NusE protein overproduction plasmid. The band representing the correct insert is indicated by the black arrow. C- pCU202 (700 bp); 2-9- Colonies picked. **B.** Amplified PCR products from the six NusB and NusE PCA vectors. 1- pCU235 (1000 bp) ;2- pCU236 (1000bp) ;3- pCU231 (600bp) ;4- pCU250 (1100bp) ;5- pCU246 (500bp) ;6- pCU247 (500bp).

3.3.2 Purification of PCA tagged NusB and NusE

The SmBiT/LgBiT fusion proteins were purified using the Ni-NTA column. For example, As illustrated in Figure 3.8A, the soluble N-SmBiT-NusB was overproduced shown by the protein band representing the expected molecular weight in the clarified cell lysate. The band of the corresponding size was diminished in the flow-through fraction and detected in the elution fractions. The result proved that the His-tagged NusB bound to the Ni-NTA column and was eventually washed out at high imidazole concentrations. To remove any Ni^{2+} ion leaked from the column, the purified proteins were dialyzed into storage buffer (Appendix I) with EDTA and DTT added. The protein concentrations were estimated by Bradford assay (Thermofisher) before storage at -80^{o}C. The summary gel was run to show the purified SmBiT/LgBiT fusion NusB and NusE (Figure 3.8B). Although some minor impurities of proteins existed, the contaminations were not expected to interfere with the assay.

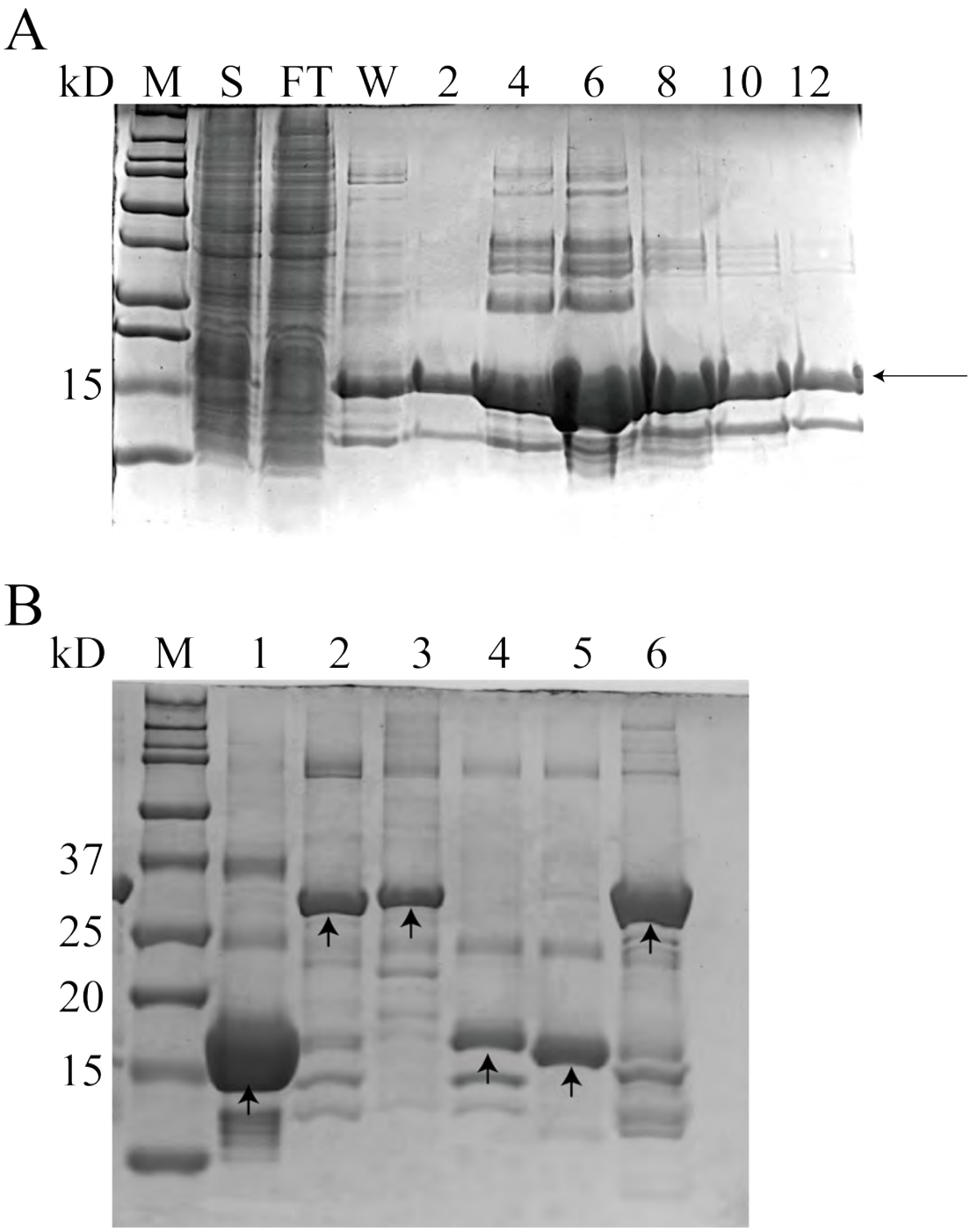

Figure 3.8 A. Purification gel for N-SmBiT-NusB showing the clarified supernatant of cell lysate, flow-through, 40 mM imidazole wash and six elution fractions. SmBiT-NusB is illustrated by the black arrow. M- marker; S- supernatant of cell lysate; FT- flow through; W- 40 mM imidazole wash; 2, 4, 6, 8, 10, 12- elution fractions. **B.** Summary gel of the PCA tagged NusB and NusE purified in this investigation. The recombinant NusB and NusE are indicated by black arrows. 1- N-SmBiT-NusB (19 kD); 2- N-LgBiT-NusE (32 kD); 3- C-LgBiT-NusE (33 kD); 4- N-SmBiT-NusE (16 kD); 5- C-SmBiT-NusE (16 kD); 6- N-LgBiT-NusB (36 kD).

3.3.3 Studying of NusB-NusE PPI by NanoLuc PCA

N-SmBiT-NusB, N-LgBiT-NusE, C-LgBiT-NusE, N-LgBiT-NusB, N-SmBiT-NusE, and C-SmBiT-NusE were purified. The SmBiT/LgBiT fusion NusB and NusE provided four combinations for testing the NanoLuc reconstitution (SmBiT-NusB + LgBiT-NusE and LgBiT-NusB + SmBiT-NusE). To measure the luminescence from different combinations, the fusion NusB and NusE were incubated for the PPIs to occur. The signals were quantified from the NusB-NusE mixtures or from the LgBiT fusion protein as shown in Figure 3.9. No significant light emission was detected when N-SmBiT-NusB was mixed with the LgBiT fusion NusE. Conversely, the interaction between N-LgBiT-NusB and the SmBiT fusion NusE generated 100-fold brighter signal compared to N-LgBiT-NusB alone. Since the interaction of N-LgBiT-NusB and C-SmBiT-NusE demonstrated the optimal luminescence emission, the NusB-NusE titration and the inhibitor tests were performed using N-LgBiT-NusB and C-SmBiT-NusE.

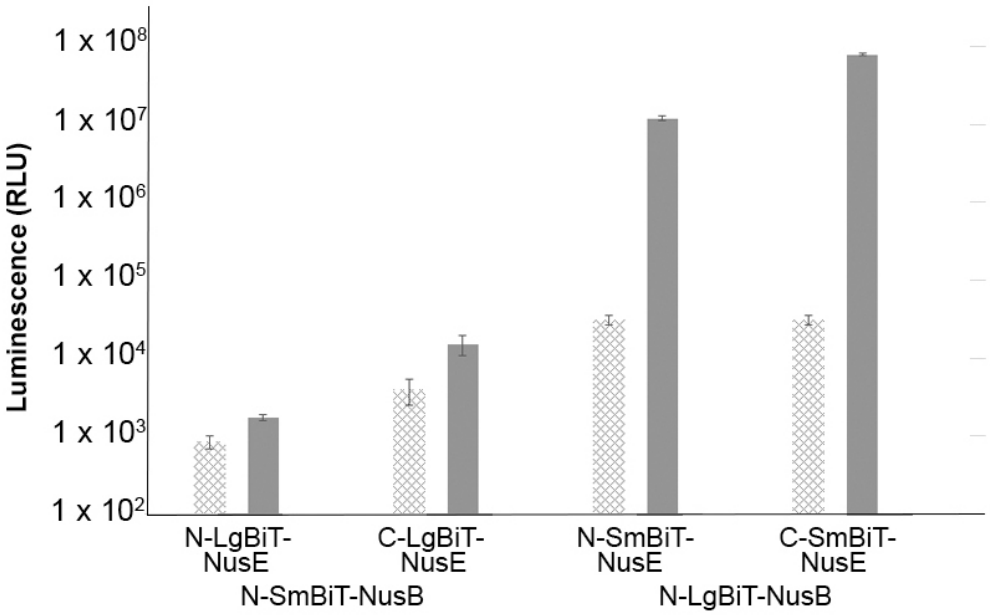

Figure 3.9 The luminescence signal emitted from each combination of the PCA tagged NusB and NusE. The patterned columns represent the signal from the LgBiT tagged proteins, whereas the solid columns represent the signal from each interaction (Tsang *et al*., 2019).

The optimal NanoLuc fragment complementation could be estimated by the protein models in Figure 3.10. When N-SmBiT-NusB and C-LgBiT-NusE were interacting, two PCA tags were spatially separated. In contrast, the SmBiT and LgBiT tags came into sufficient contact during the PPI of N-LgBiT-NusB and C-SmBiT-NusE, favoring the enzyme refolding.

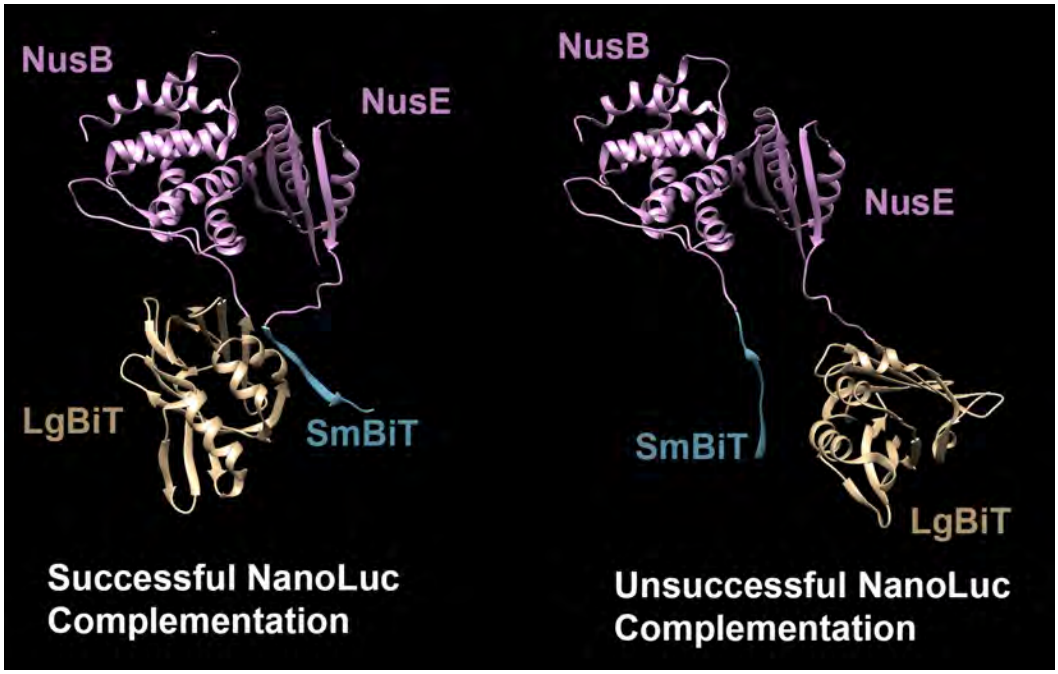

Figure 3.10 The PPI estimations for N-LgBiT-NusB with C-SmBiT-NusE and N-SmBiT-NusB with C-LgBiT-NusE (Tsang *et al*., 2019).

To evaluate the NusB-NusE binding affinity, N-LgBiT-NusB at 1 μM was titrated against C-SmBiT-NusE at various concentrations. With an increasing amount of C-SmBiT-NusE, the luminescence signal increased until reaching the plateau phase (Figure 3.11). The NusB-NusE binding affinity was evaluated by calculating dissociation constant (K_d): The concentration at which 50% NusE molecules was interacting with NusB. In the titration of N-LgBiT-NusB and C-SmBiT-NusE, the calculated K_d meant the N-SmBiT-NusE concentration that gave 50% light intensity compared to the maximal value. The K_d was calculated to be 1.5 $\pm$ 0.3 μM. Likewise, the similar value (1.1 $\pm$ 0.1 μM) was obtained from the previous study (Yang *et al*., 2017). The result evidenced that the *in vitro* NanoLuc PCA could be used to investigate the NusB-NusE PPI.

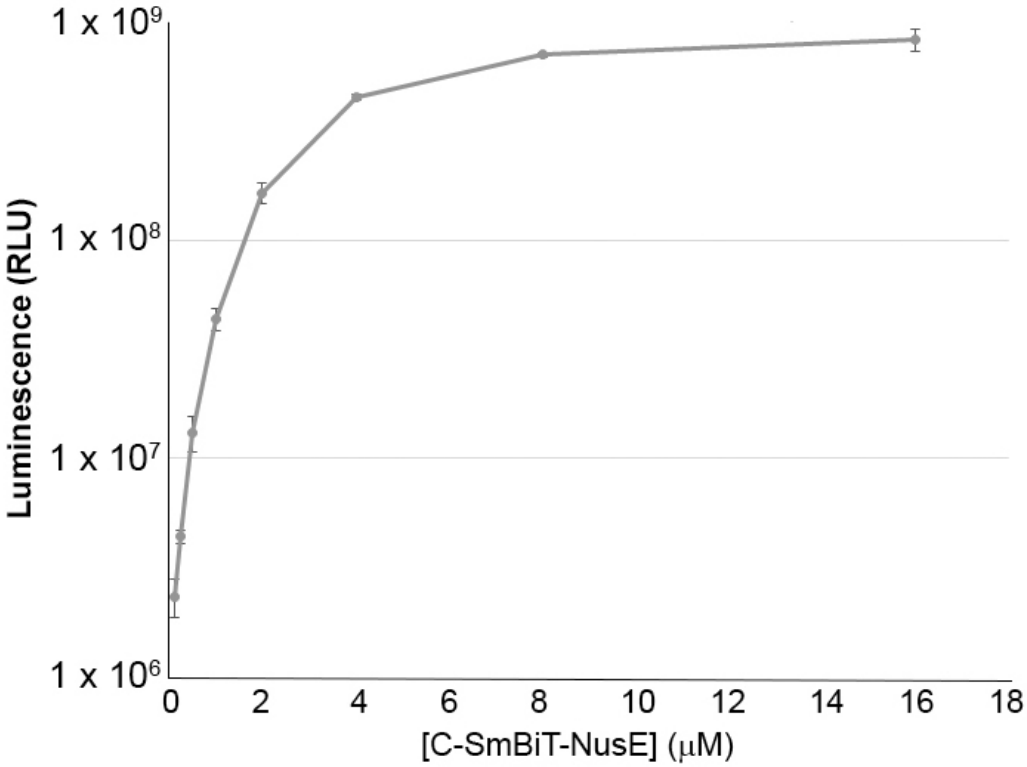

Figure 3.11 Titration of N-LgBiT-NusB with C-SmBiT-NusE at different concentrations (Tsang *et al*., 2019).

Before the PPI inhibitor tests, an appropriate protein concentration was determined to show the PPI disruption . When N-LgBiT-NusB was in excess, the PPI inhibitory effect might be masked. However, when N-LgBiT-NusB was inadequate, high level of PPI inhibition could be frequently observed regardless to the strengthen of PPI inhibitors. According to the titration curve of N-LgBiT-NusB and C-SmBiT-NusE (Figure 3.11), the concentration of 1 μM was at the middle part of the exponential phase. As this concentration was not located at the plateau, the apparent decrease in luminescence could be observed when the PPI inhibition occurred. Therefore, 1 μM N-LgBiT-NusB and 1 μM C-SmBiT-NusE were used for examining the PPI inhibitory effect of nusbiarylins.

3.3.4 Examination of the PPI inhibitory effects by MC4 and its derivatives

The PPI of N-LgBiT-NusB and C-SmBiT-NusE favored NanoLuc refolding, which was prevented by PPI inhibitors. Thus, decrease in the luminescence emission was inversely correlated to the inhibitor performance.

The NusB-NusE PPI represents the potential drug target as aforementioned. By structure-based pharmacophore design and *in silico* screening, the initial compound MC4 (Figure 3.12A) was spotted. MC4 showed the specific interaction with *B. subtilis* NusB and the repressed RNA production in *S. aureus* (Yang *et al*., 2017). Aa illustrated in the docking model, MC4 was designed to interact with NusB through the alkyne group in a hydrophobic interaction with R76, the phenol group bonding to E81, and the nitrate group interacting with Y16 (Figure 3.12B). MC4 was used to test the feasibility of the *in vitro* NanoLuc PCA because MC4 was previously shown to inhibit the NusB-NusE interaction by the ELISA-based assay (Yang *et al*., 2017). 1 μM N-LgBiT-NusB and 1 μM C-SmBiT-NusE were titrated against MC4 at a series of concentrations, the result was interpreted as the percentage inhibition (Figure 3.12C). With the increasing MC4 amounts, the percentage inhibition increased and reached the plateau at high doses (Figure 3.12C). To evaluate the PPI inhibition by MC4, half-maximal inhibitory concentration (IC_{50}) was calculated to find the MC4 concentration that interacted with 50% N-LgBiT-NusB molecules. The dose-dependent curve in Figure 3.12C was mathematically interpreted as $y = 11.135 \ln(x) + 14.256$. At 50% inhibition ($y = 50$), the corresponding MC4 concentration (x) was approximate 24.8 μM, meaning the IC_{50}. In the prior study, the similar IC_{50} value was obtained using the

ELISA-based assay (Yang *et al*., 2017). Therefore, the *in vitro* NanoLuc PCA was proven feasible for characterizing the NusB-NusE PPI inhibitors. We hereby extended the study to screen for new nusbiarylin compounds.

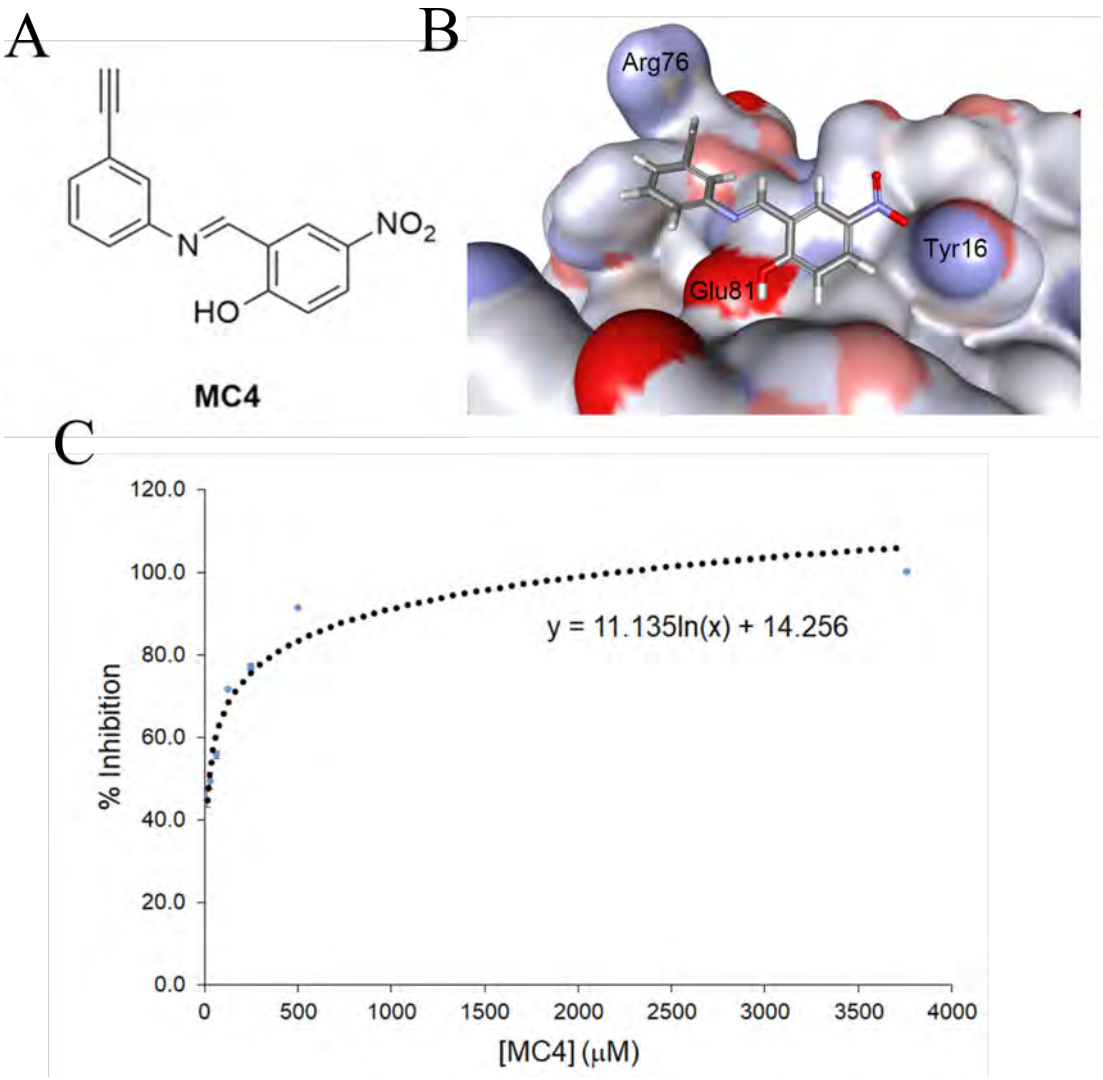

Figure 3.12 A. The chemical structure of MC4 (Tsang *et al*., 2019). **B.** The docking model of MC4 on the NusB surface (Tsang *et al*., 2019). **C.** MC4 PPI inhibitory effects on the NusB-NusE interaction measured by the *in vitro* NanoLuc PCA (Tsang *et al*., 2019).

Three new MC4 analogues, MC4-19, MC4-33 and MC4-92 (Figure 3.13), were synthesized for testing the *in vitro* NanoLuc PCA in PPI inhibitor screening. Three MC4 derivatives had the C-N single bond instead of the imine group as the imine group could contribute to non-specific interaction with proteins. The compounds were titrated with N-LgBiT-NusB and C-SmBiT-NusE. MC4-19, MC4-33, and MC4-92 demonstrated PPI inhibitory effects with different IC_{50} values (Table 3.1). The result suggested that the *in vitro* NanoLuc PCA could be applied to compare the PPI inhibitory effects of the nusbiarylin compounds. To assess the antimicrobial activity, broth microdilution assay was performed to find out the minimum inhibitory concentration (MIC). In definition, MIC means the minimum antibiotic concentration that suppresses the bacterial growth. Since MRSA is the most prevalent multidrug resistant bacteria (Hassoun *et al*., 2017), antimicrobial susceptibility test was conducted on *S. aureus*, MRSA and other common Gram-positive pathogens. Correspondingly, these strains were found susceptible to MC4-19, MC4-33 and MC4-92 (Table 3.1). Compared to MC4, the derivatives were less efficient for inhibiting the NusB-NusE PPI shown by the higher IC_{50} values. Nevertheless, MC4-92 showed similarly strong antimicrobial activities against *S. aureus* and MRSA (HA W235 ST5) as MC4 did. The possible explanation was that the antimicrobial activity could be attributed to other factors beyond the PPI inhibition such as cell membrane permeability.

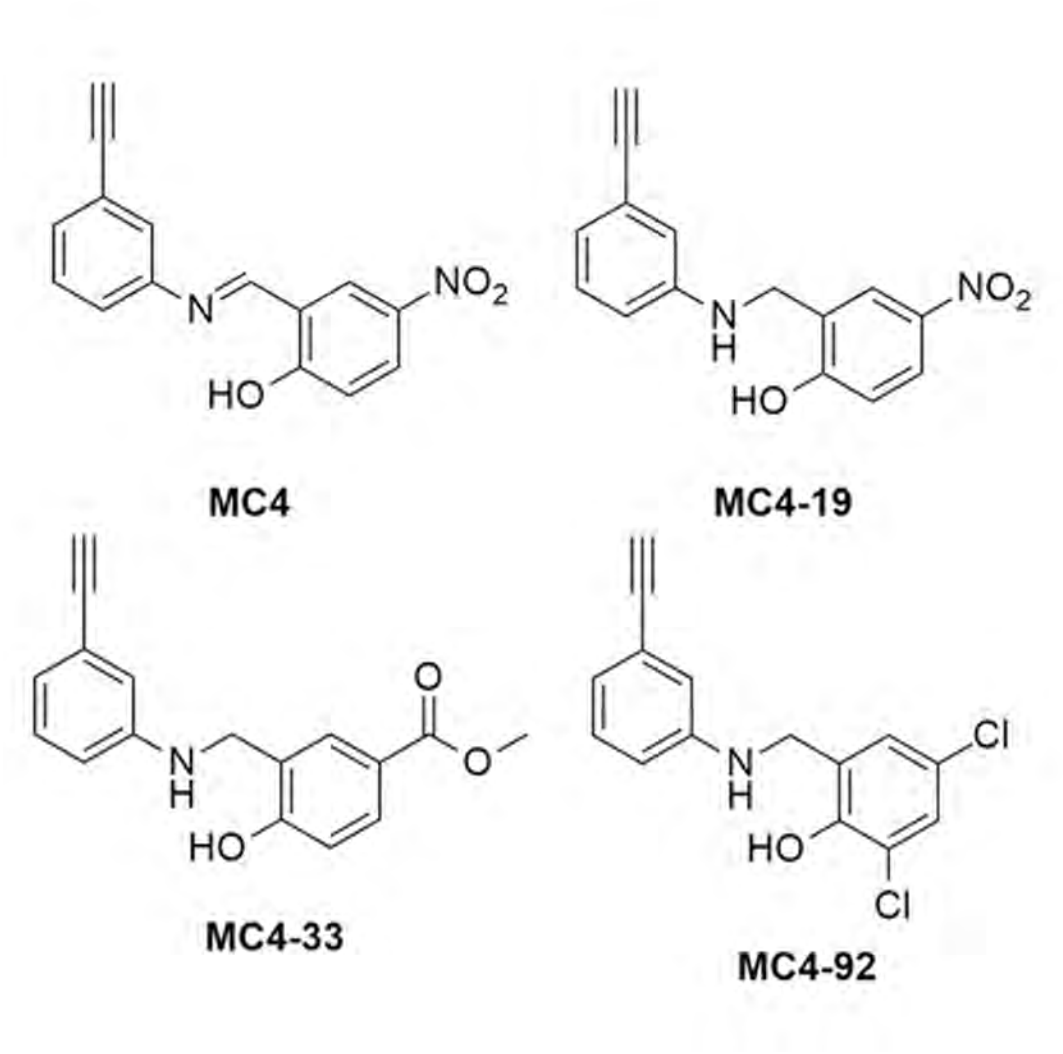

Figure 3.13 The chemical structures of MC4, MC4-19, MC4-33 and MC4-92 (Tsang *et al*., 2019).

To improve the efficiency of the *in vitro* NaonLuc PCA for large-scale screening, the assay could be simplified to test a single concentration correlating to the IC_{50}. Therefore, lots of compounds could be tested in one trial. For nusbiarylins, 125 μM was the concentration reflecting the IC_{50} (Table 3.1). By doing so, the *in vitro* NanoLuc PCA could be applied to screen for new NusB-NusE PPI inhibitors.

Table 3.1. Antimicrobial activities and PPI inhibitions of the MC4 compounds against *S. aureus* and common Gram-positive pathogens (Tsang *et al*., 2019).

		compound						
		MC4	MC4-19	MC4-33	MC4-92	V[a]	O[b]	G[c]
		IC_{50} (μM)						
		24.8 ± 0.3	80.2 ± 2.0	83.4 ± 3.8	72.8 ± 0.9			
		% inhibition (125 μM)						
		71.7 ± 0.4	50.2 ± 0.7	47.9 ± 3.4	50.6 ± 4.9			
S. aureus	ATCC 25923	8	16	32	2	1	1	1
	ATCC 29213	16	16	16	4	1	0.3	1
	ST239	16	16	>64	>64	1	>64	>64
	ATCC BAA-43	8	16	>64	>64	1	>64	>64
	ATCC BAA-44	32	16	>32	>64	2	>64	>64
	HA W-231 ST45	32	16	32	64	1	4	16
	CA W-47 ST30	16	16	32	64	2	4	0.3
	CA W-45 ST59	16	32	>64	64	1	8	1
	CA W-46 ST59	16	16	32	32	1	8	1
	USA 300	16	16	32	32	1	32	1
	ST22	16	16	32	16	1	64	0.3
	CA W-4 ST338	16	16	32	16	1	1	0.3
	CA W-48 ST217	8	16	32	32	1	64	1
	HA W-235 ST5	8	16	32	8	1	>64	>64
Gram-(+)[d]	ECAS 25788	16	64	>64	>64	4	32	4
	SEPI 12228	>64	8	32	64	2	0.3	0.1
	SSAP 15305	16	32	32	>64	1	1	0.1
	SPNE 49619	>64	16	16	16	2	2	32
	SPYO 19615	32	16	16	>64	2	0.1	8
	SAGA 12386	256	16	>64	>64	1	0.5	32

[a]V: vancomycin. [b]O: oxacillin. [c]G: gentamicin. [d]ECAS: *Enterococcus casseliflavus*; SEPI: *Staphylococcus epidermidis*; SSAP: *Staphylococcus saprophyticus*; SPNE: *Streptococcus pneumonia*; SPYO: *Streptococcus pyogenes*; SAGA: *Streptococcus agalactiae.*

The new nusbiarylin compounds were tested by the *in vitro* NanoLuc PCA. MC4-134 and MC4-135 were shown to strongly inhibit the growth of *S. aureus* (Table 3.2) (performed by Miss Lin Lin). In the *in vitro* NanoLuc PCA, PPI inhibition by MC4-134 and MC4-135 was quantified as the dose-dependent curves (Figure 3.14).

Table 3.2 Antimicrobial activities of MC4-134 and MC4-135 against *S. aureus* 25923 and 29213.

	MIC (μg/mL)	
	S. aureus 25923	*S. aureus* 29213
MC4-134	0.5	0.5
MC4-135	0.25	0.5

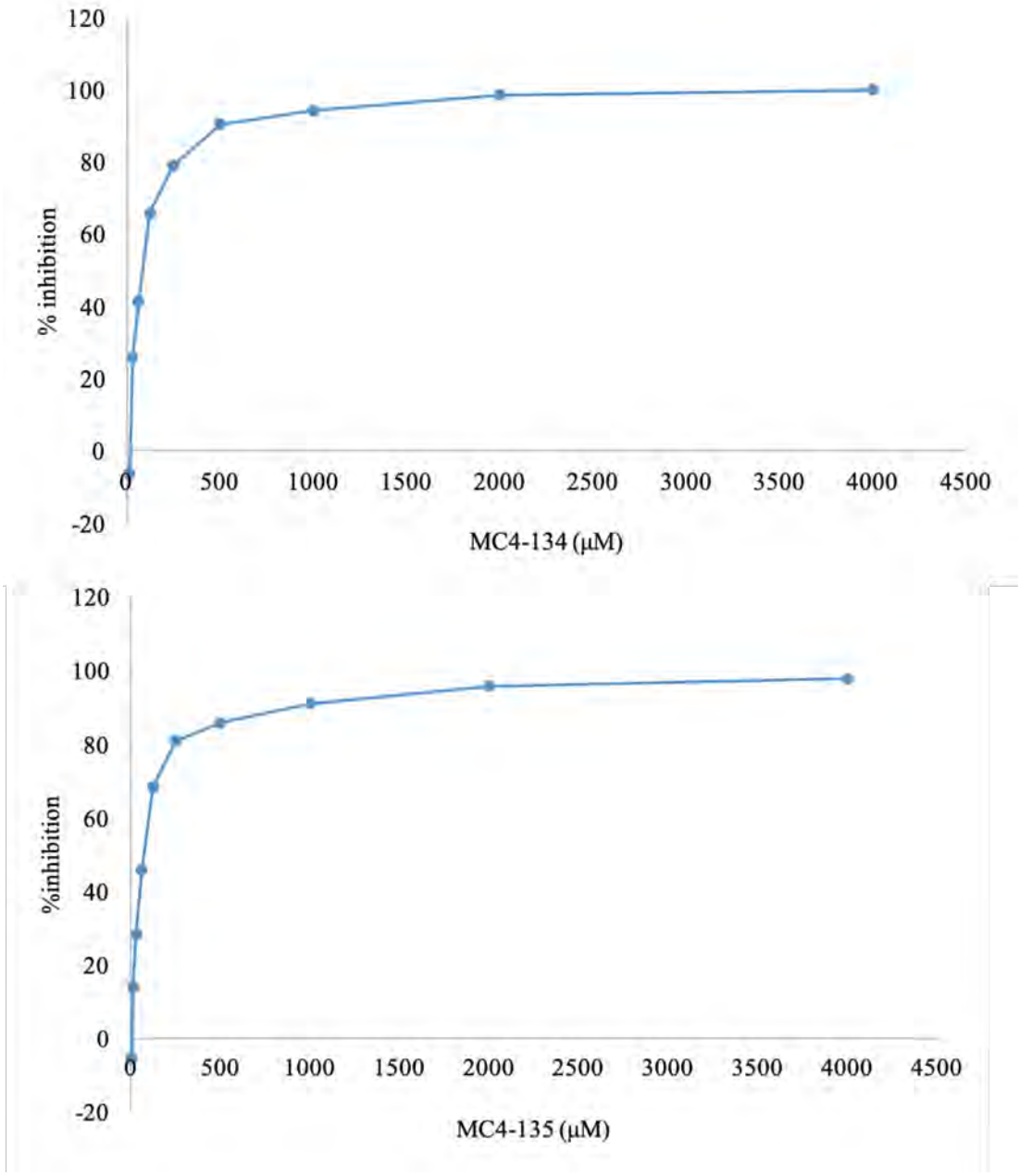

Figure 3.14 NusB - NusE PPI inhibition by MC4-134 and MC4-135 measured by the *in vitro* NanoLuc PCA.

3.4 Application of the NanoLuc PCA to study RNAP-σ^A PPI

3.4.1 Design and construction of the RNAP clamp helix fragments and σ^A overproduction plasmids

To further validate the assay, another critical PPI in bacterial transcription, the RNAP-σ^A interaction was chosen. As both σ^{70} and σ^A belong to the σ^{70} family (Narayanan *et al*., 2018; Johnston *et al*., 2009), the structure of *E. coli* holoenzyme was used to design the recombinant σ^A. The *E. coli* holoenzyme structure (Figure 3.15) revealed the σ^{70} CTD near to the RNAP CH domain. Thus, σ^A was tagged at the CTD, whereas CH was tagged at both NTD and CTD. To generate the overproduction plasmids, the gene *sigA* was cloned into pCU203 and pCU204, whereas the gene *rpoC(aa220- 315)* was cloned into pCU201, pCU202, pCU203 and pCU204 (Table 2.1).

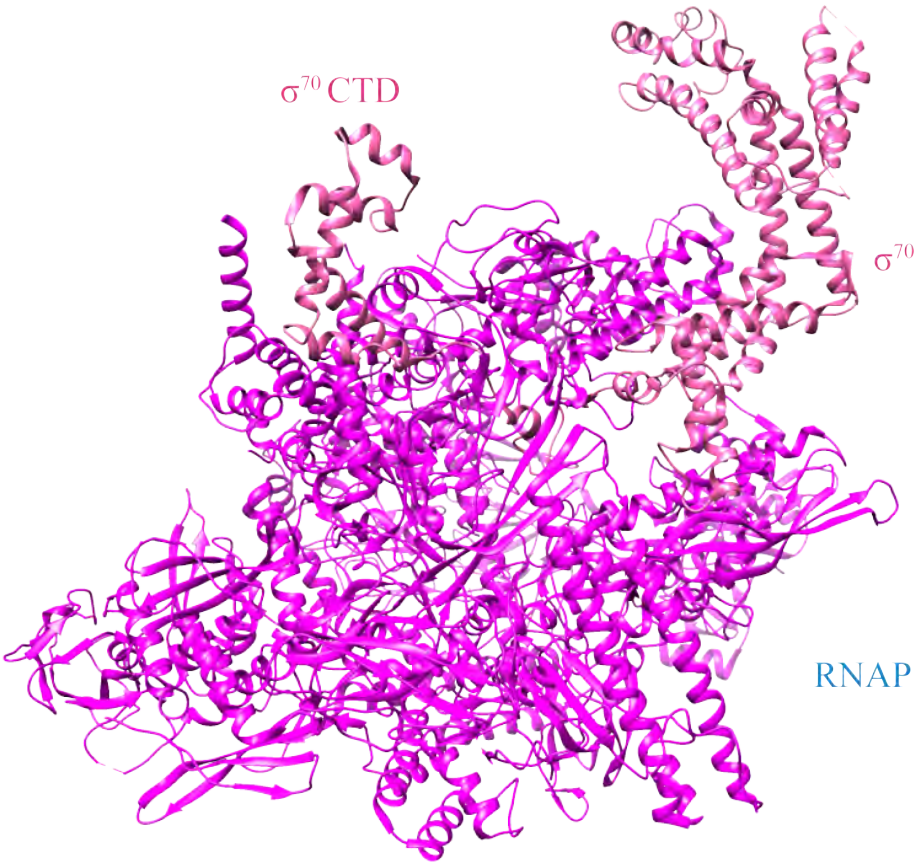

Figure 3.15 The structure of *E.coli* RNAP holoenzyme (PDB ID: 6C9Y).

3.4.2 Application of NanoLuc PCA for studying in vitro RNAP-σ^A interaction and PPI inhibitors

Small-scale protein overproduction was performed to check protein solubility. C-SmBiT-σ^A was pooly produced in the *E. coli* host, whereas C-LgBiT-σ^A and the SmBiT fusion CH fragments were overproduced as soluble proteins. Thus, C-LgBiT-σ^A, N-SmBiT-CH and C-SmBiT-CH were purified. The optimal light emission was identified when C-LgBiT-σ^A interacted with C-SmBiT-CH (data not shown).

C-LgBiT-σ^A was titrated against C-SmBiT-CH at a series of concentrations. As illustrated in Figure 3.16, two proteins reacted in a dose-dependent manner with the

K_d of approximate 0.71 μM. In contrast to the NusB - NusE interaction (K_d was approximate 1.5 μM), the RNAP - σ^A PPI gave a lower K_d. The difference in the K_d values meant 0.71 μM CH could interact with 50% molecules of σ^A, whereas NusE had to be at 1.5 μM to bind to 50% molecules of NusB. Thus, the data from the *in vitro* NanoLuc PCA suggested the PPI of RNAP - σ^A had stronger affinity. This is consistent to the fact that the RNAP-σ^A PPI is stronger than the NusB-NusE PPI. The inhibitor test was conducted using the previously identified RNAP-σ^A PPI inhibitor C5 (Yang *et al*., 2015; Figure 3.17A). The IC_{50} was found to be approximate 26 μM (Figure 3.17B). The result proved that the *in vitro* NanoLuc PCA could be used in characterizing PPIs of different strengths and PPI inhibitors.

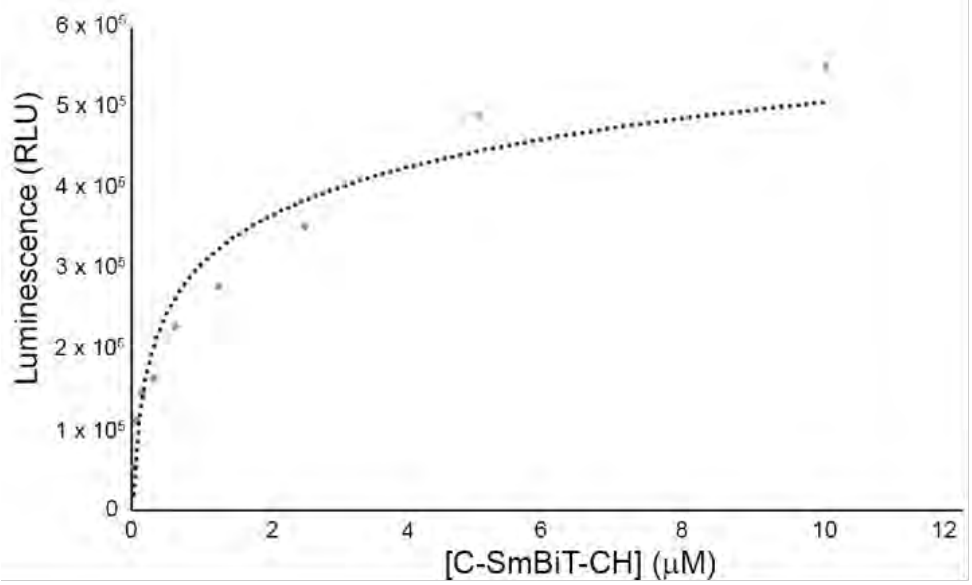

Figure 3.16 Titration of C-LgBiT-σ^A and C-SmBiT-CH at different concentrations (Tsang *et al*., 2019).

A

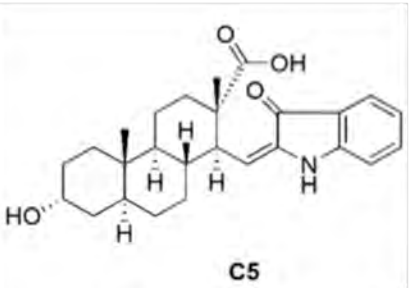

C5

B

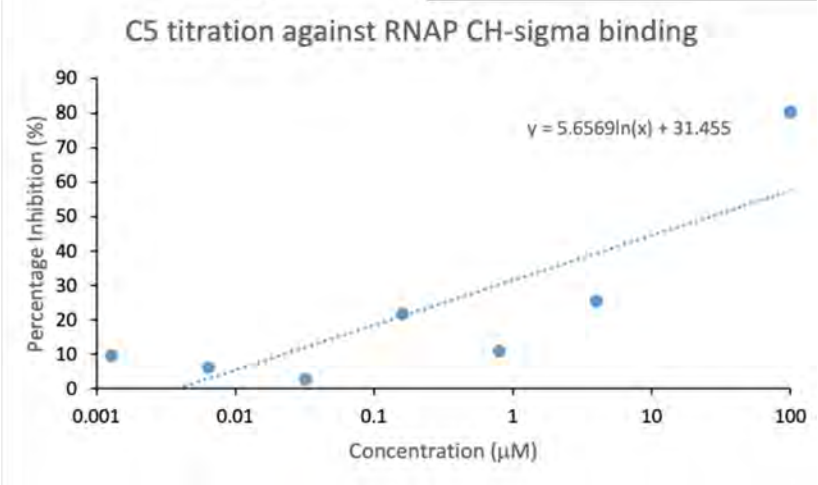

Figure 3.17 A. The chemical structure of C5. (Ye *et al*., 2019). **B.** Inhibition of C5 on the *in vitro* C-LgBiT-σ^A and C-SmBiT-CH interaction tested by the *in vitro* NanoLuc PCA (Tsang *et al*., 2019).

3.5 Discussion

3.5.1 Establishment of the PCA vector system

We generated the PCA plasmid system for tagging proteins with a 6 x His tag and the NanoLuc fragments (SmBiT or LgBiT). For proteins with resolved structures, the fusion protein could be designed based on the structural information. For two proteins with an unknown interaction mode, all combinations of the SmBiT/LgBiT tagging positions should be compared to optimize luminescence emission. Using the established PCA plasmid system, only a single cloning step was required prior to the protein overproduction plasmid constructions. Thus, the signal optimization process was simplified.

3.5.2 Experimental designs for the overproduction plasmids

In the design of recombinant proteins, the reading frame problem should be taken into account.

The gene insertion should be in the correct reading frame in order to properly transcribe the coding sequence. In fact, the PCA vectors have an additional stop codon between the *smbit*/*lgbit* genes and *MCS*. Also, the stop codon is in frame with the start codon (Figure 3.5). Thus, the stop codon should be removed during cloning to enable a complete recombinant protein. As shown in Figure 3.5. The unwanted stop codon is flanked by the set of recognition sites: *Xho*I, *Sac*I and *EcoR*I and another set of restriction sites: *Acc65*I and *Xba*I. To get rid of this stop codon, the restriction enzymes for cloning must be chosen from these two sets. For example, the overproduction plasmids of the recombinant NusB and NusE were cloned using *EcoR*I and *Acc65*I.

Factors beyond the experimental design also affected the signal optimization process. For example, C-SmBiT-σ^A was poorly produced in the *E. coli* host. To enable the protein purification, C-LgBiT-σ^A was overproduced and purified.

3.5.3 Possible improvements for the assay

We demonstrated successful applications of the *in vitro* NanoLuc PCA for quantifying PPIs. Due to the mild catalytic activity of LgBiT, the LgBiT fusion protein was used as the negative control to indicate the background signal. However, other possibilities of interference with the assay were not completely excluded in current study. For

instance, decrease in the luminescence emission could be due to PPI inhibition, but inhibition of the luciferase enzyme activity probably partly contributed to the decrease. If the compound-luciferase interaction took place, the PPI inhibition would be overestimated. To examine if any interference with the NanoLuc activity by MC4. 1 μM NanoLuc enzyme was titrated against MC4 at a series of concentrations. MC4 was indicated to have no significant interference with the NanoLuc activity (data not shown). Additionally, MC4 were similarly quantified in the investigation compared to the previous investigation (Yang *et al*., 2017). Thus, the compound-luciferase interaction did not significantly interfere with the *in vitro* NanoLuc PCA when studying nusbiarylins. Nevertheless, the control reaction of the intact NanoLuc plus inhibitors could be included for future researches of other PPI inhibitors.

To prove the NanoLuc reformation from a specific PPI only, another control reaction could be added. For example, a pair of non-interactive proteins tagged by the NanoLuc fragments could be included. This control reaction could indicate no NanoLuc reformation without a specific PPI. An engineered alkane dehydrogenase, namely HaloTag, was chosen since this enzyme has no interaction with any bacterial transcription factors. By including the LgBiT fusion HaloTag as the control reaction, we could show that the NanoLuc refolding preferably took place upon a specific PPI.

Chapter 4: Construction of reporter strains for promoter study

4.1 Construction of the *E. coli* reporter strains

4.1.1 Experimental design

E. coli reporter strains were made to examine the disruption of nusbiarylins to the bacterial rRNA transcription. To achieve this, a previously established plasmid-borne reporter system (Li *et al*., 1984) was applied. The system was composed of three plasmids pSL102, pSL103 and pSL115, expressing *chloramphenicol acetyltransferase* (*cat*) under the control of *E. coli rrnG* promoter P_2 (Figure 4.1). pSL102 was selected as the positive control to show normal transcription without disruption. pSL103 was used as the negative control to represent low read-through (Figure 4.1). pSL115 was previously engineered to have an antiterminator sequence at the leader region (Li *et al*., 1984). *boxA* (TGCTCTTTAA), *boxB* (CTGAGAAAAAGCGAAGCGGCA) and *boxC* (TGTGTGGG) were identified in pSL115. The reporter gene expression was inspected by dot blot. Theoretically, NusB enables a complete transcript when *boxA* presents. Thus, nusbiarylins treatment should be able to alter the reporter gene transcription. To avoid the assay interference by variation in the plasmid copy numbers, an additional *bla* gene in the same plasmid was used to correct the *cat* mRNA amount.

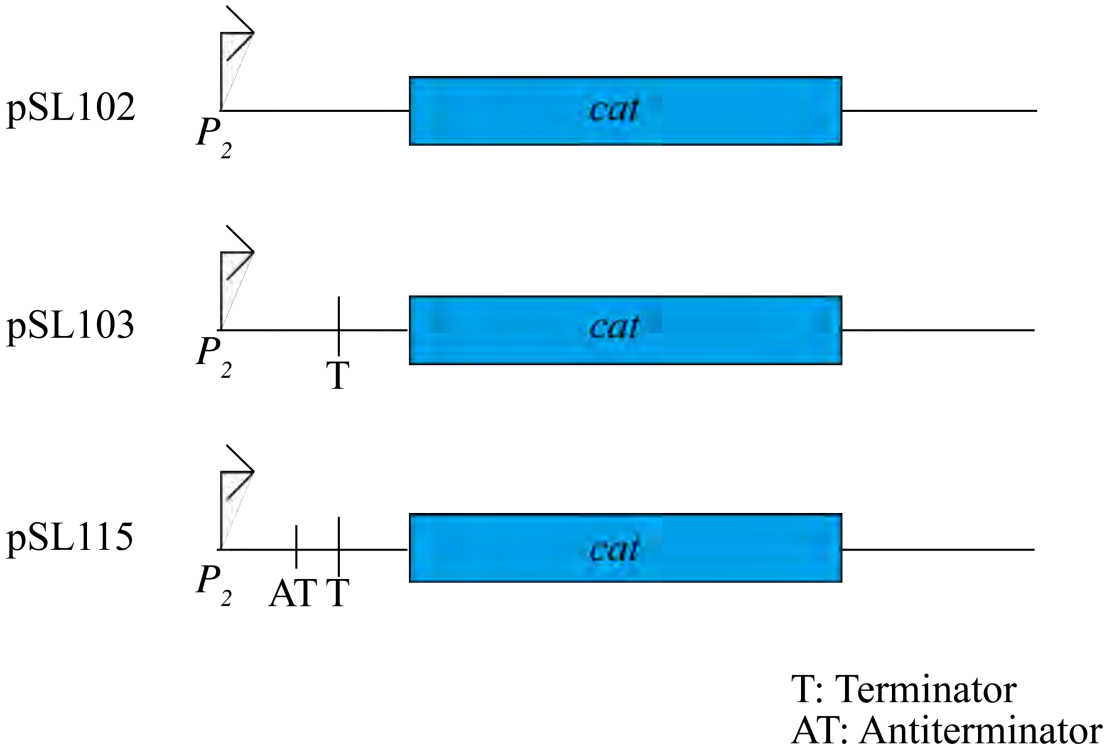

Figure 4.1 pSL102, pSL103, and pSL115 for *E. coli* reporter strain constructions. pSL102 and pSL103 were used as the positive and negative controls respectively. pSL115 was used to show the bypass of the Rho-terminator upstream the *cat* gene. P_2, *E. coli rrnG* promoter P_2; *T*, Rho-terminator; AT, antiterminator; *cat*, *chloramphenicol acetyltransferase*. Adapted from Li *et al*., 1984.

In this study we applied the plasmid-borne system to investigate the reporter gene transcription when the bacterial cells were treated with MC4-134. Since MC4-134 showed MIC of 32 μg/mL against *E. coli* 25922 in the broth microdilution assay (performed by Miss Lin Lin).

4.1.2 Optimization of non-radioactive RNA dot blot detection

Three reporter plasmids pSL102, pSL103 and pSL115 were obtained from the Coli Genetic Stock Center in Yale University. The prior researches made use of the plasmid-borne system in exploring the NusB role in rRNA transcription (Li *et al*., 1984; Torres *et al*., 2004). Hereby we exploited the same system to highlight the transcriptional effects of nusbiarylins.

To analyze the reporter gene expression, total RNA was extracted from *E. coli* for dot blot. Previous studies used radioactive DNA probes for RNA detection (Torres *et al*., 2004). Because of the difficulties in handling radioactive substances, non-radioactive approaches were decided for our study. A non-radioactive label biotin was selected for detection. The detection was based on the interaction between biotin and streptavidin conjugated horseradish peroxidase (HRP). As the change in the detection method, we first tested the feasibility of biotin-based dot blot detection for inspecting the reporter gene expression.

In the first test, the *E. coli* reporter strain carrying pSL102 was investigated as the *bla* and *cat* genes could be constitutively expressed. 1.5 μg total RNA from the *E. coli* transformants were extracted and hybridized with 30 ng/mL *bla* probe at 55^{o}C. The *bla* expression could be specifically detected from the transformant cellular RNA as shown in Figure 4.2. However, the background signal was higher than expected potentially due to the non-specific binding of the probe. In the second test, the *bla* and *cat* probes were used to detect the *bla* and *cat* transcripts using 1.5 μg and 10 μg

cellular RNA. To minimize the background signal from non-specific probing, the hybridization temperature was lowered to improve the probe binding and a more stringent wash was used to remove the non-specific bindings. As shown in Figure 4.2, the signal to noise ratio was improved. The dot intensities escalated with the increasing amounts of the input RNA. Notably, faint dots were found when the wildtype *E. coli* RNA was probed. The non-specific interaction could be due to the high concentration (100 ng/mL) of *bla* probe (Figure 4.2). Refinement of the probe concentrations will be carried out in the future studies.

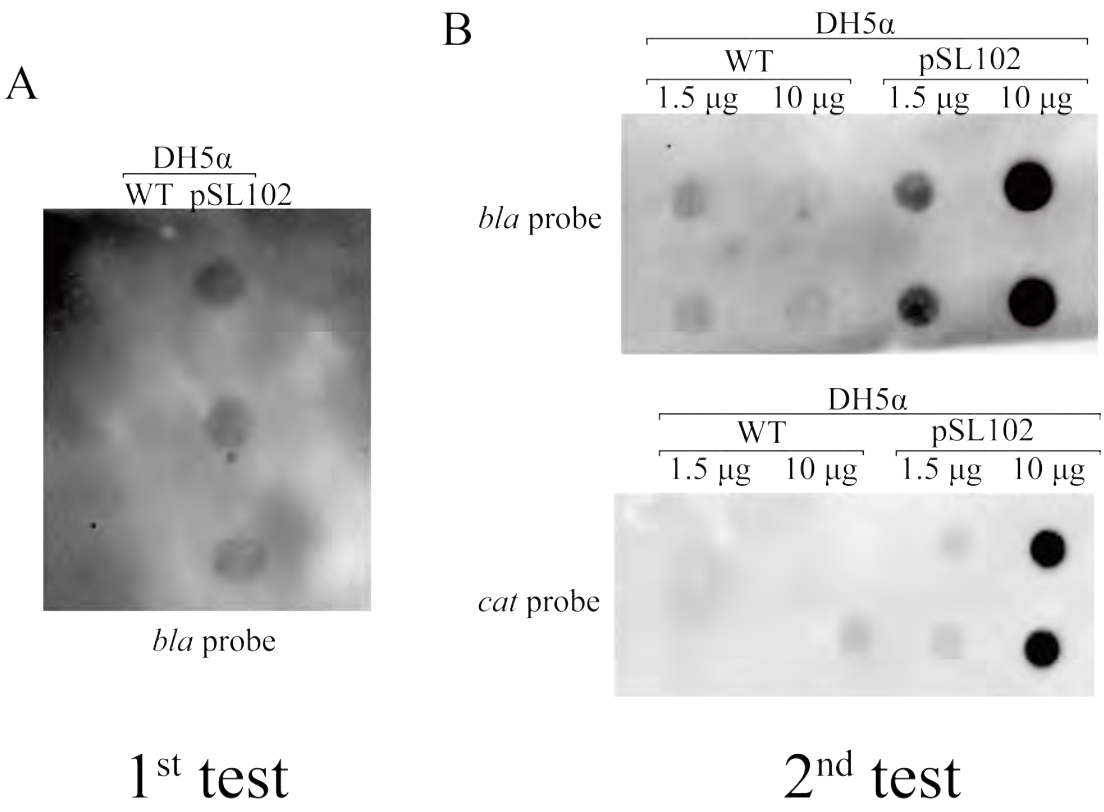

Figure 4.2 Dot blot results of inspecting the *bla* and *cat* gene expressions in the reporter strain carrying pSL102. **A.** The detection of the *bla* gene expression in the pSL102 transformant. The hybridization temperature was performed at 55^{o}C and the low stringency wash was applied. **B.** The detection of the *bla* and *cat* gene expressions in the pSL102 transformant. The hybridization was performed at 50^{o}C and the higher stringency wash was done.

4.2 Development of the *B. subtilis* reporter strains

4.2.1 Construction of the NanoLuc reporter plasmid

Most nusbiarylin compounds did not inhibit *E. coli* growth. Thus, the *E. coli* reporter strains could not be applied to some MC4 analogues that strongly suppressed the growth of Gram-positive bacteria only. Instead, *B. subtilis* reporter strain provided an alternative choice to characterize the transcription inhibitors.

pSG1729 was a plasmid designed to fuse a reporter gene into the *B. subtilis amyE* gene in the previous studies (Lewis and Marston, 1999). In the investigation, pSG1729 was selected as the parent vector to make the NanoLuc reporter plasmid pCU314 (Figure 4.3). A xylose-inducible promoter controlled the reporter gene expression. Following transformation, the reporter gene and the promoter could be inserted into the *B. subtilis amyE* locus through double cross over (Figure 4.4). During the investigation, we examined the possibility of NanoLuc as the reporter enzyme in *B. subtilis*. The gene *nanoLuc* was cloned into pSG1729, resulting in the NanoLuc reporter plasmid pCU314 (Figure 4.3). pCU314 was then transformed into the *B. subtilis* 168 strain.

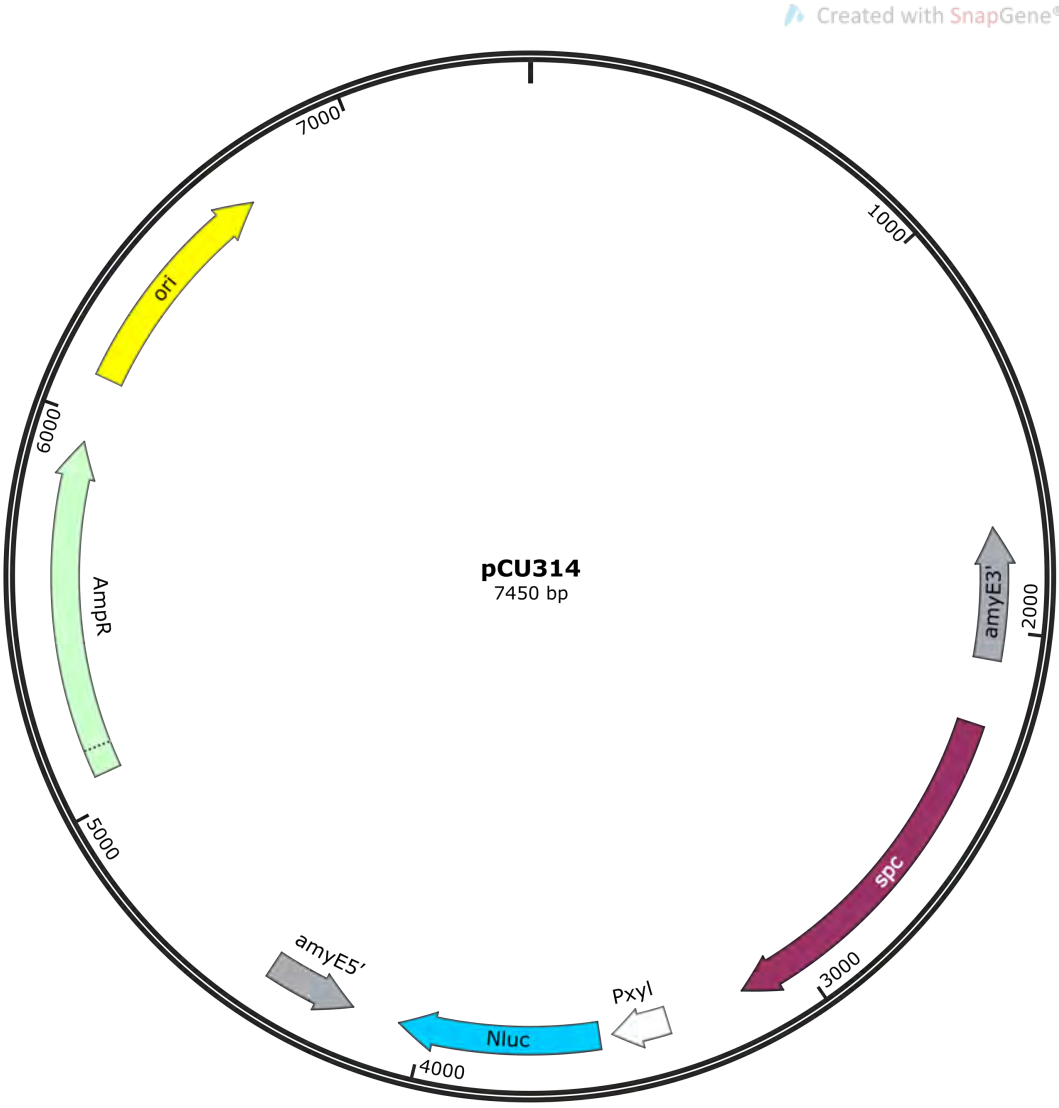

Figure 4.3 The NanoLuc reporter plasmid pCU314. The *nanoLuc* gene expression is under the control of xylose inducible promoter P_{xyl}. *spc* is the selective marker for the transformant. The *amyE* gene fragments facilitated double crossover for the *nanoLuc* gene insertion into the *B. subtilis amyE* gene.

The gene *amyE* is responsible for synthesizing an enzyme amylase that hydrolyzes starch into glucose monomers (Liu *et al*., 2015). The insertion of P_{xyl} and *nanoLuc* into the *amyE* locus inactivated the amylase biosynthesis. As a result, the transformant did not produce the functional amylase to hydrolyze starch. To distinguish the pCU314 transformant from the wildtype *B. subtilis* 168, the colonies resulting from the

transformation were grown with 1% starch on a LB agar. Eventually, the colonies were stained by iodine solution. If the intact starch existed, dark blue color would develop in the colonies. This suggested the disruption of amylase biosynthesis and thus the gene insertion at the *amyE* locus.. Successful recombinant *B. subtilis* strain was named BS2019 (Table 2.1).

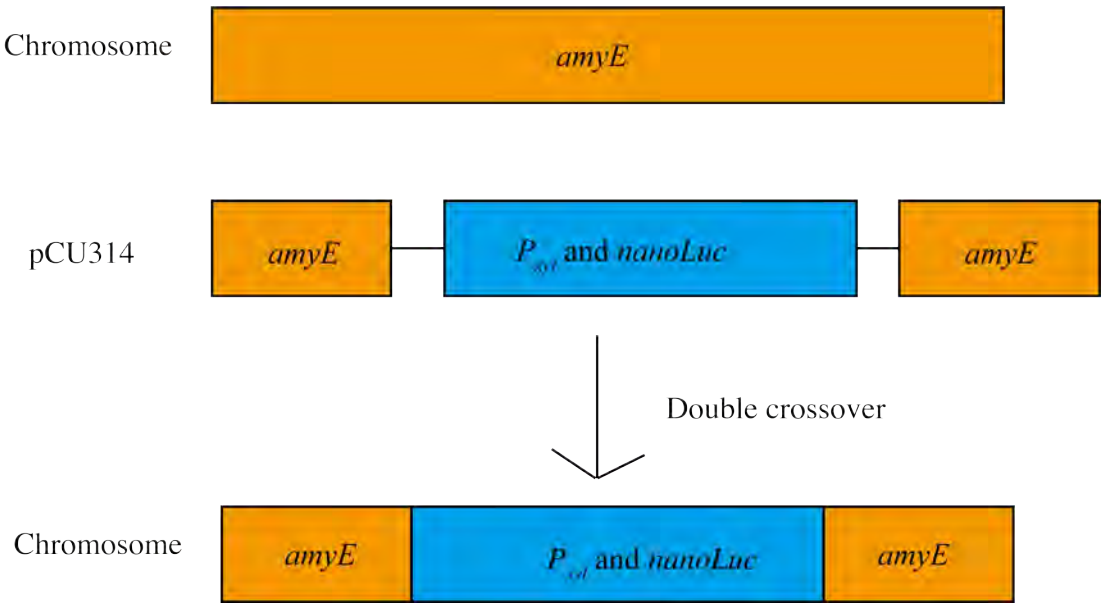

Figure 4.4 Schematic diagram presenting the double crossover between the *B. subtilis* chromosome and pCU314 plasmid. The homologous part of *amyE* gene in the pCU314 aligns with the *amyE* gene in the chromosome, resulting in the chromosomal incorporation of the promoter-*nanoLuc* gene construct by double cross over.

4.2.2 Examination of the *NanoLuc production in recombinant B. subtilis*

Experiment was then conducted to examine if functional NanoLuc was made by BS2019. BS2019 was grown in LB media supplemented with or without 1% xylose. The overnight culture was harvested and lyzed. The luminescence emission due to the NanoLuc enzyme activity was measured from the cell lysate. With the xylose induction, the cell lysate released 70-fold brighter luminescence than the no xylose control group (Figure 4.5). The data suggested that the *nanoLuc* gene expression was induced by xylose treatment and the active enzyme was synthesized.

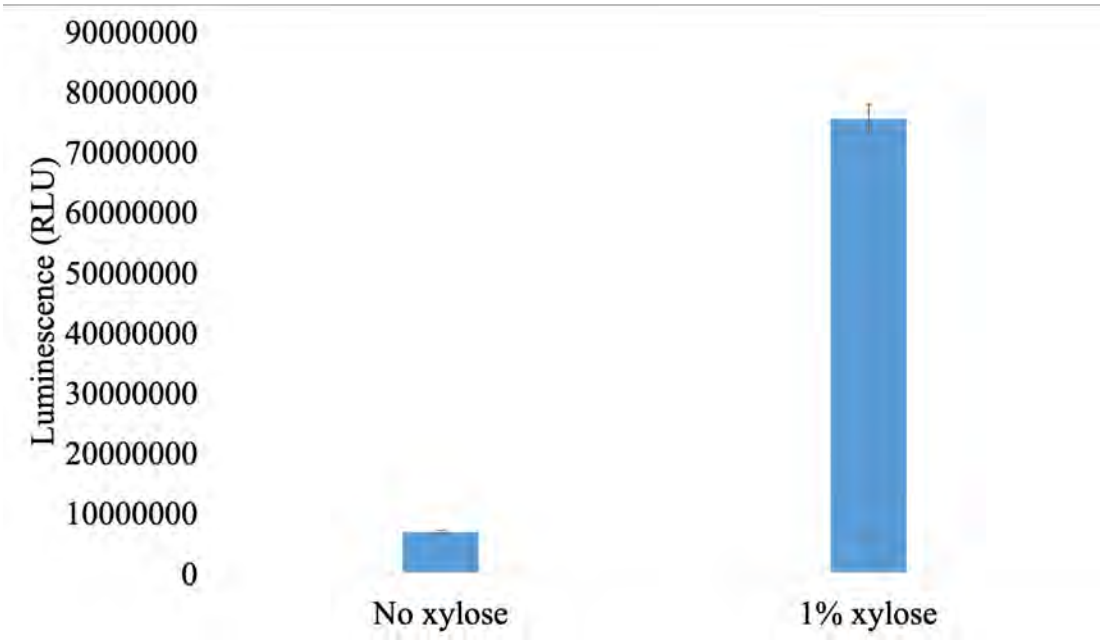

Figure 4.5 The luminescence signal generated from BS2019 with or without the xylose induction

4.3 Discussion

4.3.1 Optimization and test using the E. coli reporter strain

Using the cellular RNA from *E. coli* pSL102 transformants, the constitutive expression of *bla* and *cat* were successfully detected by the biotin-based RNA detection. Nonetheless, the signal optimization was required. In the first test, the *bla* mRNA was detected but the signal-to-noise ratio was low (Figure 4.2). This could be mainly attributed to two factors: the insufficient RNA input and the suboptimal hybridization procedure. First, pSL102, pSL103, and pSL115 are low copy number plasmids. Consequently, the *bla* mRNA could be scarce in cellular RNA. To deal with this issue, amounts of input RNA and DNA probes were increased to improve the positive signal. Second, the background noise signal could be high when the hybridization was not performed properly. For example, the high hybridization temperature hindered DNA probe binding to the complementary RNA and the low stringency wash could not fully remove non-specific binding. Therefore, the hybridization temperature was lowered and a higher stringency wash was adapted in the second test. As a consequence, the dot intensity was apparently improved in the second test. 10 μg total RNA were found to give the dense dots when detected by the *bla* and *cat* probes (Figure 4.2).

In spite of the improved signal-to-noise ratio, minor non-specific bindings were seen when the wildtype *E. coli* cellular RNA was hybridized with the *bla* or *cat* probes. Since the non-specific signals were not observed when 1.5 μg cellular RNA was hybridized with the *cat* probes, the non-specific signals could be attributed to the elevated input of RNA or DNA probes. Further optimization will be required.

4.3.2 Substitution of the reporter genes for studying transcription and translation effects

Nusbiarylins were designed to inhibit the bacterial rRNA transcription. To clarify the consequence of transcription inhibition, the reporter gene translation could be examined. Since the reporter enzyme chloramphenicol acetyltransferase did not result in the release of luminescence or fluorescence, the current *E. coli* reporter strains were not readly be used for examining the change in the reporter gene translation. For future researches, the gene *nanoLuc* could be used as the reporter. The *nanoLuc* gene expression could be checked by dot blot and the measurement of NanoLuc activity could reflect the reporter gene translation. Consequently, the inhibitory effects of nusbiarylins could be examined at the levels of transcription and translation by the reporter strain carryinging the *nanoLuc* gene.

4.3.3 Modification of pCU314 for B. subtilis reporter strains to study MC4 compounds

BS2019 demonstrated successful production of functional NanoLuc. To make the reporter strain specialized for the nusbiarylins study, the *B. subtilis rrnB* promoter P_1, the *nut* site, and the Rho-terminator could be cloned into the promoter region of pCU314. Supposedly, the NusB-NusE PPI could result in antitermination to enable the reporter gene expression. If nusbiarylins inhibited the NusB-NusE interaction, the *nanoLuc* gene expression would be suppressed by the Rho-terminator. The resulting gene expression level could be evaluated by dot blot.

Chapter 5: Crystallographic investigation of NusB-nusbiarylins interactions

5.1 Purification of *T. maritima* NusB

5.1.1 Construction of the NusB overproduction plasmid

To identify the NusB-nusbiarylins interaction mode to atomic resolution, crystallographic approach was carried out to determine the crystal structures of NusB-nusbiarylin complexes. Co-crystallization was applied to obtain the NusB-nusbiarylin crystals. To enable the NusB stability throughout co-crystallization with the nusbiarylin compounds, NusB original from the thermophilic bacteria *T. maritima* was selected.

To make the protein overproduction plasmid of TmaNusB, the *tmanusB* gene of 400 bp was cloned into pNG209. In PCR colony screening, the PCR product of 400 bp was detected in DNA gel electrophoresis. Thereby the gene insertion was extrapolated. No mutation was identified in Sanger sequencing. The resulting protein overproduction plasmid was termed pCU173 (Table 2.1), encoding the non-tagged TmaNusB.

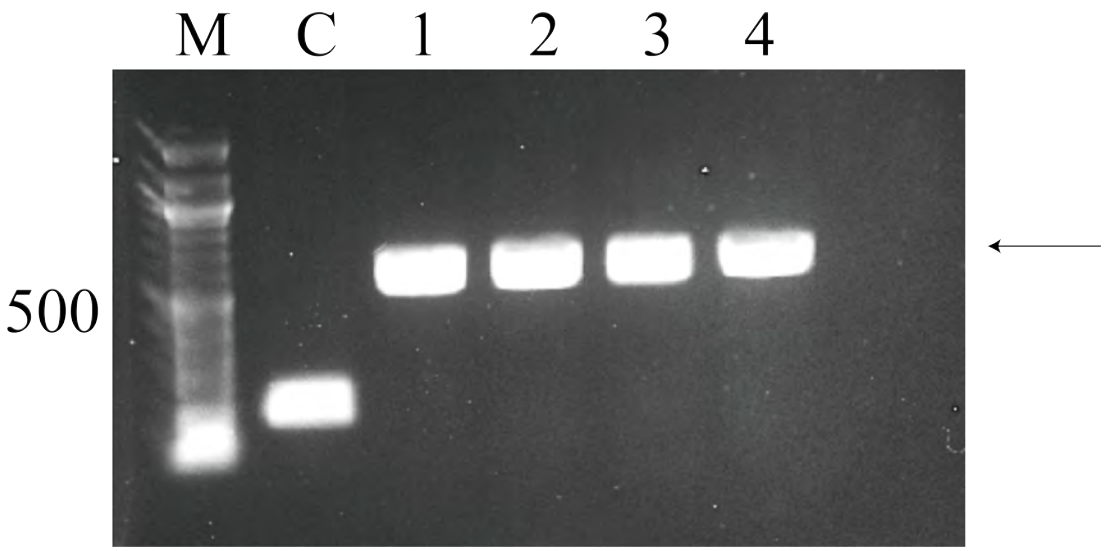

Figure 5.1 Colony screening for *T. maritima nusB* cloned into the pNG209. 1- pNG209 (200 bp); 2 - 5- colonies picked.

5.1.2 Purification of NusB for crystallization

With reference to the prior study (Bonin *et al*., 2004), TmaNusB was initially purified through 80^{o}C heat shock and gel filtration. Following the 80^{o}C heat shock, TmaNusB was purified by gel filtration but the resulting protein purity was inadequate for structural study. During gel filtration, multiple elution peaks were observed (Figure 5.2A), suggesting the impurities that were not removed by heat shock. Although the summary gel showed a dense band representing the expected molecular weight of TmaNusB (Figure 5.2B), some minor impurities existed. In the first crystallization experiment, only small needle crystals were observed, probably due to these minor impurities.

A

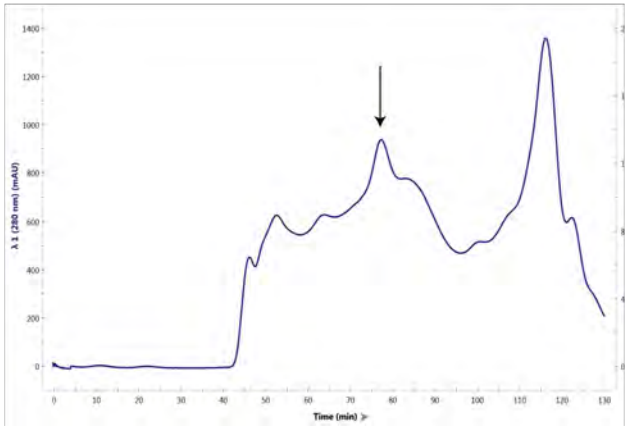

B

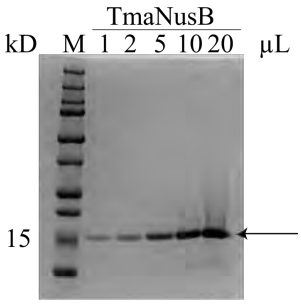

Figure 5.2 The first TmaNusB purification result. **A.** The elution profile of the *E. coli* heat-resistant fraction during gel filtration. The black arrow indicates the elution peak of TmaNusB. **B.** Summary gel of TmaNusB purification. The black arrow indicates the band representing TmaNusB.

To improve the protein purity, the heparin column was applied to purify TmaNusB because NusB is an RNA binding protein. As illustrated by the purification gel in Figure 5.3A, a 15 kD band corresponding to TmaNusB presented in the heat-resistant fraction and the elution fractions. This implied that TmaNusB bound to the column and was eluted by the NaCl gradient. The TmaNusB fractions were further purified by gel filtration. The elution profile was monitored by the absorbance at 280 nm. A major peak was obtained around 77 mL (Figure 5.3B), the peak fractions were pulled together. The purified protein was concentrated to 17 mg/mL prior to the crystallization. In the summary gel of TmaNusB purification, the dense band corresponding to the TmaNusB molecular weight presented (Figure 5.3C). On the other hand, a major impurity between 25 kD and 37 kD existed, potentially attributed to the NusB dimerization. The purified TmaNusB was then crystallized alone or with nusbiarylins before X-ray diffraction.

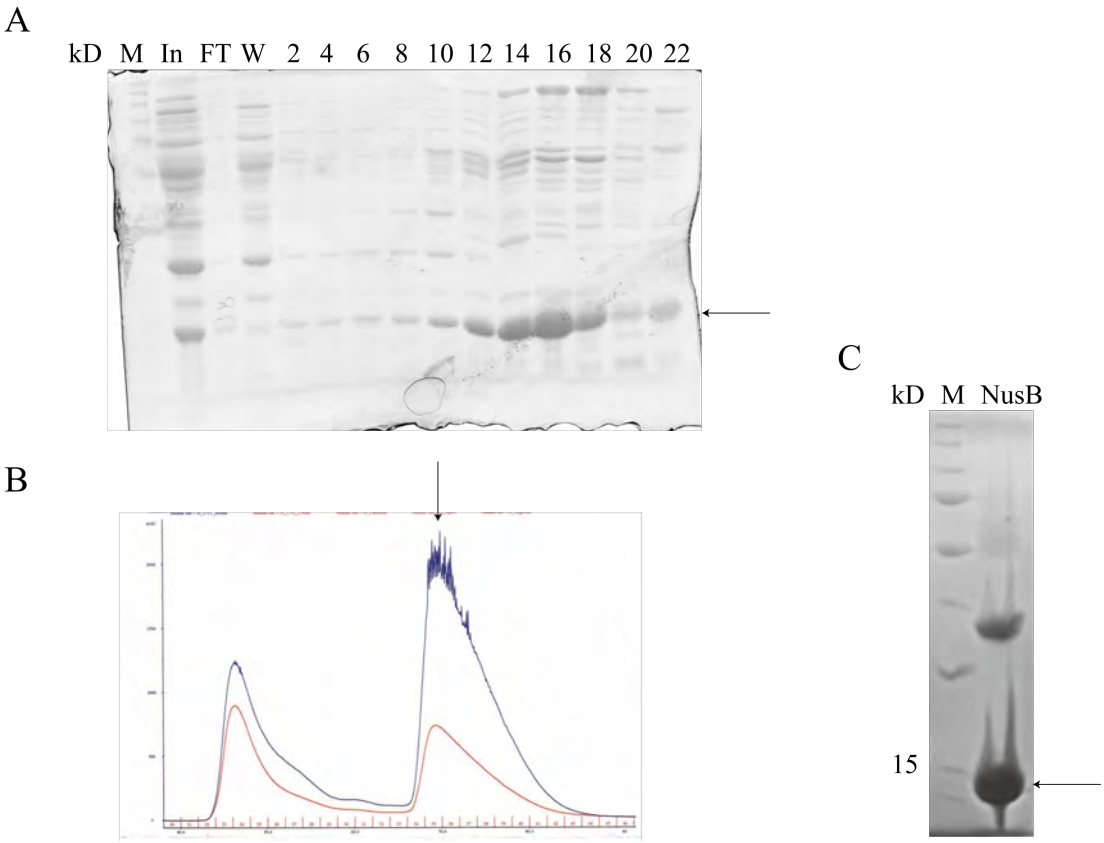

Figure 5.3 A. Purification of TmaNusB from the heparin column. The black arrow indicates the band representing TmaNusB. M- marker; In- input; FT- flow through; W- wash; 2, 4, 6, 8, 10, 12, 14, 16, 18, 20- elution fractions. **B.** Elution profile from gel filtration. **C.** Summary gel of the TmaNusB purification. The band representing TmaNusB is indicated by the black arrow.

5.2 Structural studies of NusB-MC4 compounds interaction

5.2.1 NusB crystallization

The NusB crystallization condition was screened using the commercial kits. Total 13 conditions gave crystals of different shapes, such as needle clusters and single needle crystals. The most promising one was the cubic-shaped crystals in 2.8 M sodium acetate trihydrate at pH 7.0 (Figure 5.4A). To maximize the crystal size, sodium acetate trihydrate concentrations ranging from 2 to 3.4 M were tested. Crystals did not develop

at low salt concentrations from 2 to 2.4 M. The small cubic crystals developed in 2.6 to 2.8 M sodium acetate, whereas the larger crystals were found when the salt concentration was above 3 M (Figure 5.4B).

To distinguish between salt and protein crystals, the unknown crystals were stained by the protein dye (Figure 5.5). After incubation, the blue crystals were observed, meaning proteins. The reason was that only protein crystal had a solvent channel that absorbed dye, whereas salt crystal without the solvent channel did not absorb any blue dye molecule.

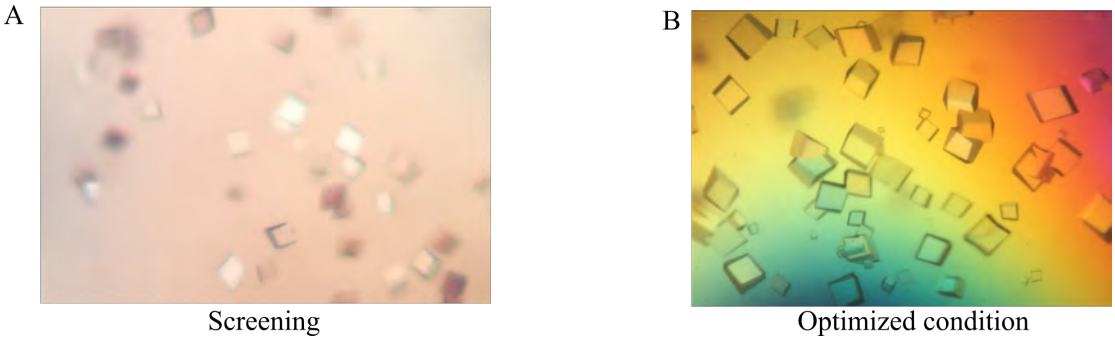

Figure 5.4 A. The crystal image from initial screening using TmaNusB alone. **B.** Optimized crystals by altering the sodium acetate concentration.

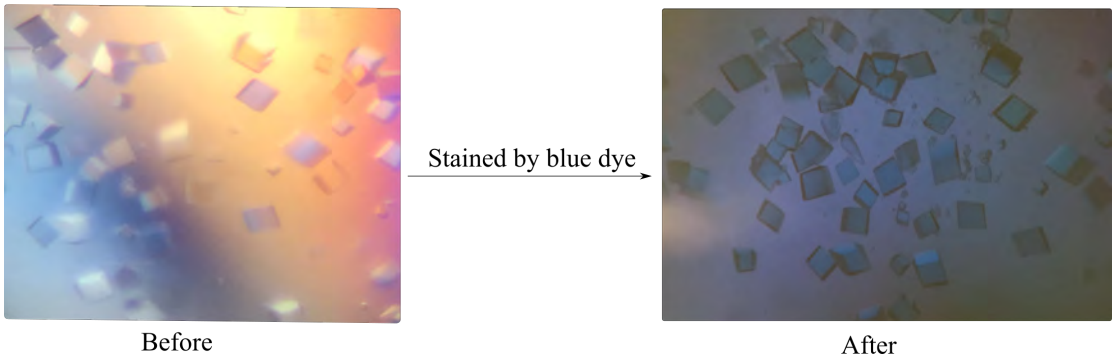

Figure 5.5 The test to confirm protein crystals. The droplet containing unknown crystals was mixed with the dye, incubated at room temperature for at least 5 minutes. The incubation resulted in the crystals in blue color.

5.2.2 Co-crystallization of NusB with MC4-134 or MC4-150 or MC4-152

Three nusbiarylin compounds, MC4-134, MC4-150 and MC4-152, were chosen for crystallographic examination because of the strong antimicrobial activities against *S. aureus* (performed by Miss Lin Lin) (Table 5.1). The structural determinations were attempted by soaking and co-crystallization. For the compounds to form complex with TmaNusB in the crystal form, the optimized protein crystals were transferred into the inhibitor droplets with 0.1 or 1% DMSO. After overnight incubation, the protein crystals remained intact.

Table 5.1 Antimicrobial activities of MC4-134, MC4-150 and MC4-152 against the *S. aureus* strains.

	MIC (μg/mL)		
	MC4-134	MC4-150	MC4-152
S. aureus 25923	0.5	0.5	0.5/1
S. aureus 29213	0.5	0.5	0.5/1

Alternatively, co-crystallization was performed to obtain the NusB-nusbiarylin complex crystals. The purified TmaNusB and the compounds were mixed for complex assembly. The crystallization condition was screened using the commercial kits, crystals developed in different shape. The crystal development suggested that TmaNusB or the compounds or the TmaNusB-compound complex formed the crystals. When TmaNusB was co-crystallized with the MC4-150, hexagonal crystals were repeatedly observed in various conditions (Figure 5.5). Apparently the existences of the hexagonal crystals suggested MC4-150 crystals. To identify if TmaNusB presented

in the unknown crystals. SDS-PAGE was performed. The 15 kD band representing the NusB molecular weight was found (data not shown). The result manifested that the hexagonal crystal could be formed by TmaNusB or TmaNusB in complex with MC4-150. When NusB was co-crystallized with MC4-150 or MC4-152, numerous conditions resulted in the crystal development. The conditions that gave 3D and large crystals were optimized to acquire the high-quality crystals (Figure 5.6).

To get rid of the nusbiarylin compound crystals, the mixture of TmaNusB and MC4-150 was dialyzed to remove the unbound inhibitors. The protein or the protein-ligand complex was concentrated to 10 mg/mL. Due to lower protein concentration, the mixture was incubated at 22^{o}C to facilitate the crystal development. Eventually the planar 2D crystals developed as shown in Figure 5.6.

Crystal 1

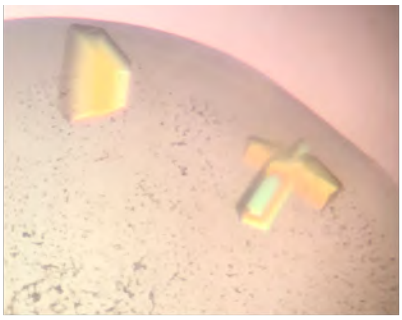

Crystal 2

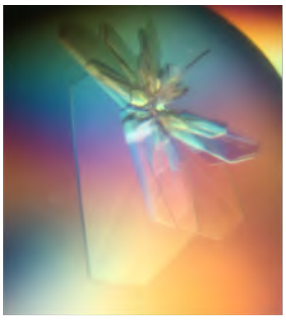

Crystal 3

	Crystal 1	Crystal 2	Crystal 3
TmaNusB + MC4-150/152	MC4-150	MC4-152	MC4-152
Methods to complex assembly	Incubation at 30°C	Incubation at 30°C	Dialysis at 4°C
Crystallization conditions	0.2 M $MgCl_2$ 0.1 M Tris pH 8.5 25% w/v PEG 3350	0.2 M Succinic acid pH 7.0 15% w/v PEG 3350	0.2 M Ammonium acetate 0.1 M Tris pH 8.5 25 % w/v PEG 3350

Figure 5.6 Crystal images and crystallization conditions in the study.

5.3 Diffraction data

The protein crystals from TmaNusB or the TmaNusB-nusbiarylins mixture were subjected to X-ray diffraction in the synchrotron facility BESSY II. The data were analyzed using molecular replacement in Phenix and the inspection of electron density representing the compound was done by Coot. In the electron density map of the expected nusbiarylins-interacting site, no electron density of nusbiarylins could be found in the expected position (Figure 5.7).

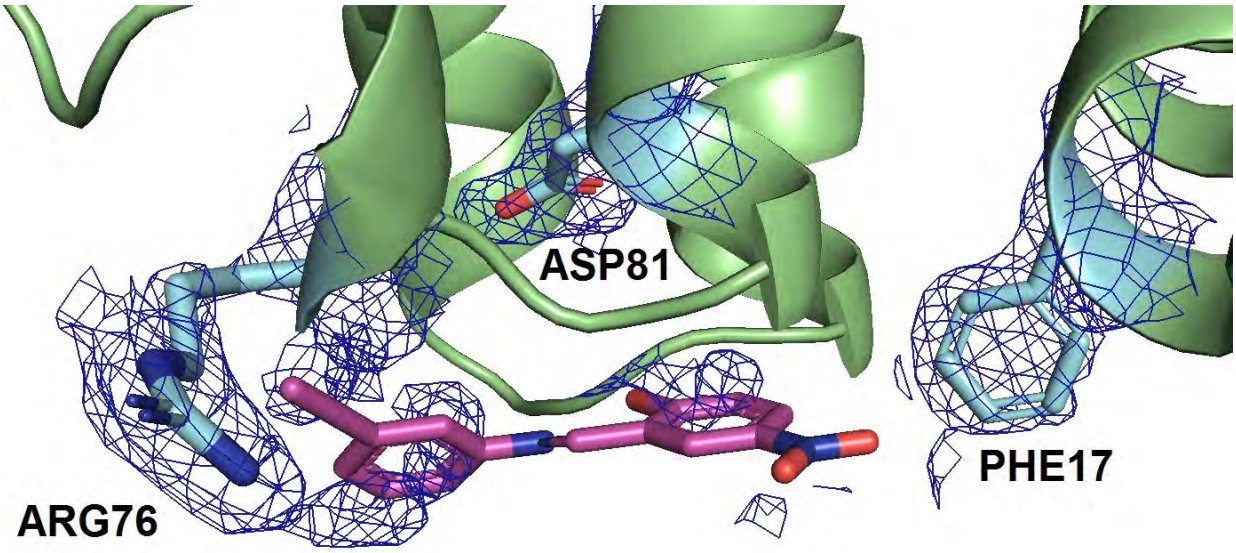

Figure 5.7 The electron density map constructed from analyzing the diffraction data. No compound molecule, MC4-134, was identified in the expected interaction surface on NusB.

5.4 Discussion

5.4.1 TmaNusB purification for structural study

For the crystallographic study, NusB from the thermophilic bacteria *T. maritima* was chosen for the high protein stability. The protein overproduction plasmid of the non-tagged TmaNusB was made by inserting a stop codon upstream of the *6 x his* gene.

Initially, TmaNusB was purified by heat shock and gel filtration. However, the resulting protein purity was low. The possible reason was probably the suboptimal purification procedure. Although most *E. coli* proteins were denatured and removed by heat shock, some heat-stable proteins could not be fully destroyed. As a result, these proteins contributed to the low protein purity. To obtain the highly pure TmaNusB, an affinity purification step using the heparin column was performed prior to gel filtration. With the two-step purification for the heat-resistant fraction, the pure TmaNusB was

obtained.

5.4.2 Crystals of TmaNusB for structural determination

The purified TmaNusB was used for structural characterization of NusB-nusbiarylin complexes. As aforementioned, the suboptimal purification procedure gave TmaNusB of low protein purity. The impure TmaNusB was used for crystallization but only small needle crystals developed. Following the optimization of purification process, crystallization was repeated with the pure TmaNusB. Eventually the 3D cubic protein crystals were obtained. However, the summary gel showed a major impurity of around 25 to 37 kD (Figure 5.3C). Since the NusB dimerization was observed in several prior studies (Altieri *et al*., 2000; Gopal, 2000; Bonin *et al*., 2004), the impurity was deduced to be the NusB dimer of around 30 kD.

To acquire the NusB-nusbiarylin complex in the crystal forms, soaking and co-crystallization were performed. In soaking, the NusB crystals were placed in the inhibitor droplets, theoretically the inhibitors diffused into the NusB crystals when interaction occured. As nusbiarylins favor DMSO as the solvent, the protein crystals were incubated at various DMSO concentrations to examine the crystal stability. After overnight incubation, the TmaNusB crystals remained intact at up to 5% DMSO, probably due to the high protein stability. Nevertheless, the crystals soaked with the compounds were not used for X-ray diffraction because the nusbiarylins were not expected to efficiently interact with the NusB crystals. The initial compound MC4 was designed according to the NusB conformation in complex with NusE. Upon NusE

binding, E75 of NusB could be shifted to the position near to the R16 residue of NusE (Luo *et al*., 2008). Thus, this conformational change was probably required for nusbiarylins to function. However, the NusB conformation should be inflexible when NusB was in crystal form. Thereby, the interaction between the nusbiarylin compounds and NusB crystals was estimated to be minimized. Instead, during co-crystallization the NusB-nusbiarylin complex formed before being crystallized. Therefore, co-crystallization was preferred.

During the co-crystallization, TmaNusB and the compounds were mixed prior to crystallization. To maximize the amounts of TmaNusB-nusbiarylin complexes in the mixture, the protein was mixed with excess compounds at the 1 to 5 ratio. The crystals of different shapes were observed in the initial screening. However, the obtained crystals could be TmaNusB or the compounds or the TmaNusB-nusbiarylin complexes. As mentioned above, the hexagonal crystals were repeatedly observed in multiple conditions when NusB was co-crystallized with MC4-150. SDS-PAGE was applied to clarify if the hexagonal crystals contained the protein. The protein band representing the TmaNusB molecular weight was observed (data not shown). Interestingly, the band that might represent the NusB dimer was not found compared to the summary gel (Figure 5.3C). The possible reason was that the TmaNusB-nusbiarylin complex formation or the NusB monomer crystallization shifted the equilibrium to the NusB monomer, reducing the dimer concentration to an undetectable amount by Coomassie blue dye.

To completely exclude the nusbiarylins crystals, the protein-ligand complex was assembled during dialysis. Since the dialysis membrane held TmaNusB or the TmaNusB-nusbiarylin complex only, the free compounds will be dialyzed out of the reaction mixture. Only the free protein and the protein-ligand complex were expected to exist in the mixture. However, the protein concentration was lowered compared to the concentration before the assembly, probably due to the protein loss during dialysis. Thus, crystallization was performed at the higher temperature to maximize the physical contact between the protein molecules. A longer incubation period was required for the crystal development.

Chapter 6: Discussion and conclusions

6.1 Development of an *in vitro* HTS method for PPI inhibitor screening and characterization

Our work established the use of an *in vitro* NanoLuc PCA for PPI inhibitor screening. A series of vectors were made encoding the 6 x His and NanoLuc fragment tags for protein overproduction. We have also demonstrated the feasibility of the *in vitro* NanoLuc PCA by studying the PPIs between NusB-NusE and RNAP-σ^A . The *in vitro* NanoLuc PCA serves as a novel and simple method in characterizing PPI and inhibitors.

The *in vitro* NanoLuc PCA can be further modified to become an automated and cost-effective method. In the study, the *in vitro* NanoLuc PCA was simplified for the large-scale screening purpose with an automated pipetting equipment. This makes the routine work easy and fast. In addition, consumption of experimental materials can make the assay inexpensive. For instance, the NanoLuc substrate was previously diluted twenty-fold before use. In the NusB-NusE PPI study, the substrate could be diluted hundred-fold to give a similar signal.

Compared to the ELISA-based assay, the *in vitro* NanoLuc PCA is a rapid and inexpensive assay. The ELISA-based assay was previously employed to assess the PPI inhibition (Yang *et al*., 2015; Yang *et al*., 2017). However, ELISA is not an optimized HTS for PPI inhibitors. The turnaround time of ELISA-based assay could be over one day, hindering the large scale screening. In the earlier study (Yang *et al*., 2017), the

ELISA-based assay included overnight incubation steps for NusB coating and BSA blocking prior to multiple incubations for PPI and detection by costly antibodies. In contrast to the ELISA-based assay, the *in vitro* NanoLuc PCA required only two 15-minute incubations prior to the signal measurement in the present investigation, resulting in the turnaround time of about 40 minutes. Even the reliable data could be obtained through both the *in vitro* NanoLuc PCA and ELISA-based assay, the *in vitro* NanoLuc PCA system developed in the present study has shorter turnaround time, reduced material cost for each run, and simpler procedure.

6.2 Study of MC4 derivatives by *in vitro* NanoLuc PCA

By employing the *in vitro* NanoLuc PCA, we compared the performances of the MC4 analogues MC4-19, MC4-33 and MC4-92. The compounds showed antimicrobial activities in the antibiotic susceptibility test and demonstrated PPI inhibitions in the *in vitro* NanoLuc PCA (Table 3.1). Compared to MC4, the derivatives made to have the C-N single bond gave rise to improved flexibility. The flexible chemical structure introduced steric hindrance during the NusB-nusbiarylins interaction. As a result, the weaker PPI interferences were detected in the *in vitro* NanoLuc PCA compared to MC4. Notably, MC4-92 had a lower MIC value against *S. aureus* 25922 compared to MC4, meaning improved antimicrobial activity (Table 3.1), This discrepancy pointed out that the antimicrobial activity did not fully rely on the PPI inhibition. Indeed, MC4-92 was synthesized with two additional chloride groups. The functional group modifications might result in different properties such as membrane permeability and metabolism in bacterial cells. The *in vitro* study indicated

that the minor modifications in the MC4 structures altered the PPI inhibition and the antimicrobial activity.

6.3 Investigation the effects of MC4-series compounds on rRNA transcription by *in vivo* assay

Our work enabled further studies in the MC4-series compounds and other transcription inhibitors. The *E. coli* reporter strains were made and the reporter gene expression were detected by dot blot. The investigations on nusbiarylin compounds will be carried out subsequently. To demonstrate the compound interference with antiterminaton. The reporter strains will be grown with the compounds at the non-lethal dose. The cellular RNA will be extracted and analyzed by dot blot. Changes in the reporter gene expression could be detected if the nusbiarylins suppressed the reporter gene transcription. Further experiments could be conducted to correlate the NusB-nusbiarylins interaction to the transcription inhibition. The NusB knockout and mutant strains, obtained from the Coli Genetic Stock Center in Yale University, will be used to show the reporter gene transcription without a functional NusB. A plasmid carrying the *nusB* gene will be used for complementation to rescue the defective transcription. This recovery would be altered if nusbiarylins acted on NusB. This work can characterize the action of nusbiarylins on the bacterial rRNA transcription.

The use of the plasmid-borne system was limited to Gram-negative bacteria. On the other hand, some Gram-positive bacteria like *S. aureus* are important pathogens targeted for the development of new antibiotics. Thus, the corresponding reporter

strain should be generated. Our work proved that NanoLuc is suitable as a reporter enzyme in *B. subtilis*. The current reporter plasmid pCU314 could be further modified. First, the xylose-inducible promoter could be substituted by the *rrn* promoters. The reporter gene could be replaced by the genes *mCherry* and *lacZ*, the classic reporter genes for promoter characterization. The use of reporter strains can correlate the nusbiarylins effect to *rrn* antitermination.

6.4 Structural characterization of nusbiarylins

We attempted to determine the crystal structures of NusB-nusbiarylin complexes to identify the essential residues involved in the interaction. However, no compound molecule was identified in the diffraction data set, suggesting the crystals used in X-ray diffraction contained TmaNusB only. Potentially it was due to the failure of TmaNusB-nusbiarylin complex formation during the co-crystallization steps. Before repeating co-crystallization, experiments could be conducted to confirm the complex formation by other means, such as mass spectrometry, in which the peak shift between spectra implies the complex formation.

6.5 Future work

Investigations will be executed to explore the NusB-nusbiarylins interaction mode. The crystal structure determination of NusB-compound complex can elucidate the essential residues in the interaction but was not achieved in the present study. Apart from the structural determination, the essential residues could be examined by other means like NusB mutagenesis. The residues to be mutated could be selected from the

NusB-nusbiarylins docking model. To generate the NusB mutants, PCR splicing (Figure 6.1) could be applied for cloning the protein overproduction plasmids of the NusB mutants. The purified mutant proteins will be analyzed by ITC to quantify the change in the NusB-nusbiarylins interaction. The work to clarify the interaction mode can improve the pharmacophore model for the design of stronger PPI inhibitiors.

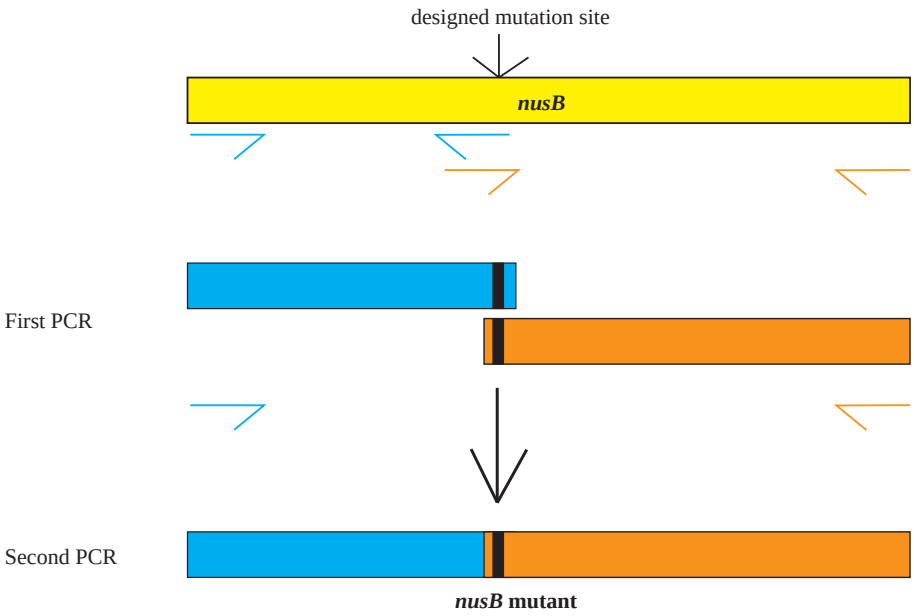

Figure 6.1 Schematic diagram for mutagenesis by PCR splicing. The *nusB* gene is amplified as two fragments containing the mutation (Black region) in the overlapping regions, followed by PCR reactions to synthesize the complete *nusB* gene with the desired mutation.

Currently some of the nusbiarylin compounds demonstrated antimicrobial activities against some clinically significant pathogens such as MRSA and *S. pneumoniae* (Yang *et al*, 2017; Qiu *et al*., 2019). To fully validate the nusbiarylins as the antimicrobial drug candidates, investigations should be conducted on these strains. For example, the reporter assay could be amended to make *S. aureus* and *S. pneumoniae* reporter

strains. A reporter plasmid encoding NanoLuc under the control of the *rrn* promoter region could be designed and introduced to the *S. aureus* strain by electroporation (Malone *et al*., 2009). The reporter strain will be grown with nusbiarylins at the non-lethal dose and the reporter gene mRNA amount will be determined by dot blot. The data can directly show the effects of nusbiarylins on the *S. aureus rrn* operons.

6.6 Conclusions

A group of chemicals called nusbiarylins were designed for blocking the NusB-NusE PPI for bacterial rRNA transcription. Previous studies focused on their antimicrobial activities against various pathogens and simply proved the specific interaction between NusB and MC4. Hereby we extended the study to characterize the nusbiarylin compounds at the molecular level. In this study, we developed the simple and fast *in vitro* NanoLuc PCA for PPI inhibitor screening and successfully applied the assay in the nusbiarylins study. We also generated the *E. coli* and *B. subtilis* reporter strains containing the *rrn* promoter and modified the non-radioactive RNA detection method. Further experiments will be conducted to examine any change in the reporter gene transcription. The NusB-compound crystal structure was not determined in the crystallographic study. Other methods could be applied in confirming the NusB-nusbiarylins complex such as the mass spectrometry. The assay systems developed in this study provided valuable tools for the discovery and characterization of other bacterial transcription inhibitors as novel antimicrobial agents.

References

Aboulhouda, S., Di Santo, R., Therizols, G., & Weinberg, D. (2017). Accurate, streamlined analysis of mRNA translation by sucrose gradient fractionation. *Bio-protocol, 7*(19), e2573. doi:10.21769/BioProtoc.2573

Altieri, A. S., Mazzulla, M. J., Horita, D. A., Coats, R. H., Wingfield, P. T., Das, A., Court, D. L., & Byrd, R. A. (2000). The structure of the transcriptional antiterminatior NusB from *Escherichia coli*. *Nature Structural Biology*, *7*(6), 470-474. doi:10.1038/75869

Artsimovitch, I., Svetlov, V., Anthony, L., Burgess, R. R., & Landick, R. (2000). RNA polymerases from *Bacillus subtilis* and *Escherichia coli* differ in recognition of regulatory signals *in vitro*. *Journal of Bacteriology, 182*(21), 6027–6035. doi:10.1128/jb.182.21.6027-6035.2000

Balleza, E., López-Bojorquez, L. N., Martínez-Antonio, A., Resendis-Antonio, O., Lozada-Chávez, I., Balderas-Martínez, Y. I., Encarnación, S., & Collado-Vides, J. (2009). Regulation by transcription factors in bacteria: beyond description. *FEMS microbiology reviews*, 33(1), 133–151. https://doi.org/10.1111/j.1574-6976.2008.00145.x

Belogurov, G. A., Sevostyanova, A., Svetlov, V., & Artsimovitch, I. (2010). Functional regions of the N-terminal domain of the antiterminator RfaH. *Molecular Microbiology, 76*(2), 286–301. doi: 10.1111/j.1365-2958.2010.07056.x

Berg K. L., Squires C., & Squires C. L. Ribosomal RNA operon anti-termination. Function of leader and spacer region *boxB-boxA* sequences and their conservation in diverse micro-organisms. *Journal of Molecular Biology*. 1989; 209:345–358. doi:10.1016/0022-2836(89)90002-8

Bocchetta, M., Xiong, L. & Mankin, A. S. (1998). 23S rRNA positions essential for tRNA binding in ribosomal functional sites. *Proceedings of the National Academy of Sciences of the United States of America, 95*(7), 3525–3530. doi:10.1073/pnas.95.7.3525

Bonin, I., Robelek, R., Benecke, H., Urlaub, H., Bacher, A., Richter, G., & Wahl, M. C. (2004). Crystal structures of the antitermination factor NusB from *Thermotoga maritima* and implications for RNA binding. *The Biochemical journal, 383*(Pt. 3), 419–428. doi:10.1042/BJ20040889

Borukhov, S., Lee, J., & Laptenko, O. (2005). Bacterial transcription elongation factors: new insights into molecular mechanism of action. *Molecular Microbiology, 55*(5), 1315-1324. doi:10.1111/j.1365-2958.2004.04481.x

Borukhov, S., & Nudler, E. (2008). RNA polymerase: the vehicle of transcription. *Trends in Microbiology*. *16*, 126–134. doi:10.1016/j.tim.2007.12.006

Burmann, B. M., Luo, X., Rösch, P., Wahl, M. C., & Gottesman, M. E. (2010). Fine tuning of the *E. coli* NusB:NusE complex affinity to *boxA* RNA is required for processive antitermination. *Nucleic acids research, 38*(1), 314–326. doi:10.1093/nar/gkp736

Burmann, B. M., & Rösch, P. (2011). The role of *E. coli* Nus-factors in transcription regulation and transcription:translation coupling: from structure to mechanism. *Transcription, 2*(3), 130–134. doi:10.4161/trns.2.3.15671

Burmann, B. M., Schweimer, K., Luo, X., Wahl, M. C., Stitt, B. L., Gottesman, M. E., & Rosch, P. (2010). A NusE:NusG complex links transcription and translation. *Science, 328*(5977), 501–504. doi:10.1126/science.1184953

Burova, E., Hung, S. C., Sagitov, V., Stitt, B. L., & Gottesman, M. E. (1995). *Escherichia coli* NusG protein stimulates transcription elongation rates *in vivo* and *in vitro*. *Journal of bacteriology*, 177(5), 1388–1392. doi:10.1128/jb.177.5.1388-1392.1995

Browning, D. F., & Busby, S. J. (2004). The regulation of bacterial transcription initiation. *Nature Reviews Microbiology*, *2*(1), 57-65. doi:10.1038/nrmicro787

Brueckner, F., Ortiz, J., & Cramer, P. (2009). A movie of the RNA polymerase nucleotide addition cycle. *Current Opinion in Structural Biology, 19*(3), 294–299. doi:10.1016/j.sbi.2009.04.005

Carter, R., & Drouin, G. (2009). Structural differentiation of the three eukaryotic RNA polymerases. *Genomics*, *94*(6), 388-396. doi:https://doi.org/10.1016/j.ygeno.2009.08.011

Das A. (1992). How the phage lambda N gene product suppresses transcription termination: communication of RNA polymerase with regulatory proteins mediated by signals in nascent RNA. *Journal of bacteriology, 174*(21), 6711–6716. doi:10.1128/jb.174.21.6711-6716.1992

Das, R., Loss, S., Li, J., Waugh, D. S., Tarasov, S., Wingfield, P. T., Byrd, R. Q., & Altieri, A. S. (2008). Structural biophysics of the NusB:NusE antitermination complex. *Journal of molecular biology, 376*(3), 705–720. doi:10.1016/j.jmb.2007.11.022

Dangkulwanich, M., Ishibashi, T., Bintu, L., & Bustamante, C. (2014) Molecular mechanisms of transcription through single-molecule experiments. *Chem Reviews. ,114*(6):3203–3223. doi:10.1021/cr400730x

Devito, J., & Das, A. (1994). Control of transcription processivity in phage lambda: Nus factors strengthen the termination-resistant state of RNA polymerase induced by N antiterminator. *Proceedings of the National Academy of Sciences of the United States of America, 91*(18), 8660–8664. doi:10.1073/pnas.91.18.8660.

Dixon, A. S., Schwinn, M. K., Hall, M. P., Zimmerman, K., Otto, P., Lubben, T. H., Butler, B. L., Binkowski, B. F., Machleidt. T., Kirkland, T. A., Wood. G. M., Eggers. C.T., Encell, L. P., & Wood, K. V. (2015). NanoLuc complementation reporter optimized for accurate measurement of protein interactions in cells. *ACS Chemical Biology*, *11*(2), 400-408. doi:10.1021/acschembio.5b00753

Dennis, P. P., Ehrenberg, M., & Bremer, H. (2004). Control of rRNA synthesis in *Escherichia coli*: a systems biology approach. *Microbiology and molecular biology reviews, 68*(4), 639–668. doi:10.1128/MMBR.68.4.639-668.2004

Dudenhoeffer, B. R., Schneider, H., Schweimer, K., & Knauer, S.H. (2019). SuhB is an integral part of the ribosomal antitermination complex and interacts with NusA. *Nucleic acids research, 47*(12), 6504–6518. doi:10.1093/nar/gkz442

Feklistov A. (2013). RNA polymerase: in search of promoters. *Annals of the New York Academy of Sciences, 1293*, 25–32. doi:10.1111/nyas.12197

Friedman, D. I., Baumann, M., & Baron, L. (1976). Cooperative effects of bacterial mutations affecting λ N gene expression. *Virology, 73*(1), 119–127. doi:10.1016/0042-6822(76)90066-0

Friedman, D. I., Schauer, A. T., Baumann, M. R., Baron, L. S., & Adhya, S. L. (1981). Evidence that ribosomal protein S10 participates in control of transcription termination. *Proceedings of the National Academy of Sciences of the United States of America*, 78(2), 1115–1118. doi:10.1073/pnas.78.2.1115

Friedman, L. J., Mumm, J. P., & Gelles, J. (2013). RNA polymerase approaches its promoter without long-range sliding along DNA. *Proceedings of the National Academy of Sciences of the United States of America, 110*(24), 9740–9745. doi:10.1073/pnas.1300221110

Gentry, D. R., & Burgess, R. R. (1993) Cross-linking of *Escherichia coli* RNA polymerase subunits: identification of beta as the binding site of omega. *Biochemistry, 32*, 11224–11227. doi:10.1021/bi00092a036

Ghosh, B., Grzadzelska, E., Bhattacharya, P., Prealta, E., DeVito, J., & Das, A. (1991). Specificity of antitermination mechanisms suppression of the terminator cluster T1-T2 of *Escherichia coli* ribosomal RNA operon, *rrnB*, by phage λ antiterminators. *Journal of Molecular Biology*. *1*, 59-66. doi:10.1016/0022-2836(91)90737-q

Ghosh, P., Ishihama, A. and Chatterji, D. (2001). *Escherichia coli* RNA polymerase subunit ω and its N-terminal domain bind full-length β' to facilitate incorporation into the α to subassembly. *European Journal of Biochemistry*, 268(17), 4621-4627. doi:10.1046/j.1432-1327.2001.02381.x

Glyde, R., Ye, F., Jovanovic, M., Kotta-Loizou, I., Buck, M., & Zhang, X. (2018). Structures of bacterial RNA polymerase complexes reveal the mechanism of DNA loading and transcription initiation. *Molecular Cell*, *70*(6), 1111-1120. doi:10.1016/j.molcel.2018.05.021

Gong, F., & Yanofsk, C. (2002). Instruction of translating ribosome by nascent peptide. *Science*, *297*(5588), 1864-1867. doi:10.1126/science.1073997

Gopal, B., Haire, L., Cox, R., Colston, M., Major, S., Brannigan, J., Smerdon, S. J., & Dodson, G. (2000). The crystal structure of NusB from *Mycobacterium tuberculosis*. *Natural Structural Biology*, *7*, 475-478. doi:10.1042/BJ20040889

Gource, R. L., Gaal, T., & Barlett, M. S., (1996). rRNA transcription and growth rate-dependent regulation of ribosome synthesis in *Escherichia coli*. *Annual Review of Microbiology*, *50*, 645-677. doi:10.1146/annurev.micro.50.1.645

Grinwald, M., & Ron, E. Z. (2013). The *Escherichia coli* translation-associated heat shock protein YbeY is involved in rRNA transcription antitermination. *PLoS ONE*, *8*(4), e62297. doi:10.1371/journal.pone.0062297

Grundy, F. J., Winkler, W. C., & Henkin, T. M. (2002). tRNA-mediated transcription antitermination *in vitro*: codon-anticodon pairing independent of the ribosome. *Proceedings of the National Academy of Sciences of the United States of America*, *99*(17), 11121–11126. doi:10.1016/s0092-8674(01)00582-7

Gusarov, I., & Nudler, E. (2001). Control of intrinsic transcription termination by N and NusA. *Cell*, *107*(4), 437-449. doi:10.1016/s0092-8674(01)00582-7

Hall, M. P., Unch, J., Binkowski, B. F., Valley, M. P., Butler, B. L., Wood, M. G., Otto, P., Zimmerman, K., Vidugiris, G., Machleidt, T., Rober, M. B., Benink, H. A., Eggers, C. T., Slater. M. R., Meisenheimer, P. L., Klaubert, D. H., Fan. F., Encell, L.P., & Wood, K. V. (2012). Engineered luciferase reporter from a deep sea shrimp utilizing a novel imidazopyrazinone substrate. *ACS chemical biology*, *7*(11), 1848–1857. doi:10.1021/cb3002478

Hassoun, A., Linden, P. K., & Friedman, B. (2017). Incidence, prevalence, and management of MRSA bacteremia across patient populations-a review of recent developments in MRSA management and treatment. *Critical care (London, England)*, *21*(1), 211. doi:10.1186/s13054-017-1801-3

Hiblot, J., Yu, Q., Sabbadini, M. D., Reymond, L., Xue, L., Schena, A., Sallin, O., Hill, N., Griss, R., & Johnsson, K. (2017). Luciferases with tunable emission wavelengths. *Angewandte Chemie,129*(46), 14748-14752. doi:10.1002/anie.201708277

Ishihama, A. (1992). Role of the RNA polymerase alpha subunit in transcription activation. *Molecular Microbiology, 6*(22), 3283–3288. doi:10.1111/j.1365-2958.1992.tb02196.x

Janda, J. M., & Abbott, S. L. (2007). 16S rRNA gene sequencing for bacterial identification in the diagnostic laboratory: pluses, perils, and pitfalls. *Journal of clinical microbiology, 45*(9), 2761–2764. doi:10.1128/JCM.01228-07

Johnston, E. B., Lewis, P. J. & Griffith, R. (2009). The interaction of *Bacillus subtilis* σ^A with RNA polymerase. *Protein Science, 18*(11), 2287–2297. https://doi.org/10.1002/pro.239

Juang, Y. L., & Helmann, J. D. (1994). The delta subunit of *Bacillus subtilis* RNA polymerase. An allosteric effector of the initiation and core-recycling phases of transcription. *Journal of molecular biology*, 239(1), 1-14. doi: 10.1006/jmbi.1994.1346

Juang, Y. L, & Helmann, J. D. (1994). A promoter melting region in the primary σ factor of *Bacillus subtilis*. Journal of Molecular Biology, 235(5), 1470-1488. doi:10.1006/jmbi.1994.1102

Keller, A. N., Yang, X., Wiedermannová, J., Delumeau, O., Krásný, L., & Lewis, P. J. (2014). ε, a new subunit of RNA polymerase found in gram-positive bacteria. *Journal of bacteriology, 196*(20), 3622–3632. doi:10.1128/JB.02020-14

Kireeva, M. L., Kashlev, M., & Burton, Z. F. (2013). RNA polymerase structure, function, regulation, dynamics, fidelity and roles in gene expression. *Chemical Reviews, 113*(11), 8325-8330. doi:10.1021/cr400436m

Krupp, F., Said, N., Huang, Y. H., Loll, B., Bürger, J., Mielke, T., Spahn, C. M. T., & Wahl, M. C. (2019). Structural basis for the action of an all-purpose transcription anti-termination factor. *Molecular Cell, 74*(1). doi: 10.1016/j.molcel.2019.01.016

Lee, J., & Borukhov, S. (2016). Bacterial RNA Polymerase-DNA interaction—the driving force of gene expression and the target for drug action. *Frontiers in Molecular Biosciences, 3.* doi:10.3389/fmolb.2016.00073

Lewis, P. J., & Marston, A. L. (1999). GFP vectors for controlled expression and dual labelling of protein fusions in *Bacillus subtilis*. *Gene, 227*(1), 101-109. doi:10.1016/s0378-1119(98)00580-0

Li, P., Wang, L., & Di, L. J. (2019). Applications of protein fragment complementation assays for analyzing biomolecular interactions and biochemical networks in living cells. *Journal of Proteome Research, 18*(8), 2987–2998. doi: 10.1021/acs.jproteome.9b00154

Li, S. C., Squires, C. L., & Squires, C. (1984). Antitermination of *E. coli* rRNA transcription is caused by a control region segment containing lambda *nut*-like sequence. *Cell, 38* (3), 851-860. doi: 10.1016/0092-8674(84)90280-0

Liu X, Jia W, An Y, Cheng, L., Wang, M., Yang, S., Chen, H. (2015). Screening, gene cloning, and characterizations of an acid-stable α-amylase. *Journal of Microbiology and Biotechnology*, 25(6):828-836. doi:10.4014/jmb.1409.09094

Luo, X., Hsiao, H. H., Bubunenko, M., Weber, G., Court, D. L., Gottesman, M. E., Urlaub, H., & Wahl, M. C. (2008). Structural and functional analysis of the *E. coli* NusB-S10 transcription antitermination complex. *Molecular Cell, 32*(6), 791–802. doi:10.1016/j.molcel.2008.10.028

Ma, C., Yang, X., & Lewis, P. J. (2016). Bacterial transcription as a target for antibacterial drug development. *Microbiology and Molecular Biology Reviews, 80*(1), 139–160. doi:10.1128/MMBR.00055-15

Maeda, M., Shimada, T., & Ishihama, A. (2015). Strength and regulation of seven rRNA promoters in *Escherichia coli*. *PloS ONE, 10*(12), e0144697. doi:10.1371/journal.pone.0144697

Malone, C. L., Boles, B. R., Lauderdale, K. J., Thoendel, M., Kavanaugh, J. S., & Horswill, A. R. (2009). Fluorescent reporters for *Staphylococcus aureus*. *Journal of microbiological methods, 77*(3), 251–260. doi: https://doi.org/10.1016/j.mimet.2009.02.011

Mathew, R., & Chatterji, D. (2006). The evolving story of the omega subunit of bacterial RNA polymerase. *Trends in Microbiology, 14*(10), 450-455. doi:10.1016/j.tim.2006.08.002

Marr, M. T., & Roberts, J. W. (2000). Function of transcription cleavage factors GreA and GreB at a regulatory pause site. *Molecular Cell, 6*(6), 1275–1285. doi: 10.1016/s1097-2765(00)00126-x

Mayer, C., & Grummt, I. (2006). Ribosome biogenesis and cell growth: mTOR coordinates transcription by all three classes of nuclear RNA polymerases. *Oncogene, 25*(48), 6384–6391. doi: 10.1038/sj.onc.1209883

Mehta, P., Woo, P., Venkataraman, K., & Karzai, A.W. (2012). Ribosome purification approaches for studying interactions of regulatory proteins and RNAs with the ribosome. *Methods in Molecular Biology, 905*, 273–289. doi:10.1007/978-1-61779-949-5_18

Michnick, S. W., Ear, P. H., Landry, C., Malleshaiah, M. K., & Messier, V. (2011). Protein-fragment complementation assays for large-scale analysis, functional dissection and dynamic studies of protein–protein interactions in living cells. *Methods in Molecular Biology Signal Transduction Protocols*, 395–425. doi: 10.1007/978-1-61779-160-4_25

Molnar, C., & Gair., J. (2019) Concept of Biology-1st Canadian Edition. Retrieved from https://opentextbc.ca/biology/

Murakami, S. K. (2015). Structural biology of bacterial RNA polymerase. *Biomolecules*, *5*(20), 848-864. doi: 10.3390/biom5020848

Murayama, S., Ishikawa, S., Chumsakul, O., Ogasawara, N., & Oshima, T. (2015). The role of α-CTD in the genome-wide transcriptional regulation of the *Bacillus subtilis* cells. *PloS ONE, 10*(7), e0131588. doi:10.1371/journal.pone.0131588

Nachtergaele, S., & He, C. (2017). The emerging biology of RNA post-transcriptional modifications. *RNA biology, 14*(2), 156–163. doi:10.1080/15476286.2016.1267096

Nadiras, C., Schwartz, A., Delaleau, M., & Boudvillain, M. (2018). Evaluating the effect of small RNAs and associated chaperones on Rho-dependent termination of transcription *in vitro*. *Methods in Molecular Biology* (Clifton, N.J.), 1737, 99–118. https://doi.org/10.1007/978-1-4939-7634-8_7

Narayanan, A., Vago, F. S., Li, K., Qayyum, M. Z., Yernool, D., Jiang, W., & Murakami, K. S. (2018). Cryo-EM structure of *Escherichia coli* σ70 RNA polymerase and promoter DNA complex revealed a role of σ non-conserved region during the open complex formation. *The Journal of biological chemistry, 293*(19), 7367–7375. doi:10.1074/jbc.RA118.002161

Neben, C. L., Lay, F. D., Mao, X., Tuzon, C. T., & Merrill, A. E. (2017). Ribosome biogenesis is dynamically regulated during osteoblast differentiation. *Gene, 612*, 29–35. doi:10.1016/j.gene.2016.11.010

Neylon, C., Brown, S. E., Kralicek, A. V., Miles, C. S., Love, C. A., & Dixon, N. E. (2000). Interaction of the *Escherichia coli* replication terminator orotein (Tus) with DNA: A model derived from DNA-Binding studies of mutant proteins by surface plasmon resonance. *Biochemistry,39*(39), 11989-11999. doi:10.1021/bi001174w

Nickels, B. E., & Hochschild, A. (2004). Regulation of RNA polymerase through the secondary channel. *Cell, 118*(3), 281–284. doi: 10.1016/j.cell.2004.07.021

Nudler, E. (2009). RNA polymerase active center: The molecular engine of transcription. *Annual Review of Biochemistry, 78*(1), 335-361. doi:10.1146/annurev.biochem.76.052705.164655

Oda, M., Kobayashi, N., Fujita, M., Miyazaki, Y., Sadaie, Y., Kurusu, Y., & Nishikawa, S. (2004). Analysis of HutP-dependent transcription antitermination in the *Bacillus subtilis* hut operon: identification of HutP binding sites on hut antiterminator RNA and the involvement of the N-terminus of HutP in binding of HutP to the antiterminator RNA. *Molecular Microbiology, 51*(4), 1155–1168. doi: 10.1046/j.1365-2958.2003.03891.x

Opalka, N., Brown, J., Lane, W. J., Twist, K. A., Landick, R., Asturias, F. J., & Darst, S. A. (2010). Complete structural model of *Escherichia coli* RNA polymerase from a hybrid approach. *PLoS Biology, 8*(9), e1000483. doi:10.1371/journal.pbio.1000483

Orosz, A., Boros, I., & Venetianer, P. (1991). Analysis of the complex transcription termination region of the *Escherichia coli rrnB* gene. *European Journal of Biochemistry, 201*, 653-659.

Potter, K. D., Merlino, N. M., Jacobs, T., & Gollnick, P. (2011). TRAP binding to the *Bacillus subtilis* trp leader region RNA causes efficient transcription termination at a weak intrinsic terminator. *Nucleic acids research, 39*(6), 2092–2102. doi:10.1093/nar/gkq965

Porrua, O., Boudvillain, M., & Libri, D. (2016). Transcription termination: Variations on common themes. *Trends in Genetics, 32*(8), 508-522. doi:10.1016/j.tig.2016.05.007

Qiu, Y., Chan, S. T., Lin, L., Shek, T. L., Tsang, T. F., Barua, N., Zhang, Y., Ip. M., Chan P. K. S., Blanchard, N., Hanquet, G., Zuo, Z., Yang, X., & Ma, C. (2019). Design, synthesis and biological evaluation of antimicrobial diarylimine and –amine compounds targeting the interaction between the bacterial NusB and NusE proteins. *European Journal of Medicinal Chemistry, 178*, 214–231. doi: 10.1016/j.ejmech.2019.05.090

Qiu, Y., Chan, S. T., Lin, L., Shek, T. L., Tsang, T. F., Zhang, Y., Ip, M., Chan, P. K. S., Blanchard, N., Hanquet, G., Zuo, Z., Yang, X., & Ma, C. (2019). Nusbiarylins, a new class of antimicrobial agents: Rational design of bacterial transcription inhibitors targeting the interaction between the NusB and NusE proteins. *Bioorganic Chemistry, 92*, 103203. doi: 10.1016/j.bioorg.2019.103203

Ray-Soni, A., Bellecourt, M. J., & Landick, R. (2016). Mechanisms of bacterial transcription termination: All good things must end. *Annual Review of Biochemistr*y, *85*(1), 319-347. doi:10.1146/annurev-biochem-060815-014844

Rees, W. A., Weitzel, S. E., Yager, T. D., Das, A., & von Hippel, P. H. (1996). Bacteriophage lambda N protein alone can induce transcription antitermination *in vitro*. *Proceedings of the National Academy of Sciences of the United States of America, 93*(1), 342–346. doi:10.1073/pnas.93.1.342

Revyakin, A., Liu, C., Ebright, R. H., & Strick, T. R. (2006). Abortive initiation and productive initiation by RNA polymerase involve DNA scrunching. *Science, 314*(5802), 1139–1143. doi:10.1126/science.1131398

Saecker, R. M., Record, M. T., & Dehaseth, P. L. (2011). Mechanism of bacterial transcription initiation: RNA polymerase - promoter binding, isomerization to initiation-competent open complexes, and initiation of RNA synthesis. *Journal of Molecular Biology, 412*(5), 754-771. doi:10.1016/j.jmb.2011.01.018

Said, N., Krupp, F., Anedchenko, E., Santos, K. F., Dybkov, O., Huang, Y. H., Lee, C. T., Loll, B., Behrmann, E., Bürger, J., Mielke, T., Loerke, J., Urlaub, H., Spahn. C. M. T., Weber, G. F., & Wahl, M. C. (2017). Structural basis for λN-dependent processive transcription antitermination. *Nature Microbiology, 2*(7). doi: 10.1038/nmicrobiol.2017.62

Santangelo, T. J., & Artsimovitch, I. (2011). Termination and antitermination: RNA polymerase runs a stop sign. *Nature Reviews Microbiology*, *9*(5), 319–329. https://doi.org/10.1038/nrmicro2560

Selby, C. P. (2017). Mfd protein and transcription-repair coupling in *Escherichia coli*. *Photochemistry and Photobiology, 93*(1), 280–295. doi: 10.1111/php.12675

Serganov, A., Yuan, Y. R., Pikovskaya, O., Polonskaia, A., Malinina, L., Phan, A. T., Hobartner, C., Micura, R., Breaker, R. R., & Patel, D. J. (2004). Structural basis for discriminative regulation of gene expression by adenine- and guanine-sensing mRNAs. *Chemistry & Biology, 11*(12), 1729–1741. doi:10.1016/j.chembiol.2004.11.018

Shajani, Z., Sykes, M. T., & Williamson, J. R. (2011) Assembly of bacterial ribosomes. *Annual Review of Biochemistry, 80*, 501-26. Doi: 10.1146/annurev-biochem-062608-160432

Sharrock, R. A., Gourse, R. L., & Nomura, M. (1985). Defective antitermination of rRNA transcription and derepression of rRNA and tRNA synthesis in the nusB5 mutant of *Escherichia coli*. *Proceedings of the National Academy of Sciences, 82*(16), 5275–5279. doi: 10.1073/pnas.82.16.5275

Shi, J., Gao, X., Tian, T., Yu, Z., Gao, B., Wen, A., You, L., Chang, S., Zhang, X., Zhang, Y., & Feng, Y. (2019). Structural basis of Q-dependent transcription antitermination. *Nature Communications, 10*(1). doi: 10.1038/s41467-019-10958-8

Singh, N., Bubunenko, M., Smith, C., Abbott, D. M., Stringer, A. M., Shi, R., Court., D. L., & Wade, J. T. (2016). SuhB associates with Nus factors to facilitate 30S ribosome biogenesis in *Escherichia coli*. *mBio, 7*(2). doi:10.1128/mBio.00114-16

Squires, C. L., Greenblatt, J., Li, J., Condon, C., & Squires, C. L. (1993). Ribosomal RNA antitermination *in vitro*: requirement for Nus factors and one or more unidentified cellular components. *Proceedings of the National Academy of Sciences of the United States of America*, *90*(3), 970–974. doi:10.1073/pnas.90.3.970

Stagno, J. R., Altieri, A. S., Bubunenko, M., Tarasov, S. G., Li, J., Court, D. L., Byrd., R. A., & Ji, X. (2011). Structural basis for RNA recognition by NusB and NusE in the initiation of transcription antitermination. *Nucleic acids research, 39*(17), 7803–7815. doi:10.1093/nar/gkr418

Stracy, M., & Kapanidis, A. N. (2017). Single-molecule and super-resolution imaging of transcription in living bacteria. *Methods, 120*, 103–114. doi:10.1016/j.ymeth.2017.04.001

Szymanski, M., Barciszewska, M. Z., Erdmann, V. A., & Barciszewski, J. (2002). 5S ribosomal RNA database. *Nucleic acids research, 30*(1), 176–178. doi:10.1093/nar/30.1.176

Torres, M., Balada, J. M., Zellars, M., Squires, C., & Squires, C. L. (2004). *In vivo* effect of NusB and NusG on rRNA transcription antitermination. *Journal of bacteriology*, *186*(5), 1304–1310.

Torres, M., Condon, C., Balada, J. M., Squires, C., & Squires, C. L. (2001). Ribosomal protein S4 is a transcription factor with properties remarkably similar to NusA, a protein involved in both non-ribosomal and ribosomal RNA antitermination. *The EMBO journal*, 20(14), 3811–3820.

Tsang, T. F., Qiu, Y., Lin, L., Ye, J., Ma, C., & Yang, X. (2019). Simple method for studying *in Vitro* protein–protein interactions based on protein complementation and its application in drug screening targeting bacterial transcription. *ACS Infectious Diseases, 5*(4), 521-527. doi:10.1021/acsinfecdis.9b00020

Wang, F., Redding, S., Finkelstein, I. J., Gorman, J., Reichman, D. R., & Greene, E. C. (2013). The promoter-search mechanism of *Escherichia coli* RNA polymerase is dominated by three-dimensional diffusion. *Nature structural & molecular biology, 20*(2), 174–181. doi:10.1038/nsmb.2472

Weisberg, R. A., & Gottesman, M. E. (1999). Processive antitermination. *Journal of Bacteriology, 181*(2), 359–367. doi: 10.1128/jb.181.2.359-367.1999

Valabhoju, V., Agrawal, S., & Sen, R. (2016). Molecular Basis of NusG-mediated Regulation of Rho-dependent Transcription Termination in Bacteria. *Journal of Biological Chemistry, 291*(43), 22386–22403. doi: 10.1074/jbc.m116.745364

Vassylyev, D. G., Sekine, S., Laptenko, O., Lee, J., Vassylyeva, M. N., Borukhov, S., & Yokoyama, S. (2002). Crystal structure of a bacterial RNA polymerase holoenzyme at 2.6 Å resolution. *Nature, 417*(6890), 712-719. doi:10.1038/nature752

Ward, D., Delong, A., Gottesman, M., & Herskowitz, I. (1983). *Escherichia coli* nusB mutations that suppress nusA1 exhibit λ N specificity. *Journal of Molecular Biology, 168*(1), 73–85. doi: 10.1016/s0022-2836(83)80323-4

Yakhnin, A.V., & Babitzke, P. (2002). NusA-stimulated RNA polymerase pausing and termination participates in the *Bacillus subtilis* trp operon attenuation mechanism *in vitro*. *Proceedings of the National Academy of Sciences, 99*, 11067-11072

Yakhnin, H., Zhang, H., Yakhnin, A. V., & Babitzke, P. (2004). The trp RNA-binding attenuation protein of *Bacillus subtilis* regulates translation of the tryptophan transport gene trpP (yhaG) by blocking ribosome binding. *Journal of bacteriology, 186*(2), 278–286. doi:10.1128/jb.186.2.278-286.2004

Yang, X., Luo, M. J., Yeung, A. C. M., Lewis, P. J., Chan, P. K. S., Ip, M., & Ma, C. (2017). First-In-Class inhibitor of ribosomal RNA synthesis with antimicrobial activity against *Staphylococcus aureus*. *Biochemistry, 56*(38), 5049–5052. doi: 10.1021/acs.biochem.7b00349

Yang, X., Ma, C., & Lewis, P. J. (2015) Identification of inhibitors of bacterial RNA polymerase. *Methods 86*, 45−50

Yang, X., Molimau, S., Doherty, G. P., Johnston, E. B., Marles-Wright, J., Rothnagel, R., Hankamer, B., Lewis, R. J., & Lewis, P. J. (2009). The structure of bacterial RNA polymerase in complex with the essential transcription elongation factor NusA. *EMBO reports, 10*(9), 997–1002. doi:10.1038/embor.2009.155

Yang, X. J., Hart, C. M., Grayhack, E. J., & Roberts, J. W. (1987). Transcription antitermination by phage lambda gene Q protein requires a DNA segment spanning the RNA start site. *Genes Development, 1*(3), 217–226. doi: 10.1101/gad.1.3.217

Yano, H., Cai, N. S., Javitch, J. A., & Ferré, S. (2018). Luciferase complementation based-detection of G-protein-coupled receptor activity. *BioTechniques, 65*(1), 9–14. doi: 10.2144/btn-2018-0039

Zhou, M., Li, Q., & Wang, R. (2016) Current experimental methods for characterizing protein-protein interactions. *ChemMedChem 11* (8), 738−756

Zimmermann, R. A., Muto, A., Fellner, P., Ehresmann, C., & Branlant, C. (1972). Location of ribosomal protein binding sites on 16S ribosomal RNA. *Proceedings of the National Academy of Sciences of the United States of America, 69*(5), 1282–1286. doi:10.1073/pnas.69.5.1282

Appendix I Media and buffer compositions

Growth Media

LB Medium

Pancreatic digest of casein	10.0 g
Yeast extract	5.0 g
NaCl	0.5 g

pH 7.0, made up to 1 L with sterile milliQ water (MQW)

Auto Induction Medium

Tryptone	10 g
Yeast extract	5 g
$(NH_4)_2SO_4$	3.3 g
KH_2SO_4	6.8 g
Na_2HPO_4	7.1 g
Glucose	0.5 g
α-Lactose	2.0 g
$MgSO_4$	0.15 g
Trace element	0.03 g

Made up to 1 L with sterile MQW

SMM Solution

$(NH_4)_2SO_4$	2 g
KH_2PO_4	14 g
K_2HPO_4	6 g
Sodium citrate dihydrate	1g
$MgSO_4$	0.2 g

Made up to 1 L with sterile MQW

MM Competence Media

SMM	10 mL
40% glucose	125 µL
2 mg/mL tryptophan	100 µL
1 M $MgSO_4$	60 µL
20% casamino acid	10 µL
Ammonium ferric citrate	5 µL

Starvation Media

SMM	10 mL
40% Glucose	125 µL
1 M $MgSO_4$	60 µL

LB Agar

Tryptone	10 g
Yeast extract	5 g
NaCl	0.5 g
Bacteriological agar	15 g

Made up to 1 L with sterile MQW

Antibiotics plates

LB Agar 100 mL

Antibiotics	Stock (mg/mL)	Volume added (μL)
Ampicillin	100 in MQW	100
Spectinomycin	15 in MQW	100

General solutions

Agarose gel

1X TBE

Tris	89 mM
Boric acid	89 mM
EDTA	2 mM

1% Agarose

Agarose powder	0.2 g
1X TBE	20 mL

Agarose powder was melt in 1X TBE by heating, then 0.2 µl SYBR Safe dye was added

SDS Gels

10 % Resolving gel

MQW	2.4 mL
40% Acrylamide	1.3 mL
1.5M Tris, pH 8.8	1.3 mL
10% SDS	0.05 mL
10% APS	0.05 mL
TEMED	0.002 mL

5 % Stacking Gel

MQW	1.5 mL
40% Acrylamide	0.25 mL
1M Tris, pH 6.8	0.25 mL
10% SDS	0.02 mL
10% APS	0.02 mL
TEMED	0.002 mL

1 X Tricine SDS running buffer

Tris, pH 8.3	100 mM
Tricine	100 mM
SDS (w/v)	0.1 %

6X Loading buffer

Tris-HCl	0.3 M
SDS (w/v)	10 %
Bromophenol blue	0.06 %
DTT	0.6 M
Glycerol (v/v)	30 %

Protein purification

His tag protein

2 X Lysis Buffer

NaH_2PO_4	40 mM
NaCl	1 M
Imidazole	40 mM

Made up to 1 L with MQW; adjusted to pH 8.0 with NaOH; diluted in B-PER™ Complete Bacterial Protein Extraction Reagent to 1X when use

Elution

NaH_2PO_4	20 mM
NaCl	500 mM
Imidazole	500 mM

Made up to 1 L with MQW; adjusted to pH 8.0 with NaOH

Wash buffer

1X Lysis buffer	96 %
Elution buffer	4 %

Heparin binding buffer

NaH_2PO_4	20 mM
NaCl	150 mM

Made up to 1 L with MQW; adjusted to pH 8.0 with NaOH

Heparin elution buffer

NaH_2PO_4	20 mM
NaCl	1 M

Made up to 1 L with MQW; adjusted to pH 8.0 with NaOH

Gel filtration buffer

NaH_2PO_4	20 mM
NaCl	150 mM

Made up to 1 L with MQW; adjusted to pH 8.0 with NaOH

Appendix II: Growth conditions for protein purification

Plasmids	Proteins	Strain	Temperatures ^{o}C	Media
pCU231	N-SmBiT-NusB	BL21	Room temperature	AIM
pCU235	N-LgBiT-NusE	BL21	Room temperature	AIM
pCU236	C-LgBiT-NusE	BL21	Room temperature	AIM
pCU250	N-LgBiT-NusB	BL21	Room temperature	AIM
pCU246	N-SmBiT-NusE	BL21	Room temperature	AIM
pCU247	C-SmBiT-NusE	BL21	Room temperature	AIM
pCU251	C-LgBiT-σ^{A}	BL21	Room temperature	AIM
pCU252	N-SmBiT-CH	BL21	Room temperature	AIM
pCU253	C-SmBiT-CH	BL21	Room temperature	AIM
pCU173	TmaNusB	BL21	37	AIM

Appendix III Publication list

Journal articles

1. **Tsang, T. F.**, Qiu, Y., Lin, L., Ye, J., Ma, C., & Yang, X. (2019). Simple method for studying *in Vitro* protein–protein interactions based on protein complementation and its application in drug screening targeting bacterial transcription. *ACS Infectious Diseases, 5*(4), 521-527. doi:10.1021/acsinfecdis.9b00020 (Supplementary cover article)

2. Qiu, Y., Chan, S. T., Lin, L., Shek, T. L., **Tsang, T. F.**, Barua, N., … Ma, C. (2019). Design, synthesis and biological evaluation of antimicrobial diarylimine and –amine compounds targeting the interaction between the bacterial NusB and NusE proteins. *European Journal of Medicinal Chemistry, 178*, 214–231. doi: 10.1016/j.ejmech.2019.05.090

3. Qiu, Y., Chan, S. T., Lin, L., Shek, T. L., **Tsang, T. F.**, Zhang, Y., … Ma, C. (2019). Nusbiarylins, a new class of antimicrobial agents: Rational design of bacterial transcription inhibitors targeting the interaction between the NusB and NusE proteins. *Bioorganic Chemistry, 92*, 103203. doi: 10.1016/j.bioorg.2019.103203

Conference poster presentations

1. American Chemical Society Symposium - Innovation at the Frontier of Chemistry and Life Science, Beijing, 2018. Poster title ‘A Simple, Rapid Method for *in Vitro* Protein-protein Interaction (PPIs) Inhibitor Screening’

ACS Infectious Diseases

APRIL 2019
VOLUME 5
NUMBER 4
pubs.acs.org/acsinfectious

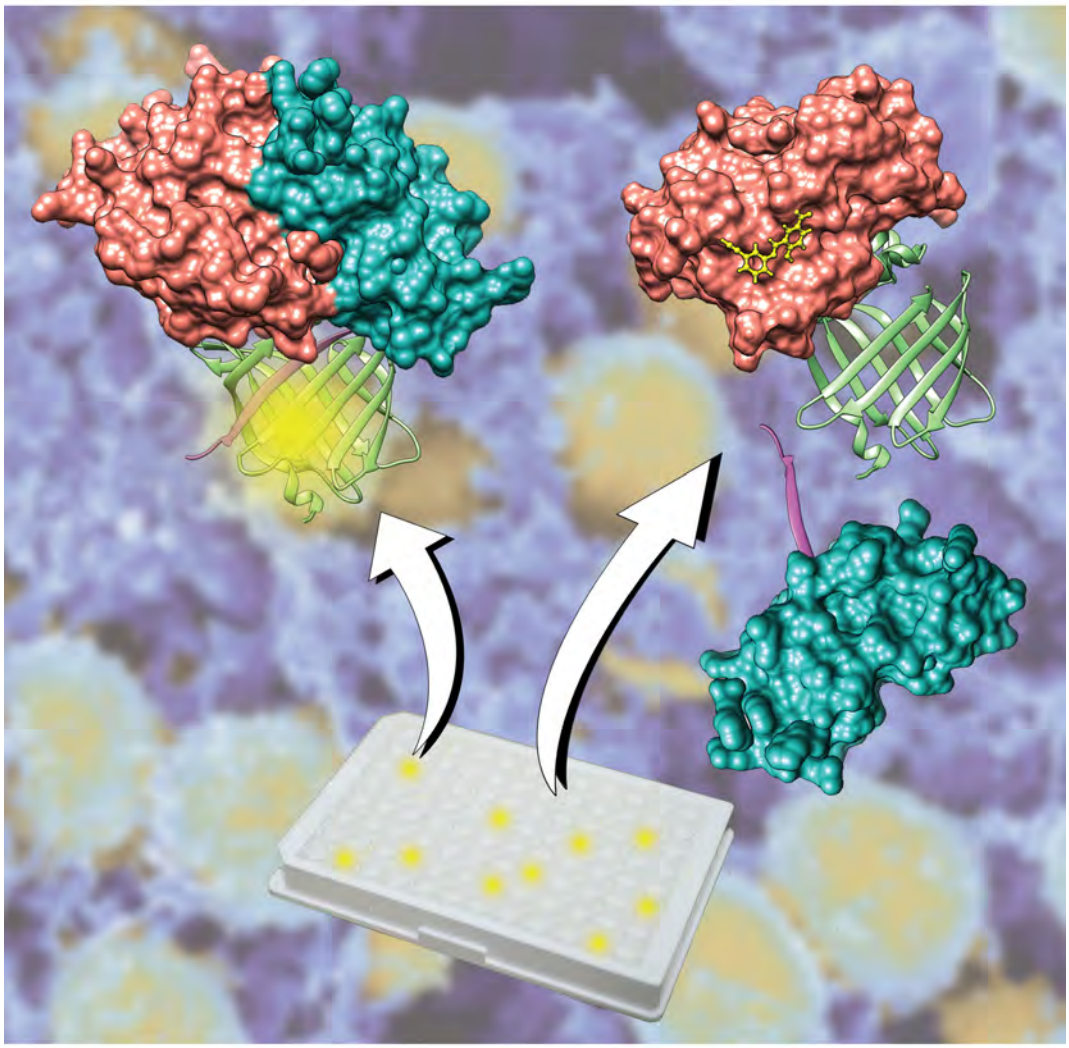

ACS Publications
Most Trusted. Most Cited. Most Read.

www.acs.org

Appendix IV Copyright clearance

Springer Nature BV - License Terms and Conditions

This is a License Agreement between Tsang Tsz Fung ("You") and Springer Nature BV ("Publisher") provided by Copyright Clearance Center ("CCC"). The license consists of your order details, the terms and conditions provided by Springer Nature BV, and the CCC terms and conditions.

All payments must be made in full to CCC.

Order Date	19-Aug-2020	Type of Use	Republish in a thesis/dissertation
Order license ID	1056712-1		
ISSN	1740-1526	Publisher	NATURE PUBLISHING GROUP
		Portion	Image/photo/illustration

LICENSED CONTENT

Publication Title	Nature Reviews Microbiology	Publication Type	Journal
Article Title	Termination and antitermination: RNA polymerase runs a stop sign.	Start Page	319
		End Page	329
		Issue	5
		Volume	9
Date	01/01/2004	URL	http://www.nature.com/nrmicro/index.html
Language	English		
Country	United Kingdom of Great Britain and Northern Ireland		
Rightsholder	Springer Nature BV		

REQUEST DETAILS

Portion Type	Image/photo/illustration	Distribution	Worldwide
Number of images / photos / illustrations	1	Translation	Original language of publication
Format (select all that apply)	Print, Electronic	Copies for the disabled?	No
		Minor editing privileges?	No
Who will republish the content?	Academic institution	Incidental promotional use?	No
Duration of Use	Life of current edition	Currency	USD
Lifetime Unit Quantity	Up to 499		
Rights Requested	Main product		

NEW WORK DETAILS

Title	Discovery and Characterization of Novel Inhibitors for Bacterial rRNA Transcription	Institution name	The Chinese University of Hong Kong
		Expected presentation date	2020-09-01
Instructor name	Dr Xiao Yang		

ADDITIONAL DETAILS

The requesting person / organization to appear on the license	Tsang Tsz Fung

REUSE CONTENT DETAILS

Title, description or numeric reference of the portion(s)	Figure 5. Processive antitermination mechanisms	Title of the article/chapter the portion is from	Termination and antitermination: RNA polymerase runs a stop sign.
Editor of portion(s)	Santangelo, Thomas J.; Artsimovitch, Irina	Author of portion(s)	Santangelo, Thomas J.; Artsimovitch, Irina
Volume of serial or monograph	9	Publication date of portion	2011-04-11
Page or page range of portion	319-329		

PUBLISHER TERMS AND CONDITIONS

If you are placing a request on behalf of/for a corporate organization, please use RightsLink.For further information visit
http://www.nature.com/reprints/permission-requests.html and
https://www.springer.com/gp/rights-permissions/obtaining-permissions/882

CCC Republication Terms and Conditions

1. Description of Service; Defined Terms. This Republication License enables the User to obtain licenses for republication of one or more copyrighted works as described in detail on the relevant Order Confirmation (the "Work(s)"). Copyright Clearance Center, Inc. ("CCC") grants licenses through the Service on behalf of the rightsholder identified on the Order Confirmation (the "Rightsholder"). "Republication", as used herein, generally means the inclusion of a Work, in whole or in part, in a new work or works, also as described on the Order Confirmation. "User", as used herein, means the person or entity making such republication.

2. The terms set forth in the relevant Order Confirmation, and any terms set by the Rightsholder with respect to a particular Work, govern the terms of use of Works in connection with the Service. By using the Service, the person transacting for a republication license on behalf of the User represents and warrants that he/she/it (a) has been duly authorized by the User to accept, and hereby does accept, all such terms and conditions on behalf of User, and (b) shall inform User of all such terms and conditions. In the event such person is a "freelancer" or other third party independent of User and CCC, such party shall be deemed jointly a "User" for purposes of these terms and conditions. In any event, User shall be deemed to have accepted and agreed to all such terms and conditions if User republishes the Work in any fashion.

3. Scope of License; Limitations and Obligations.

    3.1. All Works and all rights therein, including copyright rights, remain the sole and exclusive property of the Rightsholder. The license created by the exchange of an Order Confirmation (and/or any invoice) and payment by User of the full amount set forth on that document includes only those rights expressly set forth in the Order Confirmation and in these terms and conditions, and conveys no other rights in the Work(s) to User. All rights not expressly granted are hereby reserved.

    3.2. General Payment Terms: You may pay by credit card or through an account with us payable at the end of the month. If you and we agree that you may establish a standing account with CCC, then the following terms apply: Remit Payment to: Copyright Clearance Center, 29118 Network Place, Chicago, IL 60673-1291. Payments Due: Invoices are payable upon their delivery to you (or upon our notice to you that they are available to you for downloading). After 30 days, outstanding amounts will be subject to a service charge of 1-1/2% per month or, if less, the maximum rate allowed by applicable law. Unless otherwise specifically set forth in the Order Confirmation or in a separate written agreement signed by CCC, invoices are due and payable on "net 30" terms. While User may exercise the rights licensed immediately upon issuance of the Order Confirmation, the license is automatically revoked and is null and void, as if it had never been issued, if complete payment for the license is not received on a timely basis either from User directly or through a payment agent, such as a credit card company.

3.3. Unless otherwise provided in the Order Confirmation, any grant of rights to User (i) is "one-time" (including the editions and product family specified in the license), (ii) is non-exclusive and non-transferable and (iii) is subject to any and all limitations and restrictions (such as, but not limited to, limitations on duration of use or circulation) included in the Order Confirmation or invoice and/or in these terms and conditions. Upon completion of the licensed use, User shall either secure a new permission for further use of the Work(s) or immediately cease any new use of the Work(s) and shall render inaccessible (such as by deleting or by removing or severing links or other locators) any further copies of the Work (except for copies printed on paper in accordance with this license and still in User's stock at the end of such period).

3.4. In the event that the material for which a republication license is sought includes third party materials (such as photographs, illustrations, graphs, inserts and similar materials) which are identified in such material as having been used by permission, User is responsible for identifying, and seeking separate licenses (under this Service or otherwise) for, any of such third party materials; without a separate license, such third party materials may not be used.

3.5. Use of proper copyright notice for a Work is required as a condition of any license granted under the Service. Unless otherwise provided in the Order Confirmation, a proper copyright notice will read substantially as follows: "Republished with permission of [Rightsholder's name], from [Work's title, author, volume, edition number and year of copyright]; permission conveyed through Copyright Clearance Center, Inc. " Such notice must be provided in a reasonably legible font size and must be placed either immediately adjacent to the Work as used (for example, as part of a by-line or footnote but not as a separate electronic link) or in the place where substantially all other credits or notices for the new work containing the republished Work are located. Failure to include the required notice results in loss to the Rightsholder and CCC, and the User shall be liable to pay liquidated damages for each such failure equal to twice the use fee specified in the Order Confirmation, in addition to the use fee itself and any other fees and charges specified.

3.6. User may only make alterations to the Work if and as expressly set forth in the Order Confirmation. No Work may be used in any way that is defamatory, violates the rights of third parties (including such third parties' rights of copyright, privacy, publicity, or other tangible or intangible property), or is otherwise illegal, sexually explicit or obscene. In addition, User may not conjoin a Work with any other material that may result in damage to the reputation of the Rightsholder. User agrees to inform CCC if it becomes aware of any infringement of any rights in a Work and to cooperate with any reasonable request of CCC or the Rightsholder in connection therewith.

4. Indemnity. User hereby indemnifies and agrees to defend the Rightsholder and CCC, and their respective employees and directors, against all claims, liability, damages, costs and expenses, including legal fees and expenses, arising out of any use of a Work beyond the scope of the rights granted herein, or any use of a Work which has been altered in any unauthorized way by User, including claims of defamation or infringement of rights of copyright, publicity, privacy or other tangible or intangible property.

5. Limitation of Liability. UNDER NO CIRCUMSTANCES WILL CCC OR THE RIGHTSHOLDER BE LIABLE FOR ANY DIRECT, INDIRECT, CONSEQUENTIAL OR INCIDENTAL DAMAGES (INCLUDING WITHOUT LIMITATION DAMAGES FOR LOSS OF BUSINESS PROFITS OR INFORMATION, OR FOR BUSINESS INTERRUPTION) ARISING OUT OF THE USE OR INABILITY TO USE A WORK, EVEN IF ONE OF THEM HAS BEEN ADVISED OF THE POSSIBILITY OF SUCH DAMAGES. In any event, the total liability of the Rightsholder and CCC (including their respective employees and directors) shall not exceed the total amount actually paid by User for this license. User assumes full liability for the actions and omissions of its principals, employees, agents, affiliates, successors and assigns.

6. Limited Warranties. THE WORK(S) AND RIGHT(S) ARE PROVIDED "AS IS". CCC HAS THE RIGHT TO GRANT TO USER THE RIGHTS GRANTED IN THE ORDER CONFIRMATION DOCUMENT. CCC AND THE RIGHTSHOLDER DISCLAIM ALL OTHER WARRANTIES RELATING TO THE WORK(S) AND RIGHT(S), EITHER EXPRESS OR IMPLIED, INCLUDING WITHOUT LIMITATION IMPLIED WARRANTIES OF MERCHANTABILITY OR FITNESS FOR A PARTICULAR PURPOSE. ADDITIONAL RIGHTS MAY BE REQUIRED TO USE ILLUSTRATIONS, GRAPHS, PHOTOGRAPHS, ABSTRACTS, INSERTS OR OTHER PORTIONS OF THE WORK (AS OPPOSED TO THE ENTIRE WORK) IN A MANNER CONTEMPLATED BY USER; USER UNDERSTANDS AND AGREES THAT NEITHER CCC NOR THE RIGHTSHOLDER MAY HAVE SUCH ADDITIONAL RIGHTS TO GRANT.

7. Effect of Breach. Any failure by User to pay any amount when due, or any use by User of a Work beyond the scope of the license set forth in the Order Confirmation and/or these terms and conditions, shall be a material breach of the license created by the Order Confirmation and these terms and conditions. Any breach not cured within 30 days of written notice thereof shall result in immediate termination of such license without further notice. Any unauthorized (but licensable) use of a Work that is terminated immediately upon notice thereof may be liquidated by payment of the Rightsholder's ordinary license price therefor; any unauthorized (and unlicensable) use that is not terminated immediately for any reason (including, for example, because materials containing the Work cannot reasonably be recalled) will be subject to all remedies available at law or in equity, but in no event to a payment of less than three times the Rightsholder's ordinary license price for the most closely analogous licensable use plus Rightsholder's and/or CCC's costs and expenses incurred in collecting such payment.

8. Miscellaneous.

    8.1. User acknowledges that CCC may, from time to time, make changes or additions to the Service or to these terms and conditions, and CCC reserves the right to send notice to the User by electronic mail or otherwise for the purposes of notifying User of such changes or additions; provided that any such changes or additions shall not apply to permissions already secured and paid for.

    8.2. Use of User-related information collected through the Service is governed by CCC's privacy policy, available online here:https://marketplace.copyright.com/rs-ui-web/mp/privacy-policy

    8.3. The licensing transaction described in the Order Confirmation is personal to User. Therefore, User may not assign or transfer to any other person (whether a natural person or an organization of any kind) the license created by the Order Confirmation and these terms and conditions or any rights granted hereunder; provided, however, that User may assign such license in its entirety on written notice to CCC in the event of a transfer of all or substantially all of User's rights in the new material which includes the Work(s) licensed under this Service.

    8.4. No amendment or waiver of any terms is binding unless set forth in writing and signed by the parties. The Rightsholder and CCC hereby object to any terms contained in any writing prepared by the User or its principals, employees, agents or affiliates and purporting to govern or otherwise relate to the licensing transaction described in the Order Confirmation, which terms are in any way inconsistent with any terms set forth in the Order Confirmation and/or in these terms and conditions or CCC's standard operating procedures, whether such writing is prepared prior to, simultaneously with or subsequent to the Order Confirmation, and whether such writing appears on a copy of the Order Confirmation or in a separate instrument.

    8.5. The licensing transaction described in the Order Confirmation document shall be governed by and construed under the law of the State of New York, USA, without regard to the principles thereof of conflicts of law. Any case, controversy, suit, action, or proceeding arising out of, in connection with, or related to such licensing transaction shall be brought, at CCC's sole discretion, in any federal or state court located in the County of New York, State of New York, USA, or in any federal or state court whose geographical jurisdiction covers the location of the Rightsholder set forth in the Order Confirmation. The parties expressly submit to the personal jurisdiction and venue of each such federal or state court.If you have any comments or questions about the Service or Copyright Clearance Center, please contact us at 978-750-8400 or send an e-mail to support@copyright.com.

v 1.1